UNIVERSIDADE ESTADUAL PAULISTA
"JÚLIO DE MESQUITA FILHO"
Campus de Botucatu

PG-BGA

EFEITO DO LASER DE BAIXA INTENSIDADE SOBRE O PERFIL TRANSCRICIONAL DE RNAm EM MIOBLASTOS C2C12

JUAREZ HENRIQUE FERREIRA

Tese apresentada ao Instituto de Biociências, Câmpus de Botucatu, UNESP, como requisito para a defesa de Doutorado no Programa de Pós-Graduação em Biologia Geral e Aplicada, Área de concentração *Biologia Celular, Estrutural e Funcional.*

Prof. Dr. Robson Francisco Carvalho

BOTUCATU – SP
2018

Instituto de Biociências - Seção Técnica de Pós-Graduação
Distrito de Rubião Júnior s/n CEP 18618-970 Cx Postal 510 Botucatu-SP Brasil
Tel (14) 3880-0780 posgraduacao@ibb.unesp.br

UNIVERSIDADE ESTADUAL PAULISTA

"Julio de Mesquita Filho"

INSTITUTO DE BIOCIÊNCIAS DE BOTUCATU

EFEITO DO LASER DE BAIXA INTENSIDADE SOBRE O PERFIL TRANSCRICIONAL DE RNAm EM MIOBLASTOS C2C12

ALUNO: JUAREZ HENRIQUE FERREIRA

ORIENTADOR: PROF. DR. ROBSON FRANCISCO CARVALHO

CO-ORIENTADOR: DR. IVAN JOSÉ VECHETTI JÚNIOR

Tese apresentada ao Instituto de Biociências, Câmpus de Botucatu, UNESP, como requisito para a defesa de Doutorado no Programa de Pós-Graduação em Biologia Geral e Aplicada, Área de concentração *Biologia Celular, Estrutural e Funcional.*

Prof. Dr. Robson Francisco Carvalho

BOTUCATU – SP
2018

FICHA CATALOGRÁFICA ELABORADA PELA SEÇÃO TÉC. AQUIS. TRATAMENTO DA INFORM.
DIVISÃO TÉCNICA DE BIBLIOTECA E DOCUMENTAÇÃO - CÂMPUS DE BOTUCATU - UNESP
BIBLIOTECÁRIA RESPONSÁVEL: ROSANGELA APARECIDA LOBO-CRB 8/7500

Ferreira, Juarez Henrique.
Efeito do laser de baixa intensidade sobre o perfil transcricional de RNAm em mioblastos C2C12 / Juarez Henrique Ferreira. - Botucatu, 2018

Tese (doutorado) - Universidade Estadual Paulista "Júlio de Mesquita Filho", Instituto de Biociências de Botucatu
Orientador: Robson Francisco Carvalho
Coorientador: Ivan José Vechetti-Júnior
Capes: 20600003

1. Ciclo celular. 2. Desenvolvimento muscular. 3. Músculo esquelético. 4. Terapia com luz de baixa intensidade. 5. Transcriptoma.

Palavras-chave: Ciclo celular; Desenvolvimento muscular; Músculo esquelético; Terapia com laser; Transcriptoma.

Dedicatória

“Dedico este trabalho a minha mãe Maria Consolação Ferreira e ao meu pai Joaquim Juarez Ferreira, por terem sempre me incentivado desde a infância, a buscar o caminho do conhecimento. Este título de doutor é para vocês!”

Agradecimentos

Agradeço primeiramente a Deus por ter iluminado meu caminho e me dado sabedoria para conquistar mais esta etapa da vida.

Agradeço ao meu orientador professor Dr. Robson Francisco Carvalho por ter acreditado em mim e me dado a oportunidade de desenvolver este trabalho sob a sua orientação e por sempre ter sido solícito e dar apoio nesta jornada. Professor obrigado pela grande contribuição na minha formação acadêmica e também pelas palavras amigas ao longo desses anos. Minha eterna gratidão.

Agradeço ao meu co-orientador Doutor Ivan José Vechetti-Júnior por toda amizade e conhecimento compartilhado. Ivan, você muito além de um co-orientador e amigo, você se tornou um irmão e uma inspiração.

Agradeço a professora Dra. Maeli Dal Pai pela contribuição constante durante a execução deste projeto e por todo apoio prestado ao longo desses anos.

Agradeço a toda a equipe LBME: Ana Omoto, Bruna Zanella, Bruno Duran, Bruno Fantinatti, Carlos Augusto, Carlos Freitas, Edson Marreco, Geysson Fernandez, Grasieli Oliveira, Ivan Vechetti, Jéssica Valente, Leonardo Nazário, Paula Freire, Rafaela Nunes, Rodrigo Souza, Rondinele Salomão, Sarah Cury e Tassiana de Paula, que sempre contribuíram de uma forma direta ou indireta para a realização deste trabalho, compartilhando seu conhecimento e amizade.

Agradeço de maneira especial a algumas pessoas que ao longo desta jornada tiveram um papel fundamental na realização deste trabalho e que sem elas não teria sido possível a sua realização. Obrigado Leonardo Nazário de Moraes, Geysson Javier Fernandez Garcia, Tassiana Gutierrez de Paula, Ana Carolina Mieko Omoto e Carlos Augusto Alves pela contribuição e amizade.

Agradeço a minha esposa Talita Mariana Morata Raposo Ferreira pelo seu apoio incondicional, por sempre ter me dado forças para seguir em frente, mesmo diante das adversidades que surgiam, pela paciência e compreensão dos meus momentos de ausência.

Agradeço ao meu cachorro Jack (em memória) por sempre ter me recebido com amor e carinho quando voltava para casa após o trabalho no laboratório.

Agradeço a toda minha família pelo apoio e por sempre terem acreditado que essa conquista seria possível.

Agradeço as agências de fomento CAPES, CNPq e FAPESP por financiarem este trabalho e acreditar no nosso potencial.

RESUMO

A irradiação pelo laser de baixa intensidade (LBI) tem sido utilizada como um método não-invasivo para promover ou acelerar a capacidade de regeneração muscular. No entanto, os mecanismos moleculares regulatórios pelos quais o LBI exerce esses efeitos, permanecem em grande parte desconhecidos. Nosso objetivo foi realizar uma análise de sequenciamento de RNA (RNA-Seq) em mioblastos C2C12 após LBI. Foram realizadas as taxas de viabilidade, migração, proliferação e os dados de RNA-Seq dos mioblastos C2C12, identificando 514 genes diferencialmente expressos após LBI. Em seguida, uma análise de ontologia genética e das vias dos genes diferencialmente expressos revelaram transcritos relacionadas ao ciclo celular, biogênese ribossômica, resposta ao estresse, migração celular, estrutura morfológica e proliferação de células musculares. Após, cruzamos nossos dados de RNA-Seq com dados de transcriptomas disponíveis em base de dados públicas, com dados de diferenciação miogênica que mostraram um total de 42 transcritos sobrepostos (mioblastos *vs* miotubos). Este conjunto de transcritos compartilhados mostrou que os mioblastos irradiados pelo LBI, possuem um perfil transcricional semelhante ao de miotubo, agrupando-se distante do perfil transcricional dos mioblastos. Concluíndo, revelamos pela primeira vez que LBI, induz a uma expressão de um grande conjunto de RNAm, que codificam proteínas reguladoras do ciclo celular que podem controlar a proliferação e diferenciação de mioblastos em miotubos. Importantemente, esse conjunto de RNAm, revelou um perfil transcricional semelhante ao dos miotubos, fornencendo novos conhecimentos para a compreensão das alterações moleculares específicas subjacentes aos efeitos da irradiação por LBI em células do músculo esquelético.

Palavras-chave: transcriptoma, terapia com laser, desenvolvimento muscular, músculo esquelético, crescimento muscular, ciclo celular.

ABSTRACT

Low-level laser irradiation (LLLT) has been used as a non-invasive method to promote or accelerate muscular regeneration capability. However, the regulatory molecular mechanisms by which LLLT exerts these effects remain largely unknown. Our goal was to perform a RNA-sequencing (RNA-Seq) analysis in C2C12 myoblasts after LLLT. C2C12 myoblasts viability, migration, proliferation and RNA-Seq were performed, identifying 514 differentially expressed genes after LLLT. Next, gene ontology and pathway analysis of the differentially expressed genes revealed transcripts among categories related to cell cycle, ribosome biogenesis, response to stress, cell migration, morphological structure and muscle cell proliferation. After, we intersected our RNA-Seq data with transcriptomes publicly available myogenic differentiation data that showed a total of 42 overlapping transcripts (myoblasts vs myotube). This set of shared transcripts showed that the LLLT-myoblasts have a myotube-like profile, clustering away from the myoblast profile. In conclusion, we revealed for the first time that LLLT induces the expression a large set of mRNAs encoding for cell cycle regulatory proteins that may control myoblasts proliferation and differentiation into myotubes. Importantly, these set of mRNA revealed a myotube-like transcriptional profile and provided new insights to the understanding of the specific molecular changes underlying the effects of LLLT irradiation on skeletal muscle cells.

Key-words: Transcriptome, Laser treatment, Muscular development, Skeletal muscle, Muscle growth, Cell cycle.

Lista de Abrviações

AsGa – Arseneto de Gálio

AsGaAl – Arseneto de Gálio e Alumínio

ATP – Adenosina trifosfato

BrdU - 5-Bromo-2′-deoxyuridine

C2C12 – Linhagem celular imortalizada de mioblastos de camundongo

CT – Grupo controle

DAPI – 4’,6-diamidino-2-fenilindol

DEG – Differentially expressed genes

DMEM – Dubelcco’s Modified Eagle Medium

DMSO – Dimetilsulfóxido

GO – Gene Ontology

HCl – Ácido clorídrico

HeNe – Hélio/Neônio

IL-1β – Interleucina 1 beta

INF-γ – Interferon gama

KEGG - *Kyoto Encyclopedia of Genes and Genomes*

Laser – Light amplification by stimulated emission radiation

LBI – Laser de baixa intensidade

Linc-YY1 - Long intervening noncoding RNA

LLLT – Low level laser irradiation

miRNA – Micro-RNAs

MRFs – Myogenic regulatory factors

mRNA – RNA mensageiro

MTT - brometo 3-(4,5-dimetilazol-2-yl)-2,5-difeniltetrazol

MyHC – Cadeia Pesada de Miosina (*do inglês: myosin heavy chain*)

MyoD – Myogenic differentiation

NF-κB – Fator Nuclear-Kappa B (do inglês: nuclear factor kappa b)

NGS – Next generation sequencing

PBS – Tampão fosfato-salina

RNA-Seq – Sequenciamento de RNA

RPM – Rotações por minuto

RT – Transcrição Reversa

RT-qPCR – Reação em cadeia da polimerase em tempo real após transcrição reversa

Setdb1 – Histona

SFB – Soro fetal bovino

TEAD – Fator transcricional

TGF-β – Fator de Crescimento Transformante Beta (*do inglês: Transforming growth factor beta*)

TGF-β1 – Transforming growth factor beta 1

TNF-α – Fator de Necrose Tumoral- α (*do inglês: Tumor necrosis fator alpha*)

TWEAK - TNF-like weak inducer of apoptosis

Lista de Figuras

SUMÁRIO

1. INTRODUÇÃO

1.1. Aspectos gerais da composição e emissão dos lasers

O termo Laser é uma abreviação para *"Light Amplification by Stimulated Emission Radiation"* que, em português, significa "amplificação da luz por emissão estimulada de radiação" [1,2]. O primeiro feixe de laser produzido no espectro de faixa visível foi emitido por Maimam, em 1960, após excitar um cristal de rubi por intermédio de um flash fotográfico [1].

O laser difere da luz comum devido suas propriedades particulares [2]; suas ondas emitidas são sincronizadas em relação ao tempo e ao espaço, viajando ordenadamente e em amplitudes iguais [3]. A colimação, nome que se dá para o processo de tornar as ondas paralelas, é obtida pela unidirecionalidade do laser, que possui um feixe de fótons paralelo ao eixo do tubo que o produz, possuindo uma divergência angular muito pequena, concentrando assim toda a energia emitida em um único ponto [4]. Essas propriedades fazem com que o laser emitido possua uma elevada precisão e eficiência para transferir energia luminosa aos tecidos biológicos [5]. Dentre as causas já descritas desse efeito bioestimulante, ou biomodulador do laser, destacam-se modificações no metabolismo celular, em especial, em reações bioquímicas nas mitocôndrias, estimulando a síntese de ATP [6–8].

O laser pode ser classificado em duas categorias: lasers de alta intensidade (superam 1 W), utilizado para procedimentos mais agressivos como cirurgias, carbonização ou desnaturação de proteínas devido ao seu efeito fototérmico [9], e lasers de baixa intensidade (inferiores a 1 W), que interagem com os tecidos de forma indireta, produzindo efeitos para reparação tecidual, alívio de dor e a obtenção de efeitos anti-inflamatórios [10].

Os lasers de baixa intensidade (LBI) podem apresentar configurações diversificadas dependentes do comprimento de onda, que pode variar entre um espectro visível do vermelho a um espectro invisível do infravermelho. Esses feixes de laser são produzidos devido a mistura de gazes diversos, sendo os mais utilizados o hélio neônio (HeNe), arseneto de gálio e alumínio (AsGaAl) e o arseneto de gálio (AsGa) [11]. Os lasers que apresentam comprimento de onda na faixa de espectro infravermelho possuem maior poder de penetração nos tecidos. No entanto, o espectro de onda vermelho tem sido mais estudado [5,12].

Para a obtenção de resultados satisfatórios com o uso do LBI deve-se considerar a escolha do conjunto dos parâmetros a serem adotados, dentre eles: 1) a potência (W) que, atualmente, é considerada um parâmetro fixo e invariável nos aparelhos terapêuticos de LBI, e indica a quantidade de energia (J) pelo tempo (s) que chegará ao tecido - essa energia corresponde à quantidade de energia que será utilizada durante a irradiação terapêutica (dose); 2) a área de secção transversa do aplicador (cm^2), que corresponde à área a ser irradiada no tecido; 3) a densidade de

potência (W/cm²), definida pela potência de saída do laser pela área de secção transversa; e, 4) a densidade de energia (J/cm²), que corresponde à quantidade total da energia que foi entregue ao tecido através área de secção transversa do aplicador [5,13].

Além do cuidado na escolha dos parâmetros citados anteriormente, o comprimento de onda (nm) do LBI é um parâmetro determinante para um efeito terapêutico satisfatório, pois esse parâmetro é que determina quais tipos de tecidos biológicos irão absorver a radiação incidente e sua capacidade de penetração nesses tecidos. Dessa forma, a densidade de energia a ser utilizada por aplicação, a densidade de energia cumulativa total, e a frequência do tratamento devem ser cuidadosamente avaliadas de acordo com cada situação [5].

1.2. Uso da irradiação laser em tecidos biológicos

O efeito bioestimulante ou biomodulador do laser de baixa intensidade (LBI), vem sendo estudado desde os anos 60 [1,14–18]. No entanto, a era da terapia laser começou literalmente muito antes do desenvolvimento do próprio laser. As propriedades terapêuticas da luz "concentrada", já eram conhecidas no século XIX, quando Finsen recebeu o Prêmio Nobel em 1903, "em reconhecimento à sua contribuição para o tratamento de doenças, especialmente, o *Lupus vulgaris*, com radiação de luz concentrada, pelo qual abriu um novo caminho para a ciência médica" [19].

O uso do LBI como opção terapêutica vem sendo muito utilizado nas últimas décadas em diversas áreas médicas, objetivando promover ação ou efeito bioestimulador nas células e nos tecidos, para restabelecimento do equilíbrio celular e, consequentemente, da hemostasia dos tecidos [20]. A terapia com LBI é um método terapêutico seguro e eficaz, devido ao uso de recurso à base de luz que possui propriedades particulares que, em contato com a célula ou tecido, promove reações biológicas, gerando como resultado efeitos de diminuição da inflamação, da dor e cicatrização [21].

Diversos estudos vêm demonstrando a capacidade do LBI modular vários processos celulares em diferentes tecidos biológicos tais como estimulação na produção de colágeno pelo tecido conjuntivo, angiogênese, estimulação e diferenciação de osteoblastos, regeneração de tecido muscular esquelético, entre outros [22–38]. Em específico, Passarela et al.[34] e Karu et al.[39], demonstraram que o LBI era capaz de gerar um potencial eletroquímico extra e aumentar a síntese de ATP no interior das mitocôndrias.

No tecido muscular esquelético, o uso do LBI vem demonstrando efeitos benéficos no processo de reparação tecidual. Durante a fase de reparo do tecido muscular, o laser reduziu os níveis de IL-1β e o número de células inflamatórias [40–42]. Na fase de reparo muscular, o LBI aumentou os níveis de expressão de importantes fatores transcricionais como a MyoD e a

miogenina [43,44], e diminui o processo de fibrose devido à redução dos níveis de TGF-β1, TGF-β e dos níveis de colágeno do músculo [35,41,43,45].

O processo de inflamação no tecido muscular após lesão é caracterizado principalmente por necrose da fibra muscular, infiltrado inflamatório, aumento local de citocinas pró-inflamatórias, presença de fatores de crescimento e enzimas proteolíticas envolvidas na fagocitose de fragmentos celulares [42,46,47]. Simultaneamente, células precursoras miogênicas, denominadas de células satélites, são ativadas, proliferam e se diferenciam podendo, posteriormente, fundir-se com fibras musculares para promover o reparo de fibras musculares lesionadas, ou então, formar uma nova fibra muscular funcional [48–50] (Figura 1).

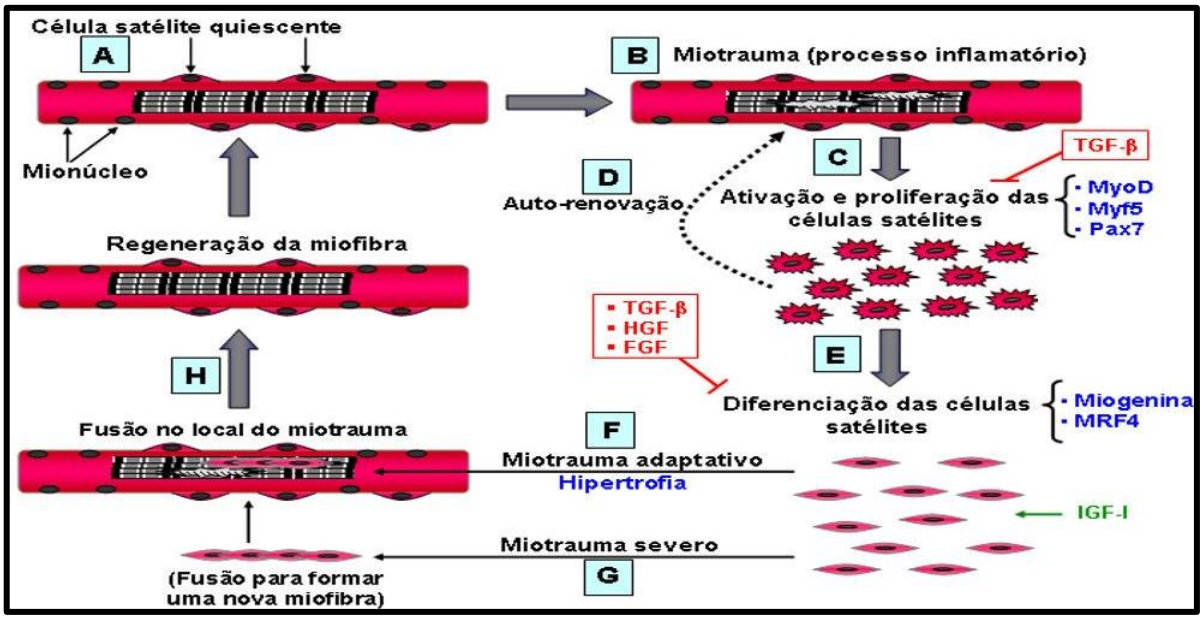

Figura 1 – Processo de regeneração Muscular. Fibra muscular normal com célula satélite quiescente e mionúcleo (A). Após um miotrauma (B), as células satélites quiescentes são ativadas, proliferam-se (C) e se diferenciam em mioblastos (E). No miotrauma adaptativo do exercício físico, os mioblastos migram para a região danificada e fundem-se à fibra muscular pré-existente para reparar o local da microlesão e/ou adicionar núcleos para ampliar a taxa síntese protéica (hipertrofia) (F). Porém, em situações de miotraumas severos que ocorra necrose das fibras (ação de toxinas e distrofia), os mioblastos poderão se alinhar e fundir-se entre si, para formar uma nova miofibra (G), e reparar o dano da fibra muscular (H). Durante o processo de regeneração, alguns mioblastos retornam ao estado quiescente e restabelecem a população de células satélites (D) (Adaptado de Chargé and Rudnick 2004 [51]).

1.3. Células C2C12

Os estudos avaliando os efeitos benéficos do LBI podem ser realizados diretamente em modelos animais ou através do uso de células de linhagem miogênicas que simulem a condição regeneração da células musculares [52,53]. Dentre as linhagens miogênicas, a linhagem C2C12 é uma

das mais utilizadas, devido sua capacidade de mimetizar o processo de miogênese ou regeneração *in vitro* [52].

As células C2C12 são mioblastos murinos derivados a partir de células satélites com o comportamento correspondente ao da linhagem progenitora [52]. Essas células são subclones de mioblastos C2 [54], que se diferenciam na cultura celular após a remoção do soro fetal bovino ou substituição pelo soro de cavalo [55,56]. O ciclo celular dos mioblastos C2C12 são comparáveis à ativação das células satélites presentes nas fibras musculares [57], tanto no estado quiescente como no estado ativado, expressam marcadores miogênicos [48] (Figura 2), chamados de fatores de regulação miogênica (MRFs, do inglês *myogenic regulatory factors*), que controlam as fases de ativação, proliferação e diferenciação durante o processo de crescimento ou reparo muscular [58].

Os mioblastos C2C12 são referência de modelo nos estudos para a compreensão dos mecanismos envolvidos no processo de reparo muscular devido ao fato de durante um processo de lesão muscular, a área afetada sofrer isquemia e consequentemente a perda de oxigênio e nutrientes [53], enquanto que, no modelo de estudo *in vitro* utilizando está linhagem celular, a diminuição dos níveis de soro fetal bovino pode mimetizar a situação de uma lesão muscular [59].

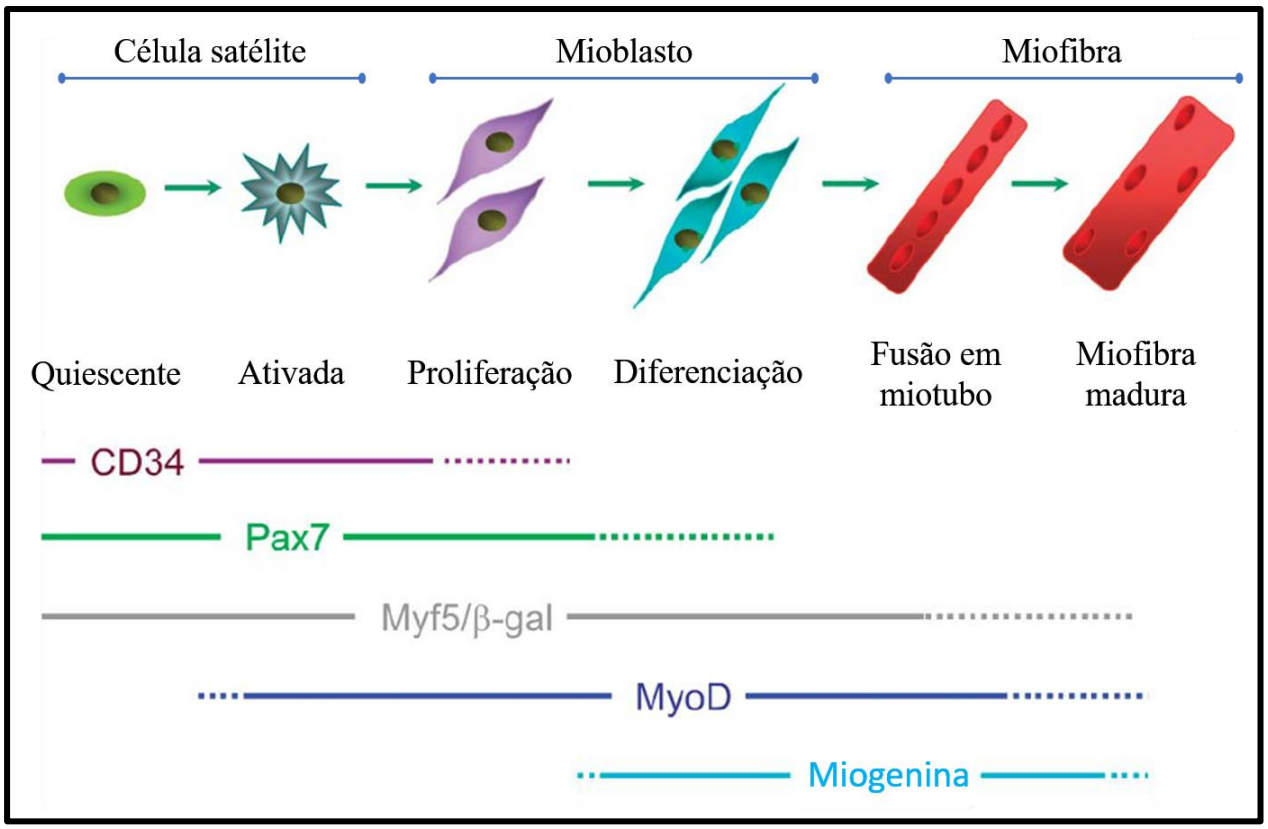

Figura 2. Representação esquemática das células satélites no crescimento muscular (adaptado de Zammit, Partridge, and Yablonka-Reuveni 2006 [60].

1.4. Perfil genômico global de mRNAs de células C2C12

Os recentes avanços de técnicas para análises globais utilizando RT-qPCR e de sequenciamento do transcriptoma, principalmente utilizando *Next-Generation Sequencing (NGS)* – permitem novos caminhos para análises de alta resolução do transcriptoma de tipos celulares específicos, o que revelou uma complexidade biológica anteriormente obscura nos estudos com tecidos inteiros [61–65].

A composição da fibra de um músculo é determinada em parte por fatores genéticos. No entanto, as fibras musculares não são unidades fixas, mas células capazes de responder a demandas funcionais alterando muito o seu fenótipo. A plasticidade funcional envolve alterações metabólicas e a expressão diferencial de MyHC e outras proteínas miofibrilares, permitindo assim, um ajuste da performance muscular [66,67]. Portanto, a real contribuição das células musculares para o fenótipo transcricional do músculo durante a regeneração muscular é ofuscada em estudos de expressão gênica com fragmentos musculares, devido a anatomia complexa do músculo esquelético e a heterogeneidade de suas fibras musculares [68]. O problema é exacerbado em doenças musculares com infiltrado de células inflamatórias ou substituição de células contráteis por células do tecido conjuntivo, como nas distrofias ou regeneração muscular [69–71]. Além disso, o perfil de expressão de uma população de fibras heterogêneas produz uma informação "média", mesmo que a doença acometa mais drasticamente um determinado tipo de célula muscular em particular [72]. O conhecimento das alterações na expressão gênica que ocorrem nas células musculares são de grande interesse para o estudo da plasticidade em relação à atividade, desuso e envelhecimento, e pode também ajudar no desenvolvimento de tratamentos para várias doenças musculares [73].

Recentes pesquisas envolvendo perfil global de expressão de mRNAs em células C2C12 têm auxiliado na identificação de importantes vias moleculares envolvidos na regeneração músculo esquelético, como descrito na tabela 1.

Condição Experimental	Pefil Genômico	Plataforma	Vias identificadas	Referência
Privação do meio de cultura (células C2C12)	mRNA	Microarray (22000*)	A,C,F,I	[74]
Tratamento com TNF-α/INF-γ (células C2C12)	mRNA	Microaray (12000*)	A,F,M,N	[75]
Tratamento com TNF-α (células C2C12)	mRNA	Microarray (25000*)	A,I,M,N,Q	[76]
Tratmento com TWEAK (células C2C12)	mRNA e miRNA	Microarray (25000*) e TLDA(650*)	A,C,F,GI,L,M,O	[77]
Regulação da miogênese por Setdb1 (Células C2C12)	mRNA	RNA-Seq e Microarray	Q	[78]
Regulação da miogênese por Linc-YY1 (Células C2C12)	mRNA	RNA-Seq	Q	[79]
Organização espacial do genoma durante miogênese (células C2C12)	mRNA	RNA-Seq	Q	[80]
Regulação da miogênese com TEAD (Células C2C12)	mRNA	RNA-Seq	Q	[81]

Tabela 1. Estudos do perfil genômico global de mRNAs em células C2C12. As principais vias/genes identificados foram: A) Sistema Proteassomal Dependente de Ubiquitina, B) Chaperonas, C) Estresse Oxidativo, D) Calpaínas, E) Proteases Lisossomais, F) Myod, G) MyhC, H) Transportador de Glutamina, I) Citocinas Inflamatórias, J) Apoptose, K) Sistema de *Splicing*, L) Sinalização Wnt, M) Sinalização NFkB , N) Sistema iNOS, O) Rede MyomiR, P) miR-23, miR-221, miR-148b e miR-338, Q) Miogênese. *: número de sondas utilizadas nos experimentos; TLDA*: TaqMan low density array (Life Technologies,EUA);* DD: *Differential Display.*

Embora os efeitos benéficos do LBI tenham sido demonstrados em diversos estudos, para nosso conhecimento, não há pesquisas relatando o perfil genômico global de mRNAs de células musculares tratadas com LBI para a elucidação dos mecanismos moleculares envolvidos na regeneração de células musculares induzida pelo tratamento com LBI. Nossa hipótese de trabalho é que a análise de dados de sequenciamento de alta performance de RNAm (*RNA-Seq*) permitirá

elucidar novas vias de regulação e mecanismos moleculares envolvidos na regeneração de células musculares tratadas com LBI.

2. OBJETIVO GERAL

Identificar as vias moleculares alteradas de mioblastos C2C12 após irradiação com laser de baixa intensidade (LBI).

2.1. Objetivos específicos

Avaliar em mioblastos C2C12 tratados com laser de baixa intensidade (LBI):

- a capacidade de proliferação e migração;
- a viabilidade celular;
- o perfil global de expressão gênica;
- o enriquecimento funcional do transcriptoma.

3. MATERIAL E MÉTODOS

3.1. Cultura celular

Os mioblastos C2C12 foram mantidos na cultura em meio de crescimento *Dulbecco's Modified Eagle Medium* (DMEM) suplementado com soro fetal bovino (SFB) (Thermo Scientific, USA) a uma concentração de 10%, penicilina 100 UI/mL e estreptomicina 100 µg/mL em uma incubadora umidificada a uma temperatura de 37ºC com uma concentração de CO_2 5%. Após as células atingirem uma confluência em torno de 70-80%, elas foram lavadas três vezes com tampão fosfato-salina (PBS) para retirada de resquícios do meio de crescimento, tripsinizadas e, então, centrifugadas a uma rotação de 1500 rpm, durante 10 minutos, a 4ºC. Em seguida, as células foram resuspendidas em DMEM suplementado com SFB 10% e, uma alíquota de 10uL foi utilizada para determinar a concentração celular em uma câmara de Neubauer. Após esse processo, as células foram transferidas para placas de 6-poços ou placas de 96-poços (viabilidade celular) de acordo com cada experimento, a uma concentração de $1x10^5$ células/poço e $5x10^3$ células/poço, respectivamente.

3.2. Irradiação pelo LBI

Os mioblastos C2C12 foram divididos em dois grupos experimentais: grupo controle (CT, n=3), constituído pelas células não irradiadas, e um grupo irradiado com o laser de baixa intensidade (LBI, n=3). O grupo LBI foi irradiado com um diodo laser de Gálio-Alumínio-Arseneto (GaAlAs), com comprimento de onda de 660 nm, energia de saída de 20 mW, área do feixe de 0,035 cm² e uma densidade de energia de 2 J/cm². O tempo de exposição foi de três segundos por ponto de aplicação. As placas de 6-poços foram irradiadas em 33 pontos (Figura 3), enquanto a placa de 96-poços foi irradiada em um único ponto. Dessa forma, pode-se obter uma cobertura total da área de cada poço da placa. O grupo CT foi submetido as mesmas condições experimentais que o grupo LBI, exceto o processo de irradiação pelo LBI. A irradiação foi realizada posicionando o feixe do laser perpendicularmente a uma distância de um centímetro da superfície inferior da placa. Todo o processo de irradiação foi realizado em ambiente escuro, para de evitar influência de outras fontes luminosas.

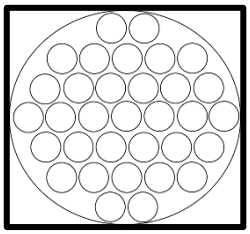

Figura 3 – Esquema de grade utilizada para a irradiação do laser de baixa intensidade nas placas de 6-poços.

3.3. Migração celular

Os mioblastos C2C12 foram cultivados em placa de 6-poços até atingirem uma confluência em torno de 80-90%. Subsequentemente, foi utilizado uma ponteira estéril de 200 µL para realizar um corte retilíneo no maior diâmetro do poço, sobre a cultura celular, obtendo-se dessa forma uma condição que simulasse uma lesão. Posteriormente, foram realizadas três lavagens com tampão PBS para remover fragmentos celulares e adicionado 2 mL de meio de cultura DMEM suplementado com SFB 5%, em cada poço, quando, então, o grupo LBI foi irradiado (Figura 4). O processo de análise da taxa de migração foi realizado através de imagens digitais logo após a irradiação pelo LBI e 6, 12, 24 e 48 horas após a irradiação. Todas as imagens foram plotadas no software ImageJ (versão 1.6.0) para mensurar a área existente entre cada margem celular.

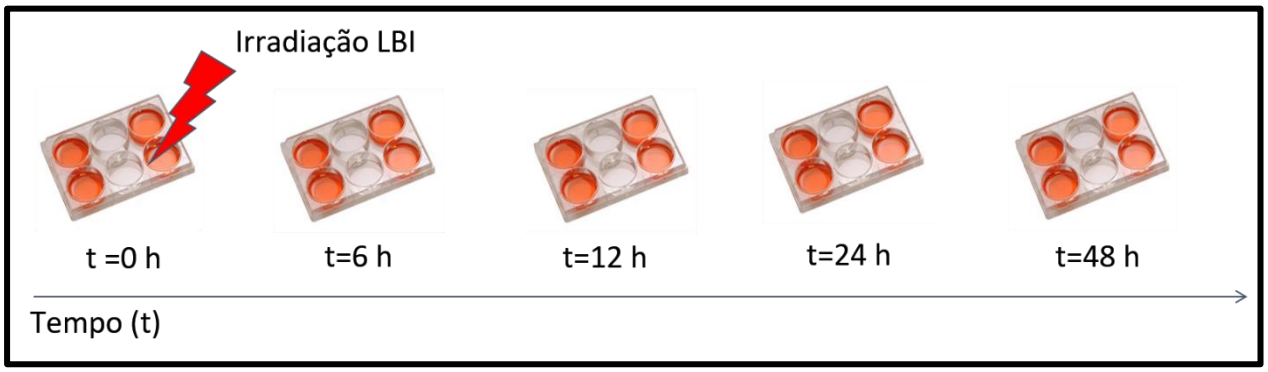

Figura 4 – Ensaio de migração/proliferação - Wound Healing.

3.4. Proliferação celular

Os mioblastos C2C12 foram submetidos a cultura sobre lamínulas de vidro inseridas em placas de 6-poços com meio de crescimento DMEM, suplementado com SFB 10%, até atingirem uma confluência de 70-80%, quando o meio de crescimento foi trocado por um meio suplementado com SFB 5% e as células foram irradiadas. Após 5 horas da irradiação, o meio foi substituído por um meio de DMEM contendo 5-Bromo-2′-deoxyuridine (BrdU; 10 µM) (Sigma-Aldrich). Após 1 hora, esse meio foi retirado e as células foram lavadas 3 vezes com tampão PBS, e então fixadas em paraformaldeído 4%, seguido de permeabilização com Triton X-100 0,1% em tampão PBS e

bloqueadas por uma hora com soro de cabra 10%, Triton X-100 1% em tampão PBS. Após o bloqueio, foi realizado a desnaturação com HCl 2 N, Triton X-100 0,5% em tampão PBS a uma temperatura de 37ºC durante 30 minutos. Após a desnaturação, foi realizado a neutralização com tampão de borato 0,1 M, pH 8,5, por 10 minutos. Subsequentemente, as células foram incubadas com anticorpo *mouse* anti-BrdU (Sigma-Aldrich) diluído em uma proporção de 1:1000, durante 1 hora e, posteriormente, *overnight* a 4ºC em uma solução de incubação composta por Triton X-100 0,3% e soro de cabra 5%. Finalmente, após a incubação *overnight*, a placa foi lavada 3 vezes com tampão PBS, e adicionado anticorpo *goat anti-mouse IgG texas red-conjugated* (Santa Cruz Biotechnology) em uma proporção 1:5000, durante 1 hora à temperatura ambiente. As lamínulas foram montadas em lâminas de vidro usando *Vectashield* (Vector Labs) e foram mantidas em ambiente privado de luz a uma temperatura de 4ºC até a leitura em microscópio de fluorescência invertido (BX61 Olympus). A análise foi realizada pela contagem dos núcleos que emitiram fluorescência, devido a incorporação do BrdU (corados em vermelho), e então foi calculado a taxa de incorporação do BrdU, em relação ao número total de núcleos celulares (corados em azul).

3.5. Viabilidade celular

A viabilidade celular dos mioblastos C2C12 foi avaliada pela função mitocondrial utilizando-se o ensaio biológico do brometo 3-(4,5-dimetilazol-2-yl)-2,5-difeniltetrazol (MTT) (Sigma-Aldrich). Esse ensaio mensura a atividade das células viáveis, via atividade da desidrogenase mitocondrial, que reduz o MTT para cristais púrpuros de formazan. Os mioblastos C2C12 foram cultivados em placas de 96-poços contendo meio de crescimento DMEM suplementado com SFB 10% até atingirem uma confluência de 70-80%, quando foram irradiados pelo LBI, o meio de cultura foi substituído por DMEM suplementado com SFB 5% por um período de 6 horas. Após esse período, o meio foi trocado e adicionado DMEM com MTT a uma concentração final de 0,5 mg/mL, e incubado por 3 horas. Seguido a incubação, os poços foram lavados 3 vezes com tampão PBS e foi adicionado 100 µL de DMSO em cada poço, para dissolver os cristais de formazan. A absorbância da solução foi mensurada em um comprimento de onda de 620 nm utilizando um leitor de microplaca (Anthos2020, Anthos Labtec Instruments).

3.6. Extração do RNA total

A extração do RNA dos mioblastos C2C12 foi realizada seis horas após a irradiação, utilizando TRIZOL (Thermo Fisher Scientific), de acordo com as instruções do fornecedor. O RNA total extraído foi quantificado por espectrofotometria usando *NanoVue* (GE Healthcare Life Sciences), e a qualidade do RNA foi obtida através do número de integridade do RNA por análises

baseadas no RNA ribossomal utilizando o *2100 Bioanalyzer system* (Agilent, USA), todas as amostras apresentaram *RIN > 9*.

3.7. Sequenciamento do RNA

Foram utilizados 5 µg de RNA total para construir as bibliotecas de RNA-seq para os grupos CT e LBI, os quais foram sequenciados em uma mesma *flow cell*, *paired-end*, 2 x 100 pb no equipamento *Illumina HiScanSQ* (Illumina, USA), segundo orientações do fornecedor. Foram gerados 25 milhões de *paired-end reads* por amostra. Os arquivos com as linhas de sequência (arquivos.fastq) foram submetidos a análise de controle de qualidade usando *FastQC* e os *Phred quality score* maior ou igual a 20 por posição de alinhamento. A linha de *paired-end reads* de fragmentos de DNAc foram alinhadas para o transcriptoma de camundongo (*RefSeq, mm10*) utilizando o software *TopHat* (versão 1.3.2) [82]. O pacote *Python HTSeq* foi utilizado para contagem dos *reads* mapeadas de cada transcrito e a expressão diferencial dos grupos controle e LBI foi identificada utilizando o pacote *DEseq* (versão 1.22.1) e reportadas como *Fold change* associado ao valor de p. Os *cutoffs* para determinar alteração nos níveis de expressão foram *Fold change* > 1,2 e valor de p <0,05. As análises foram realizadas utilizando o software R (http://www.r-project.org).

3.8. Análise de enriquecimento funcional de vias moleculares

Para uma melhor compreensão da relevância biológica dos genes que apresentaram alteração nos níveis de expressão, foi realizada uma análise de enriquecimento funcional no contexto das categorias do *Gene Ontology* (GO), *Kyoto Encyclopedia of Genes and Genomes* (KEGG), *Reactome* e base de dados *WikiPathways*. As análises das vias foram realizadas utilizando o software *Cytoscape* (versão 3.4.0) [83] em conjunto com o pacote de dados *ClueGO* (versão 2.2.5) [84]. Foram utilizados como *cutoffs* o valor de p<0,05 e um *fold* de enriquecimento maior que 10% para a identificação das categorias enriquecidas. O valor do *kappa score* foi calculado para refletir a base da relação dos termos na similaridade dos genes associados, com um *threshold* de 0,3 para fornecer uma visão da relevância das vias utilizando dados experimentais obtidos *in silico* e em base de dados de redes gênicas, interações proteína-proteína e interações funcionais [85,86]. As redes obtidas foram visualizadas e analisadas pelo *Cytoscape* [83].

3.9. Análises estatísticas

Todos os dados são apresentados como media ± desvio padrão (dp). As diferenças entre os grupos CT e LBI foram analisadas utilizando análises de teste *t* e *Mann-Whitney U* seguido de

comparações múltiplas utilizando o método proposto por *Sidak-Bonferroni*. Um valor de $p<0,05$ foi considerado significativamente estatístico. Os cálculos foram realizados através do software *GraphPad Prism* (versão 6.0.1).

4. CONSIDERAÇÕES FINAIS

A irradiação pelo LBI sobre os mioblastos C2C12 promoveu uma diminuição das taxas de proliferação e migração, com base nos dados da expressão gênica obtida pelo RNA-Seq, nossa hipótese para essa diminuição é que o LBI exerce um papel sobre as células miogênicas, fazendo com que elas inicialmente parem o seu ciclo celular, diminuindo dessa forma a sua capacidade de proliferação e migração, e, induz as células irradiadas a iniciarem o processo de diferenciação celular. No entanto, a viabilidade celular das células miogênicas que sofreram irradiação pelo LBI se manteve inalterada.

Nossos achados demonstraram pela primeira vez que os mioblastos C2C12 irradiados por LBI regulam um grande conjunto transcritos envolvidos no processo de miogênese. Importante destacar que esses conjuntos de transcritos diferencialmente expressos revelaram que os mioblastos irradiados com o LBI possuem um perfil transcricional similar ao de miotubos.

Dessa forma, podemos concluir que o LBI promove alteração no perfil transcricional dos mioblastos, tornando-os transcricionalmente mais semelhantes à miotubos já diferenciados. Esses achados fornecem nova perspectiva para a compreensão das mudanças moleculares específicas promovidas pelos efeitos do LBI sobre células musculares esqueléticas.

5. REFERÊNCIAS

1. Maiman, T. H. Stimulated Optical Radiation in Ruby. *Nature* **187,** 493–494 (1960).
2. Schawlow, A. L. Principles of lasers. *J. Clin. Laser Med. Surg.* **13,** 127–30 (1995).
3. Low, L. & Reed, A. *Eletroterapia explicada: Princípios e prática.* (Manole, 2001).
4. Kitchen, S. S. & Bazin, S. *Eletroterapia de Clayton*. (Manole, 1998).
5. Enwemeka, C. S. Intricacies of dose in laser phototherapy for tissue repair and pain relief. *Photomed. Laser Surg.* **27,** 387–393 (2009).
6. Rennó, A. C. M. *et al.* Comparative Effects of Low-Intensity Pulsed Ultrasound and Low-Level Laser Therapy on Injured Skeletal Muscle. *Photomed. Laser Surg.* **29,** 5–10 (2011).
7. Nakano, J. *et al.* Low-level laser irradiation promotes the recovery of atrophied gastrocnemius skeletal muscle in rats. *Exp. Physiol.* **94,** 1005–15 (2009).
8. Stein, A., Benayahu, D., Maltz, L. & Oron, U. Low-Level Laser Irradiation Promotes Proliferation and Differentiation of Human Osteoblasts in Vitro. *Photomed. Laser Surg.* **23,** 161–166 (2005).
9. Chavantes, M. C. & Jatene, A. D. Aplicação do laser na área cardiovascular. *Arq. Bras. Cardiol.* **54,** 63–82 (1990).
10. Parker, S. Introduction, history of lasers and laser light production. *Br. Dent. J.* **202,** 21–31 (2007).
11. Beckerman, H., de Bie, R. A., Bouter, L. M., De Cuyper, H. J. & Oostendorp, R. A. The efficacy of laser therapy for musculoskeletal and skin disorders: a criteria-based meta-analysis of randomized clinical trials. *Phys. Ther.* **72,** 483–91 (1992).
12. Enwemeka, C. S. ATTENUATION AND PENETRATION OF VISIBLE 632.8nm AND INVISIBLE INFRA-RED 904nm LIGHT IN SOFT TISSUES. *Laser Ther.* **13,** 95–101 (2001).
13. Huang, Y.-Y., Chen, A. C.-H., Carroll, J. D. & Hamblin, M. R. Biphasic Dose Response in Low Level Light Therapy. *Dose-Response* **7,** dose-response.0 (2009).
14. Geusic, J. E., Marcos, H. M. & Van Uitert, L. G. Laser oscillations in nd-doped yttrium aluminum, yttrium gallium and gadolinium garnets. *Appl. Phys. Lett.* **4,** 182–184 (1964).
15. Franken, P. A. & Ward, J. F. Optical harmonics and nonlinear phenomena. *Rev. Mod. Phys.* **35,** 23–39 (1963).
16. Patel, C. K. N. Continuous-Wave Laser Action on Vibrational-Rotational Transistions of CO_2. *Phys. Rev.* **136,** A1187–A1193 (1964).
17. Javan, A., Bennett, W. R. & Herriott, D. R. Population inversion and continuous optical maser oscillation in a gas discharge containing a He-Ne mixture. *Phys. Rev. Lett.* **6,** 106–

110 (1961).

18. Hall, R. N., Fenner, G. E., Kingsley, J. D., Soltys, T. J. & Carlson, R. O. Coherent light emission from GaAs junctions. *Phys. Rev. Lett.* **9,** 366–368 (1962).
19. Grzybowski, A. & Pietrzak, K. From patient to discoverer-Niels Ryberg Finsen (1860-1904)-the founder of phototherapy in dermatology. *Clin. Dermatol.* **30,** 451–455 (2012).
20. Dörtbudak, O., Haas, R. & Mallath-Pokorny, G. Biostimulation of bone marrow cells with a diode soft laser. *Clin. Oral Implants Res.* **11,** 540–545 (2000).
21. Enwemeka, C. S. *et al.* The efficacy of low-power lasers in tissue repair and pain control: a meta-analysis study. *Photomed. Laser Surg.* **22,** 323–329 (2004).
22. Al-Watban, F. a H. & Zhang, X. Y. The comparison of effects between pulsed and CW lasers on wound healing. *J. Clin. Laser Med. Surg.* **22,** 15–8 (2004).
23. Reddy, G. K., Stehno-Bittel, L. & Enwemeka, C. S. Laser photostimulation of collagen production in healing rabbit Achilles tendons. *Lasers Surg. Med.* **22,** 281–287 (1998).
24. Bibikova, A. & Oron, U. Attenuation of the process of muscle regeneration in the toad gastrocnemius muscle by low energy laser irradiation. *Lasers Surg. Med.* **14,** 355–361 (1994).
25. Amaral, a C., Parizotto, N. a & Salvini, T. F. Dose-dependency of low-energy HeNe laser effect in regeneration of skeletal muscle in mice. *Lasers Med. Sci.* **16,** 44–51 (2001).
26. Liebert, M. A. *et al.* Therapy on Acute Inflammatory Pain. *Photomed. Laser Surg.* **23,** 177–181 (2005).
27. Basford, J. R. Low intensity laser therapy: still not an established clinical tool. *Lasers Surg. Med.* **16,** 331–42 (1995).
28. Pessoa, E. S., Melhado, R. M., Theodoro, L. H. & Garcia, V. G. A histologic assessment of the influence of low-intensity laser therapy on wound healing in steroid-treated animals. *Photomed. Laser Surg.* **22,** 199–204 (2004).
29. Woodruff, L. D. *et al.* The efficacy of laser therapy in wound repair: a meta-analysis of the literature. *Photomed. Laser Surg.* **22,** 241–247 (2004).
30. Chagas-Júnior, O. L. Avaliação da ação do laser (λ=685 nm) sobre os mastócitos: contagem absoluta através do método esteriológico. (Pontifícia Universidade Católica - PUC, 2004).
31. Sato, Y. & Ohshima, T. The expression of mRNA of proinflammatory cytokines during skin wound healing in mice: A preliminary study for forensic wound age estimation (II). *Int. J. Legal Med.* **113,** 140–145 (2000).
32. Mendez, T. M. T. V, Pinheiro, A. L. B., Pacheco, M. T. T., Nascimento, P. M. & Ramalho, L. M. P. Dose and wavelength of laser light have influence on the repair of cutaneous

wounds. *J. Clin. Laser Med. Surg.* **22,** 19–25 (2004).

33. Do Nascimento, P. M., Pinheiro, A. L. B., Ângelo Castilho Salgado, M. & Pedreira Ramalho, L. M. A Preliminary Report on the Effect of Laser Therapy on the Healing of Cutaneous Surgical Wounds as a Consequence of an Inversely Proportional Relationship between Wavelength and Intensity: Histological Study in Rats. *Photomed. Laser Surg.* **22,** 513–518 (2004).
34. Passarella, S. *et al.* Increase of proton electrochemical potential and ATP synthesis in rat liver mitochondria irradiated in vitro by helium-neon laser. *FEBS Lett.* **175,** 95–99 (1984).
35. De Freitas, C. E. A. *et al.* High Final Energy of Low-Level Gallium Arsenide Laser Therapy Enhances Skeletal Muscle Recovery without a Positive Effect on Collagen Remodeling. *Photochem. Photobiol.* **91,** 957–965 (2015).
36. Aquino, A. E. *et al.* Can low-level laser therapy when associated to exercise decrease adipocyte area? *J. Photochem. Photobiol. B.* **149,** 21–6 (2015).
37. Alessi Pissulin, C. N., Henrique Fernandes, A. A., Sanchez Orellana, A. M., Rossi E Silva, R. C. & Michelin Matheus, S. M. Low-level laser therapy (LLLT) accelerates the sternomastoid muscle regeneration process after myonecrosis due to bupivacaine. *J. Photochem. Photobiol. B.* **168,** 30–39 (2017).
38. Pissulin, C. N. A. *et al.* GaAs laser therapy reestablishes the morphology of the NMJ and nAChRs after injury due to bupivacaine. *J. Photochem. Photobiol. B.* **167,** 256–263 (2017).
39. Karu, T., Pyatibrat, L. & Kalendo, G. Irradiation with HeNe laser increases ATP level in cells cultivated in vitro. *J. Photochem. Photobiol. B Biol.* **27,** 219–223 (1995).
40. Fernandes, K. P. S. *et al.* Effect of photobiomodulation on expression of IL-1β in skeletal muscle following acute injury. *Lasers Med. Sci.* **28,** 1043–1046 (2013).
41. Alves, A. N. *et al.* Modulating effect of low level-laser therapy on fibrosis in the repair process of the tibialis anterior muscle in rats. *Lasers Med. Sci.* **29,** 813–821 (2014).
42. Ferraresi, C., Hamblin, M. R. & Parizotto, N. A. Low-level laser (light) therapy (LLLT) on muscle tissue: Performance, fatigue and repair benefited by the power of light. *Photonics Lasers Med.* **1,** 267–286 (2012).
43. Assis, L. *et al.* Low-level laser therapy (808 nm) contributes to muscle regeneration and prevents fibrosis in rat tibialis anterior muscle after cryolesion. *Lasers Med. Sci.* **28,** 947–955 (2013).
44. Rodrigues, N. C., Brunelli, R., De Araújo, H. S. S., Parizotto, N. A. & Renno, A. C. M. Low-level laser therapy (LLLT) (660 nm) alters gene expression during muscle healing in rats. *J. Photochem. Photobiol. B Biol.* **120,** 29–35 (2013).

45. Luo, L. *et al.* Effects of low-level laser therapy on ROS homeostasis and expression of IGF-1 and TGF-β1 in skeletal muscle during the repair process. *Lasers Med. Sci.* **28,** 725–734 (2013).
46. Shin, E. H., Caterson, E. J., Jackson, W. M. & Nesti, L. J. Quality of healing: defining, quantifying, and enhancing skeletal muscle healing. *Wound Repair Regen.* **22,** 18–24 (2014).
47. Tidball, J. G. & Villalta, S. A. Regulatory interactions between muscle and the immune system during muscle regeneration. *Am J Physiol Regul Integr Comp Physiol* **298,** R1173-87 (2010).
48. Hawke, T. J. & Garry, D. J. Myogenic satellite cells Physiology to molecular biology. *J. Appl. Physiol.* **91,** 534–551 (2001).
49. Bentzinger, C. F., Wang, Y. X. & Rudnicki, M. A. Building Muscle: Molecular Regulation of Myogenesis. *Cold Spring Harb. Perspect. Biol.* **4,** a008342–a008342 (2012).
50. Shi, X. & Garry, D. J. Muscle stem cells in development, regeneration, and disease. *Genes Dev.* **20,** 1692–1708 (2006).
51. Chargé, S. B. P. & Rudnicki, M. A. Cellular and molecular regulation of muscle regeneration. *Physiol. Rev.* **84,** 209–238 (2004).
52. Burattini, S. *et al.* C2C12 murine myoblasts as a model of skeletal muscle development: morpho-functional characterization. *Eur. J. Histochem.* **48,** 223–33 (2004).
53. Shefer, G. *et al.* Low-energy laser irradiation promotes the survival and cell cycle entry of skeletal muscle satellite cells. *J. Cell Sci.* **115,** 1461–9 (2002).
54. Yaffe, D. & Saxel, O. Serial passaging and differentiation of myogenic cells isolated from dystrophic mouse muscle. *Nature* **270,** 725–727 (1977).
55. Blau, H. M., Chiu, C. P. & Webster, C. Cytoplasmic activation of human nuclear genes in stable heterocaryons. *Cell* **32,** 1171–1180 (1983).
56. Blau, H. M. *et al.* Plasticity of the differentiated state. *Science* **230,** 758–766 (1985).
57. Yoshida, N., Yoshida, S., Koishi, K., Masuda, K. & Nabeshima, Y. Cell heterogeneity upon myogenic differentiation: down-regulation of MyoD and Myf-5 generates 'reserve cells'. *J. Cell Sci.* **111,** 769–779 (1998).
58. Seale, P. & Rudnicki, M. A. A new look at the origin, function, and 'stem-cell' status of muscle satellite cells. *Dev. Biol.* **218,** 115–24 (2000).
59. Ferreira, M. P. P. *et al.* Effect of low-energy gallium-aluminum-arsenide and aluminium gallium indium phosphide laser irradiation on the viability of C2C12 myoblasts in a muscle injury model. *Photomed. Laser Surg.* **27,** 901–6 (2009).

60. Zammit, P. S., Partridge, T. A. & Yablonka-Reuveni, Z. The skeletal muscle satellite cell: the stem cell that came in from the cold. *J. Histochem. Cytochem.* **54,** 1177–91 (2006).
61. Macaulay, I. C. & Voet, T. Single cell genomics: advances and future perspectives. *PLoS Genet.* **10,** e1004126 (2014).
62. Forties, R. a & Wang, M. D. Discovering the Power of Single Molecules. *Cell* **157,** 4–7 (2014).
63. Eberwine, J., Sul, J.-Y., Bartfai, T. & Kim, J. The promise of single-cell sequencing. *Nat. Methods* **11,** 25–27 (2013).
64. Wu, A. R. *et al.* Quantitative assessment of single-cell RNA-sequencing methods. *Nat. Methods* **11,** 41–6 (2014).
65. Sandberg, R. Entering the era of single-cell transcriptomics in biology and medicine. *Nat. Methods* **11,** 22–24 (2013).
66. Baldwin, K. M. & Haddad, F. Skeletal muscle plasticity: cellular and molecular responses to altered physical activity paradigms. *Am. J. Phys. Med. Rehabil.* **81,** S40-51 (2002).
67. Flück, M. & Hoppeler, H. Molecular basis of skeletal muscle plasticity--from gene to form and function. *Rev. Physiol. Biochem. Pharmacol.* **146,** 159–216 (2003).
68. Chemello, F. *et al.* Microgenomic analysis in skeletal muscle: expression signatures of individual fast and slow myofibers. *PLoS One* **6,** e16807 (2011).
69. Hampson, R. & Hughes, S. M. Muscular expressions: profiling genes in complex tissues. *Genome Biol.* **2,** REVIEWS1033 (2001).
70. Haslett, J. N. & Kunkel, L. M. Microarray analysis of normal and dystrophic skeletal muscle. *Int. J. Dev. Neurosci.* **20,** 359–65 (2002).
71. Yan, Z. *et al.* Highly coordinated gene regulation in mouse skeletal muscle regeneration. *J. Biol. Chem.* **278,** 8826–36 (2003).
72. Raffaello, A. *et al.* Denervation in murine fast-twitch muscle: short-term physiological changes and temporal expression profiling. *Physiol. Genomics* **25,** 60–74 (2006).
73. Bassel-Duby, R. & Olson, E. N. Signaling pathways in skeletal muscle remodeling. *Annu. Rev. Biochem.* **75,** 19–37 (2006).
74. Stevenson, E. J., Koncarevic, A., Giresi, P. G., Jackman, R. W. & Kandarian, S. C. Transcriptional profile of a myotube starvation model of atrophy. *J. Appl. Physiol.* **98,** 1396–406 (2005).
75. Di Marco, S. *et al.* NF-kappa B-mediated MyoD decay during muscle wasting requires nitric oxide synthase mRNA stabilization, HuR protein, and nitric oxide release. *Society* **25,** 6533–45 (2005).

76. Bhatnagar, S. *et al.* Tumor necrosis factor-α regulates distinct molecular pathways and gene networks in cultured skeletal muscle cells. *PLoS One* **5,** (2010).
77. Panguluri, S. K. *et al.* Genomic profiling of messenger RNAs and microRNAs reveals potential mechanisms of TWEAK-induced skeletal muscle wasting in mice. *PLoS One* **5,** e8760 (2010).
78. Song, Y. J., Choi, J. H. & Lee, H. Setdb1 is required for myogenic differentiation of C2C12 myoblast cells via maintenance of MyoD expression. *Mol. Cells* **38,** 362–372 (2015).
79. Sun, K., Zhou, L., Zhao, Y., Wang, H. & Sun, H. Genome-wide RNA-seq and ChIP-seq reveal Linc-YY1 function in regulating YY1/PRC2 activity during skeletal myogenesis. *Genomics Data* **7,** 247–249 (2016).
80. Doynova, M. D., Markworth, J. F., Cameron-Smith, D., Vickers, M. H. & O'Sullivan, J. M. Linkages between changes in the 3D organization of the genome and transcription during myotube differentiation in vitro. *Skelet. Muscle* **7,** 5 (2017).
81. Joshi, S. *et al. TEAD transcription factors are required for normal primary myoblast differentiation in vitro and muscle regeneration in vivo*. *PLoS Genetics* **13,** (2017).
82. Trapnell, C. *et al.* Differential gene and transcript expressiont analysis of RNA-seq experiments with TopHat and Cufflinks. *Natures Protoc.* **7,** 562–578 (2012).
83. Shannon, P. Cytoscape: A Software Environment for Integrated Models of Biomolecular Interaction Networks. *Genome Res.* **13,** 2498–2504 (2003).
84. Bindea, G. *et al.* ClueGO: a Cytoscape plug-in to decipher functionally grouped gene ontology and pathway annotation networks. *Bioinformatics* **25,** 1091–3 (2009).
85. Aranda, B. *et al.* PSICQUIC and PSISCORE: accessing and scoring molecular interactions. *Nat. Methods* **8,** 528–9 (2011).
86. Bindea, G., Galon, J. & Mlecnik, B. CluePedia Cytoscape plugin: Pathway insights using integrated experimental and in silico data. *Bioinformatics* **29,** 661–663 (2013).

6. MANUSCRITO

Low-level laser irradiation induces a transcriptional myotube-like profile in C2C12 myoblasts

Juarez H. Ferreira[1], Sarah S. Cury[1], Ivan J. Vechetti-Júnior[1], Geysson J. F. Garcia[1], Leonardo N. Moraes[1], Carlos A. B. Alves[1], Paula P. Freire[1], Carlos E. A. Freitas[2], Maeli Dal-Pai-Silva[1] and Robson F. Carvalho[1,*]

[1] Department of Morphology

Institute of Biosciences, São Paulo State University (UNESP)

Botucatu, SP, Brazil

[2] Department of Physiotherapy

University of Western Sao Paulo (UNOESTE)

Presidente Prudente, SP, Brazil

[*]rcarvalho@ibb.unesp.br Telephone: +55 14 3880 0473

Abstract

Low-level laser therapy (LLLT) has been used as a non-invasive method to improve muscular regeneration capability. However, the molecular mechanisms by which LLLT exerts these effects remain largely unknown. We described global gene expression profiling analysis in C2C12 myoblasts after LLLT that identified 514 differentially expressed genes (DEG). Gene ontology and pathways analysis of the DEG revealed transcripts among categories related to cell cycle, ribosome biogenesis, response to stress, cell migration, and cell proliferation. We further intersected the DEG in C2C12 myoblasts after LLLT with publicly available transcriptomes data from myogenic differentiation studies (myoblasts vs myotube) to identify transcripts with potential effects on

myogenesis. This analysis revealed 42 DEG between myoblasts and myotube that intersect with altered genes in myoblasts after LLLT. Next, we performed a hierarchical cluster analysis with this set of shared transcripts that showed that LLLT-myoblasts have a myotube-like profile, clustering away from the myoblast profile. The myotube-like transcriptional profile of LLLT myoblasts was further confirmed globally considering all the transcripts detected in C2C12 myoblasts after LLLT, by bi-dimensional clustering with myotubes transcriptional profiles, and by the comparison with 154 gene sets derived from previous published in vitro omics data. In conclusion, we demonstrate for the first time that LLLT regulates a set of mRNAs that control myoblasts proliferation and differentiation into myotubes. Importantly, this set of mRNAs revealed a myotube-like transcriptional profile in LLLT-myoblasts and provide new insights to the understanding of the molecular mechanisms underlying the effects of LLLT on skeletal muscle cells.

Key-words: Transcriptome, Laser treatment, Muscle Regeneration, Myogenesis, RNA Sequencing.

Introduction

Low-level laser therapy (LLLT) has been used as a non-invasive method to promote or accelerate skeletal muscle regeneration capability [1–5]. Skeletal muscle regeneration is mainly accomplished by the proliferation and differentiation of myogenic cells derived from satellite cells (reviewed in [6]). After trauma or injury, satellite cells are activated, and become immature muscle cells or myoblasts that proliferate, migrate, and fuse into existing muscle fibers, or form new myofibers during muscle repair [7]. Consequently, several studies have been conducted in satellite cells and myogenic cell lines to understand the biological effects of LLLT on cellular and molecular mechanisms

that contribute to muscle regeneration [8–12]. These studies clearly demonstrate that myogenic cells modulate proliferation and differentiation, and change the expression of myogenic regulatory factors and cell cycle regulatory proteins in response to LLLT. Although the increasing evidence of the beneficial effects of LLLT on myogenic cells has become widely accepted, the global regulatory molecular mechanisms by which LLLT exerts these effects remain largely unknown.

Previous examinations of large scale mRNA expression generated by cDNA microarray analysis have generated insights on the molecular changes underlying the effects of LLLT in different cells types. For example, the expression levels of various genes involved in cell proliferation, apoptosis, and the cell cycle were affected by LLLT in mesenchymal stem cells [13]. Similarly, several differentially expressed genes (DEG) were identified in human fibroblasts after low-intensity red light; most of these genes either directly or indirectly participate in biologic processes related to cellular proliferation [14]. However, to the best of our knowledge, no other study has used a global mRNA expression profiling analysis by high-throughput RNA sequencing (RNA-Seq) method to study the effects of LLLT in skeletal muscle cells. This approach may provide meaningful insights into how LLLT exerts its regulatory effects in these cells and unravels laser-stimulated networks and molecular pathways. Therefore, our goal was to perform a global mRNA expression profiling analysis in C2C12 myoblasts after LLLT.

Materials and Methods

Cell culture

C2C12 myoblasts were maintained in growth medium Dulbecco's modified Eagle medium (DMEM) supplemented with 10% fetal bovine serum (Thermo Scientific, USA), 100 IU/mL penicillin, and 100 µg/mL streptomycin in a humidified incubator at 37°C

with 5% CO_2. After reach 70-80% confluence, cells were washed in phosphate-buffered saline (PBS), trypsinized, centrifuged (1500 rpm, 10 min, 4°C), resuspended in DMEM medium with FBS 10%, and counted in Neubauer chamber. Subsequently, the cells were transferred and cultured into 6-well plates ($1x10^5$ cells/well) or 96-well plates (and $5x10^3$ cells/well) in 96-well plates, according to the experiments.

Laser irradiation

Cells were divided into two experimental groups: non-irradiated control group (CT, n=3) and low-level laser irradiated group (LLL, n=3). The LLL cells were submitted to a Gallium-Aluminum-Arsenide (GaAlAs) diode laser, with 660 nm wavelength, output power of 20 mW, beam area of $0.035cm^2$, and an energy density of 2 J/cm^2. The time of exposure was 3 seconds/point. Each well plate was irradiated in 33 points (6-well plate) or 1 point (96-well plate) to ensure the complete irradiation over the entire cell-culture plate. The CT group was subjected to the same experimental conditions as the LLL, except for the irradiation. Irradiation was performed in the dark to avoid the influence of other light sources and the beam incidence angle was positioned perpendicularly (90 degree) at 1 cm of lower surface plate to the irradiation.

Cell viability assay

The viability of the proliferating C2C12 myoblasts, after LLLT, was assessed by using the 3-(4,5-dimethylthiazol-2-yl)-2,5-diphenyltetrazolium bromide (MTT) assay (Sigma-Aldrich, USA). This assay measures the activity of living cells via mitochondrial dehydrogenase activity that reduces MTT to purple formazan. The cells were seeded in a 96-well plate with DMEN, and at 0, 6, 12, 24, and 48 hours after LLLT, MTT (0.5 mg/mL) in phosphate- buffered saline (PBS) was added to each well. Following, 100 µL of DMSO was added to each well to dissolve formazan crystals. The solution absorbance

was measured at 570 nm using a microplate reader (2020, Anthos Labtec Instruments, Austria).

Wound Healing Assay

C2C12 myoblasts were plated in 6-well plate and cultured in DMEM until reach 80-90% confluence. Subsequently, a single-line scratch was mechanically generated in a cell monolayer by a 200-µl plastic tip. Cell debris were removed through two PBS washes, and 2 mL of DMEM supplemented with 5% fetal bovine serum was added to each well, when the LLL group was irradiated. The wound open area was photographed and analyzed at 0, 6, 12, 24, and 48 hours after LLLT, and the wound closure rate was determined by plotting the open wound area changes as a function of the time.

5-Bromo-2'-deoxyuridine (BrdU) incorporation

C2C12 myoblasts were plated on a glass coverslip until reach 70-80 % confluence in DMEM and then were irradiated and incubated at 37ºC with 5% CO_2 for 5 hours; subsequently, the medium was changed to a DMEM containing 10µM BrdU (Sigma-Aldrich, USA) for 60 minutes. Cells were then fixed in 4% paraformaldehyde, permeabilized with 0.1% Triton X-100 in PBS and blocked for 1 hour in 10% goat serum, 1% Triton X-100 in PBS, denatured with 2 N HCl in PBS containing 0.5% Triton X-100 at 37ºC, for 30 min, and neutralized with 0.1 M borate buffer pH 8,5 for 10 minutes. Subsequently, the cells were incubated with mouse anti-BrdU antibody (diluted 1:1000; Sigma-Aldrich, USA), for 1 hour, and next, the cells were incubated overnight in incubation solution (5% goat serum, 0,3% Triton X-100) at 4ºC. Finally, goat anti–mouse IgG texas red-conjugated (1:5000; Santa Cruz Biotechnology USA) were added to the cells for 1 hour at room temperature, and coverslips were mounted using Vectashield (Vector Labs, USA). Cells were counted in a fluorescent inverted microscope (BX61 Olympus, Japan) to calculate the ratio of $BrdU^+$ cells to the total cell number.

Total RNA Extraction

Total RNA extraction was performed using TRIZOL kit (Thermo Fisher, USA) according to the manufacturer's instructions. The RNA was quantitated by spectrophotometry using NanoVue (GE Healthcare Life Sciences, USA) and the quality of RNA was obtained by the RNA integrity number (RIN) from the analysis of ribosomal RNAs based on microfluidics, using the 2100 Bioanalyzer system (Agilent, USA).

RNA sequencing

Total RNA (5 µg) was used to construct RNA-Seq libraries for CT (n=3) and LLL (n=3) groups that were sequenced in a same flow cell, as paired-end, 2 x 100 bp, on an Illumina HiScanSQ instrument (Illumina, USA), following manufacturer's instructions, which generated an average of 25 million paired-end reads per sample. The raw sequence files (.fastq files) underwent quality control analysis using FastQC and average Phred quality scores of ≥ 20 per position were used for alignment. The raw paired-end reads of the cDNA fragments were aligned to the mouse transcriptome (RefSeq, mm10) using the TopHat (version 1.3.2) spliced junction discovery tool [15]. The Python package HTSeq was used to count mapped reads to each transcript and the differential expression across CT and LLL groups were identified using DEseq (version 1.22.1) and reported as Fold Change along with associated p-values. Cut-offs for significant changes were a fold-change > 1.2 and a p-value ≤ 0.05. The analyses were performed with software package R (http:// www.r-project.org).

Pathway and Gene Ontology Enrichment Analysis

To further understand the biological relevance of differential expressed genes, we performed functional enrichment analysis in the context of the Gene Ontology (GO) categories, Kyoto Encyclopedia of Genes and Genomes (KEGG), Reactome, and WikiPathways databases. Pathway analysis was performed using Cytoscape (v.3.4.0) [16]

with ClueGO (version 2.2.5) packages [17]. A p-value cut-off of 0.05 by group and fold enrichment greater 10% were used to identify the enriched categories. A kappa score was calculated to reflect the relationships between the terms based on the similarity of their associated genes, PSIQUIC web services with the threshold set at 0.3 was used to provide a comprehensive view on the relevant pathways using experimental and *in silico* data from gene networks, protein–protein interactions, and functional interactions [18, 19].

Identification of Transcriptionally Similar Muscle Gene Sets

Transcriptionally similar Gene Sets to the differentially expressed genes in C2C12 myoblasts after LLLT were identified by the comparison with 154 Gene Sets derived from published *in vitro* muscle microarray studies, available at SysMyo Muscle Gene Sets (http://www.sys-myo.com/). The analysis of the SysMyo Muscle Gene Sets was carried out by using Enrichr, a comprehensive gene set enrichment analysis web tools (http://amp.pharm.mssm.edu/Enrichr/) [20, 21].

Statistical Analysis

All data are presented as mean ± SD. Differences between treated and nontreated cells were analyzed using multiple-t test with Sidak-Bonferroni correction. $p < 0.05$ was considered statistically significant. The calculations and artwork were made using GraphPad software (version 6.01). Venn diagrams were created and analyzed with Venny web Server 2.1 (http://bioinfogp.cnb.csic.es/tools/venny/index.html).

Results

Low-Level Laser-Irradiation (LLLT) does not affect cell viability but reduces migration and proliferation of C2C12 myoblasts

We found no significant effects on C2C12 myoblasts viability by MTT assay at 0h, 6h, 12h, 24h, and 48h after LLLT (Fig 1a). C2C12 myoblasts migration and

proliferation were indirectly evaluated by wound healing assay at 0 h, 6 h, 12h, 24h, and 48h after LLLT treatment (Fig 1b). C2C12 myoblasts exposed to LLLT showed significantly decreased wound closure rate at 6 h, 12 h, and 24 h, when compared to the control group ($p < 0.05$) (Fig 1c). Considering these results, we selected the time-point 6 h after LLLT for the further analyses. Next, C2C12 myoblasts proliferation was measured by BrdU incorporation (Fig 1d), which showed a decreased C2C12 myoblasts proliferation ratio at 6 h after LLLT ($p<0.05$) (Fig 1e).

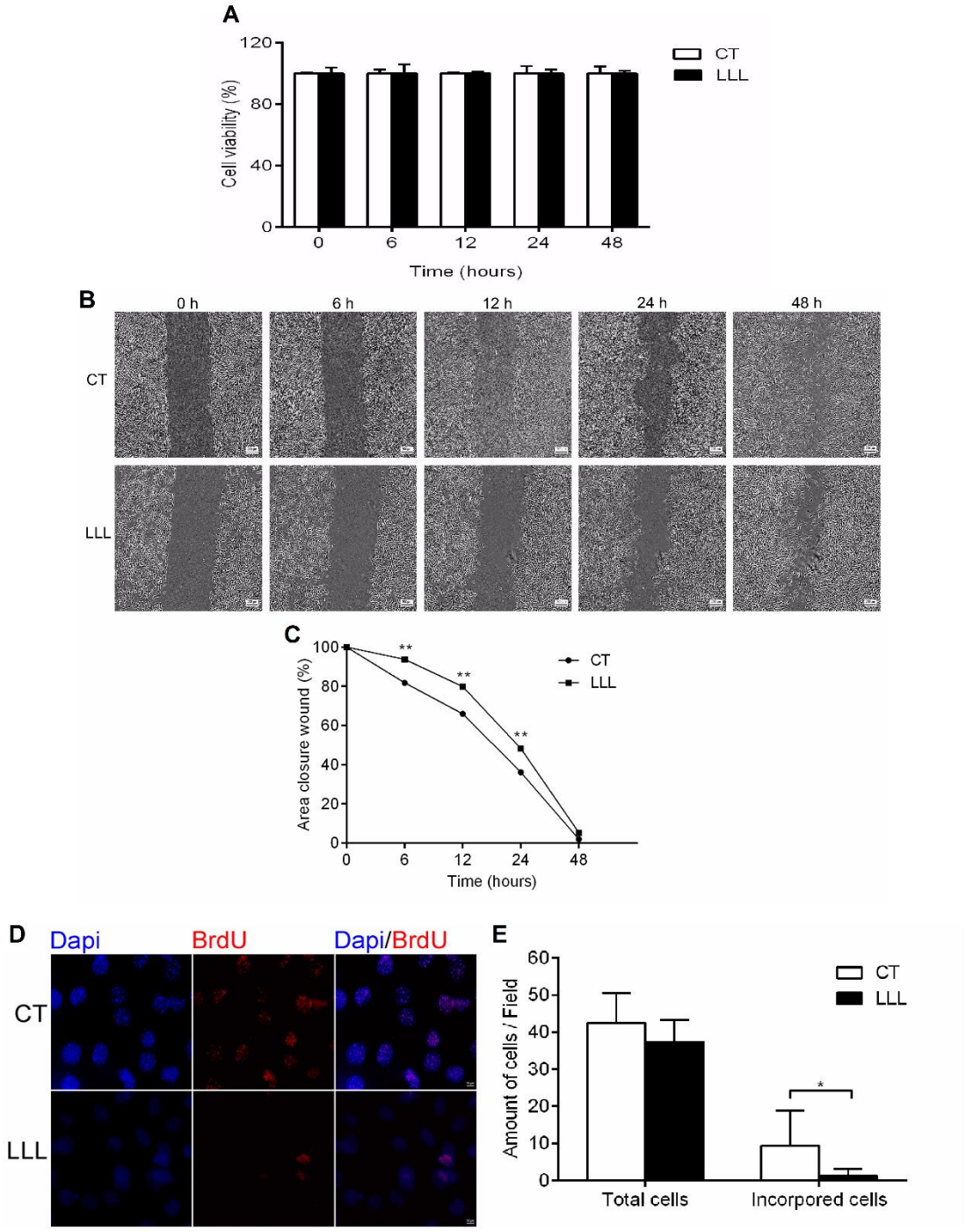

Fig 1 Low-Level Laser-Irradiation (LLLT) does not affect cell viability but reduces migration and proliferation of C2C12 myoblasts. A) Cellular viability rate analyzed by MTT assay after the LLLT of C2C12 myoblasts. Cellular viability rate was quantify considering the absorbance variation per hour between 6 h, 12 h, 24 h and 48 h related to the initial absorbance (time 0 h). B) Cellular migration and proliferation were indirectly measured by a wound-healing assay after LLLT of C2C12 myoblasts at 0 h, 6 h, 12 h, 24 h, and 48 h post-wound. C) The wound closure was quantified by measuring the remaining unmigrated area and is expressed as relative percentage (%). D) Cellular proliferation was analyzed by BrdU incorporation (red) detected 6 h after LLLT on the C2C12 myoblasts. Nuclei are counter-stained with

DAPI (blue). E) Number of BrdU+ cells per group after LLLT. Data represent mean of three independent experiments, and bars represent the standard deviation. Statistical significance was analyzed by the Student's t-tests. *$p < 0.05$, **$p < 0.002$

LLLT promotes transcriptional changes in C2C12 myoblasts

To understand the transcriptome changes associated with LLLT on C2C12 myoblasts, we performed a global mRNAs expression profiling that detected a total of 39,179 transcripts. Differential expressed genes between LLL and CT groups were selected and ranked by a combination of fold change ≥ 1.2 and adjusted p- value < 0.05 cutoff (Online Resource 1). LLLT affected the expression of 514 genes, out of which 263 and 251 were up- and down-regulated, respectively (Online Resource 1). Remarkably, the unsupervised hierarchical clustering analysis of the mRNAs expression data demonstrated biological triplicate clustering and a clear segregation between CT and LLL groups (Fig 2). All samples used in the RNA sequencing experiment presented a RIN ≥ 9.5.

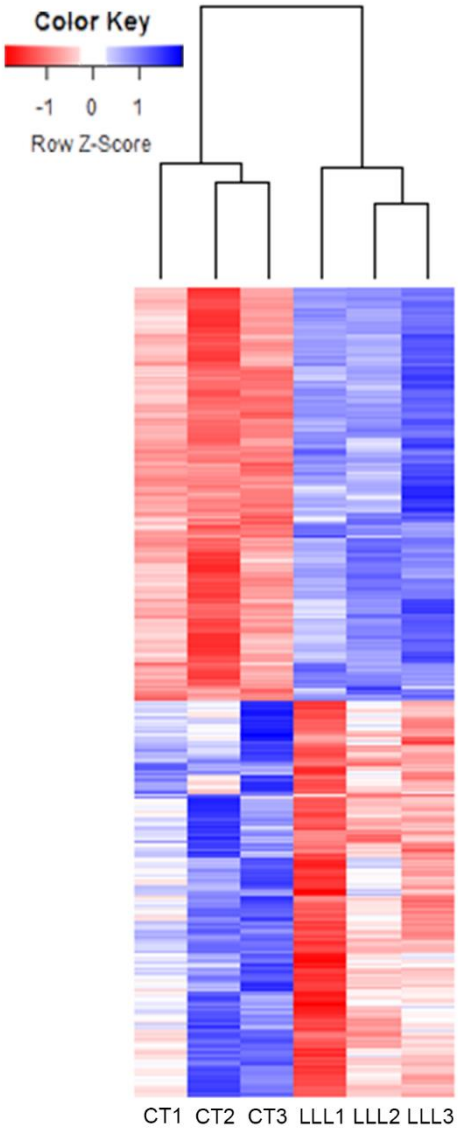

Fig 2 Low-Level Laser-Irradiation (LLLT) promotes transcriptional changes in C2C12 myoblasts. Heatmap of mRNA expression levels for the differentially expressed genes (DEG) between LLL and CT groups (1, 2, and 3 represent independent biological replicates for each group). Unsupervised hierarchical clustering analysis was performed using DEG with p-value < 0.05 and fold change > 1.2 and are shown as a color scale

LLLT induces changes in the expression of genes associated with different functional categories

To determine the biological and functional implications of the expression changes induced by LLLT treatment in C2C12 myoblasts, we performed a functional enrichment

analysis on the set of DEG (Online Resource 2). This enrichment functional analysis in C2C12 myoblasts exposed to LLLT revealed categories related to cell cycle, cell migration, response to stress, muscle cell proliferation, ribosome biogenesis, anatomical structure, DNA metabolic process, cell death, and blood vessel development (Fig 3).

To further understand the individual pathways, we also investigated the over- and under-expressed genes in each pathway. Interestingly, this analysis revealed that cell cycle pathway presented the higher enrichment (60%), and all the genes classified in this category were down-regulated (Fig 3).

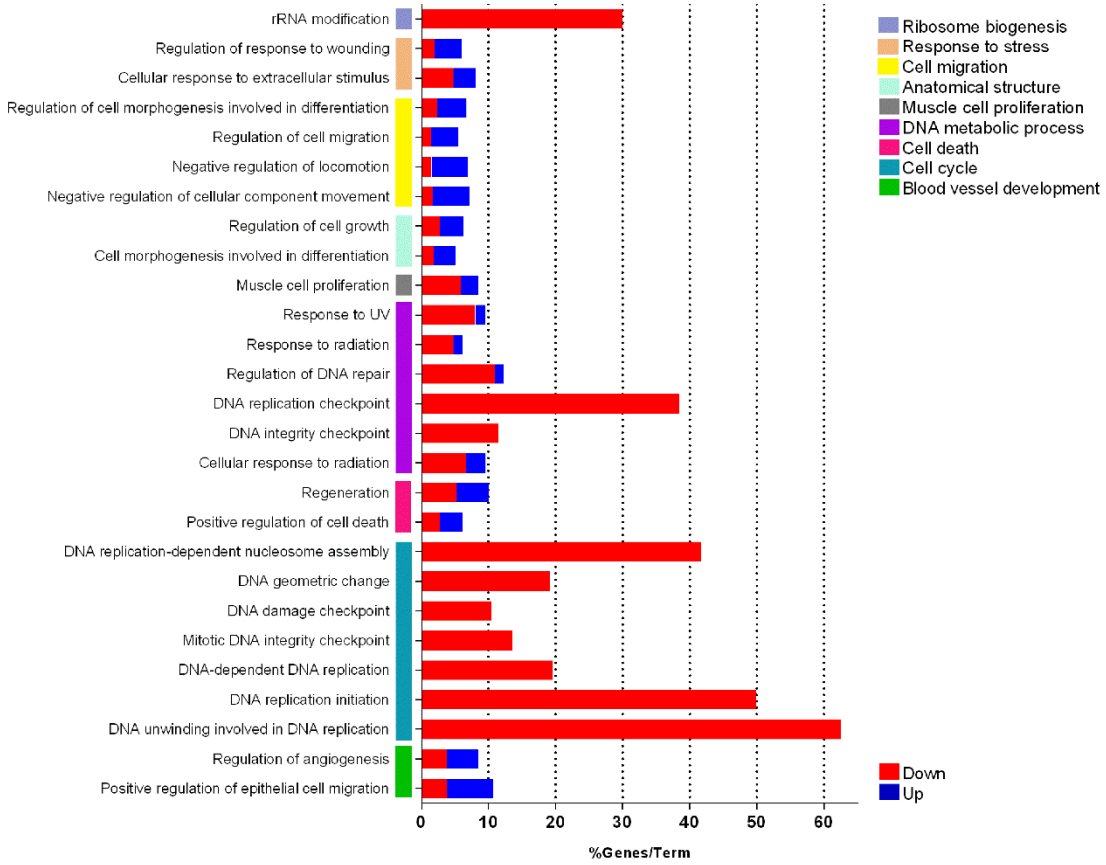

Fig 3 Low-Level Laser-Irradiation (LLLT) induces changes in the expression of genes associated with different functional categories. Pathway and Gene Ontology Enrichment Analysis of the differentially expressed genes (DEG) in C2C12 myoblasts after LLLT to identify top pathways and ontologies. Each vertical colored bars (y-axis) represent a major module; horizontal bars represent the percentage of genes presented in the data set compared to the total number of genes in each pathway/ontology. Fraction of the DEG in each pathway (red/down, blue/up; respectively) are shown in x-axis

LLLT induces distinct cell type-specific transcriptional changes

Next, we evaluated whether the gene expression changes induced by LLLT treatment in C2C12 myoblasts were distinct from different cell types that were also irradiate with LLLT. For this purpose, we compared our RNA-Seq data with previous microarrays studies that have evaluated the effect of: 1) LLLT on mesenchymal stem cell (MSCs) [13], and 2) red light irradiation on human fibroblasts (HS27) [14]. The intersection of the three studies tested showed no overlapping transcripts (Fig 4a); however, LLLT-treated myoblast had six DEG (Ada, Ccnd1, Cfh, Creld1, Gfer, and Wdr12) in common with MSCs [13], and three (Ahcy, Ppih, and Serpine1) with the HS27 [14] (Fig 4a). We also performed functional enrichment analysis on the DEG in HS27 and MSCs cells to determine the functional categories and pathways associated with LLLT treatment in these cells and, finally, we compared these results with our data. This analysis showed no overlapping functional categories and pathways, indicating that that LLLT induces distinct functional categories that are cell type-specific (Online Resource 3). Moreover, comparing our RNA-Seq data with the transcriptome data generated by microarrays technique in HS27 and MSCs [14, 13], our data presented a higher number of DEG in C2C12 (Fig 4a) and, consequently, we were able to identify a higher number of functional categories after LLLT (Fig 4b).

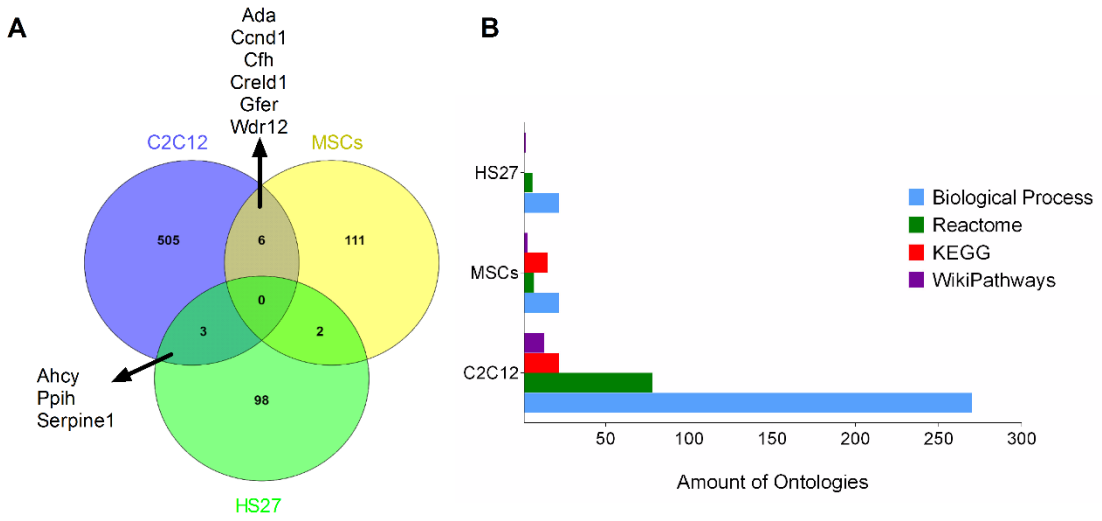

Fig 4 Low-Level Laser-Irradiation (LLLT) induces cell type-specific transcriptional changes of distinct functional categories. Comparison of our RNA-Seq data (C2C12 myoblasts after LLLT) with previous microarrays studies that have evaluated the effect of: 1) LLLT on mesenchymal stem cell (MSCs) [13], and 2) red light irradiation on human fibroblasts (HS27) [14]. A) Veen diagram showing the overlap of genes change in C2C12 myoblasts, HS27, and MSC. B) Functional enrichment analysis on the differentially expressed genes in HS27 and MSCs cells was used to determine the functional categories and pathways associated with LLLT treatment in these cells, which were compared with our data (C2C12 cells). Each horizontal bar represents the quantity of enriched ontology terms presented in the data set

LLLT induces a transcriptional myotube-like profile in C2C12 myoblasts

Considering the number of previous studies that have indicated the potential effects of LLLT on myogenesis, we compared our RNA-Seq data with literature data and asked whether a sub-set of genes in LLLT-treated myoblasts overlaps with data from two myogenesis studies [22, 23] with datasets stored at Gene Expression Omnibus (GEO; https://www.ncbi.nlm.nih.gov/gds). These studies used global microarrays analysis to evaluate the transcriptome changes during myogenesis (myoblasts and myotubes), and the data are accessible at NCBI GEO database [22, 23] by the following accession numbers: GSE3243 (not published) and GEO990 [24]. Initially, using the dataset from

these two myogenesis studies, we selected the set of DEG between myoblasts and myotubes to intersect with the genes that were changed in myoblasts after LLLT. This intersection showed a total of 42 transcripts in our data that overlaps with DEG in myotubes from GSE3243 and GEO990 (Fig 5a). Moreover, a total of 151 transcripts in our LLLT-treated myoblasts data overlaps with the DEG in myotubes from the GSE990 [24] dataset, and with 89 transcripts with the DEG in myotubes from the GSE3243 dataset (Fig 5a). We also compared these DEG that specifically overlap with the corresponding protein products from a study that evaluated the effect of LLLT on global protein expression in C2C12 myoblasts [10]. However, the proteomic data resulted in a lower number of overlapping to predict a transcriptional *myotube-like* profile. The intersection of all the four conditions tested revealed that only the protein Proliferation-associated protein 2G4 (Pa2g4), present in the proteomic study, overlaps with its corresponding transcript in the conditions that were tested (Fig 5a).

Next, we performed a hierarchical cluster analysis with the 42 transcripts differentially expressed that overlap between GSE3243, GSE990 [24] and our data by using Euclidean distance similarity. This clustering analysis showed that the LLLT-treated myoblasts have a myotube-like profile, clustering away from the myoblast profile (Fig 5b). Importantly, the myotube-like transcriptional profile of the LLLT myoblasts was globally confirmed by a bi-dimensional clustering of the 1156 transcripts detected in our RNA-Seq data that specifically overlaps with the DEG from the GSE990 [24] dataset (Fig 5c). To further confirm the global myotube-like transcriptional profile of the LLLT myoblasts, we also compared the differentially expressed genes in C2C12 myoblasts after LLLT with 154 Gene Sets derived from published in vitro muscle microarray studies. This analysis revealed that, out of the 25 top-ranked most transcriptionally similar Gene Sets (overlapping genes) to the 514 DEG in myoblasts after

LLLT, 23 are derived from differentiated myotubes and one is from a cardiotoxin injury model for the study of muscle regeneration in mice [25] (Online Resource 4).

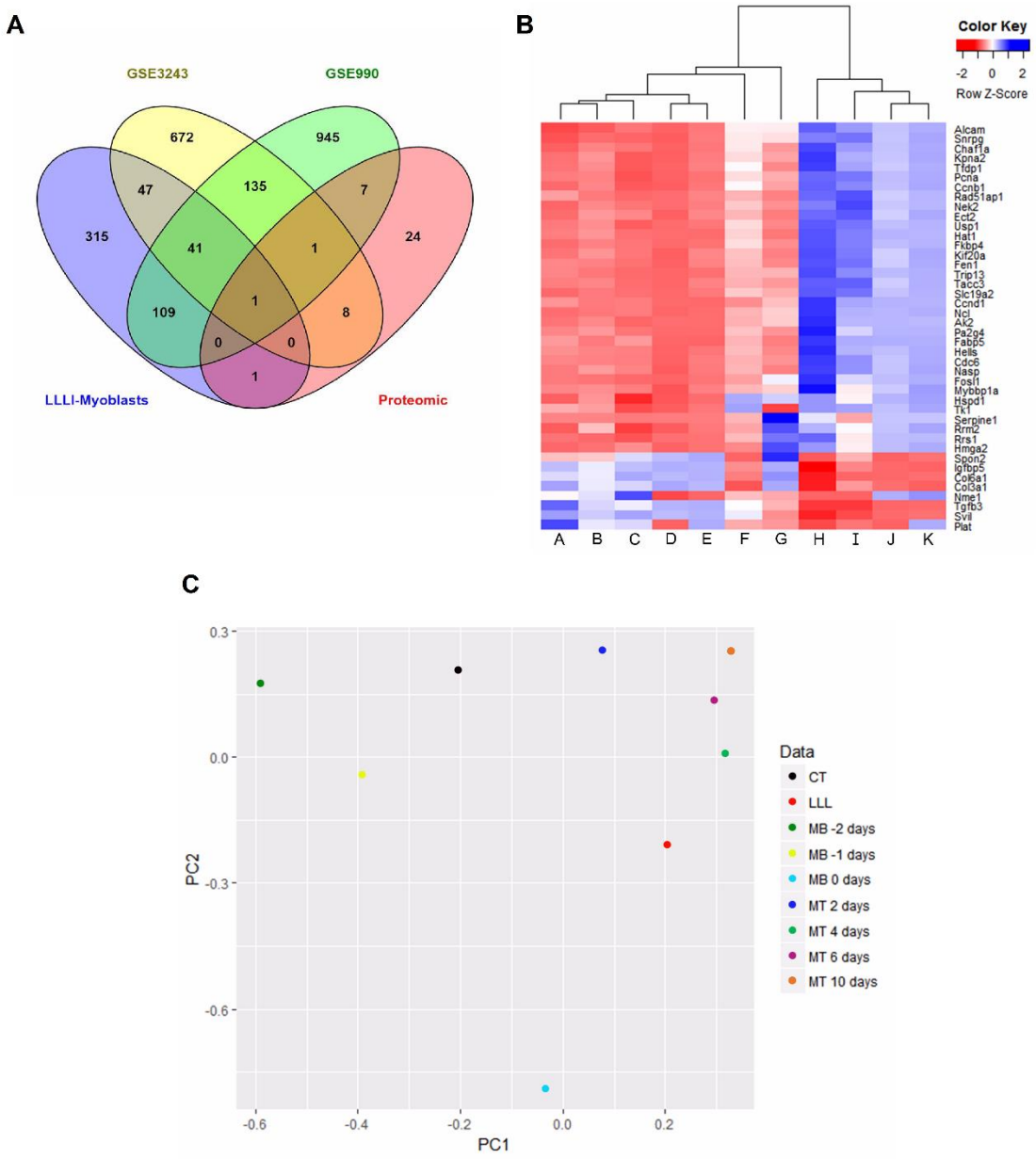

Fig 5 Low-Level Laser-Irradiation (LLLT) LLLT induces a transcriptional myotube-like profile in C2C12 myoblasts. A) Venn Diagram showing the differentially expressed genes (DEG) of our RNA-Seq data from LLLT-treated myoblasts that overlaps with global microarrays data from two previously published studies that have evaluated the transcriptome changes during myogenesis (DEG between myoblasts and myotubes). These data are accessible at NCBI GEO database by the following accession numbers: GSE3243 (not published) and GEO990 [24]. The DEG from the three transcriptomics studies are also compared with the corresponding protein products from a study that evaluated the effect of LLLT on

global protein expression in C2C12 myoblasts [10]. B) Clustering analysis of the 42 DEG of our RNA-Seq data from LLLT-treated myoblasts that are shared with GSE3243 and GEO990 [22]. GSE990 myotubes: A = 10 days, B = 6 days, C = 4 days, and F = 2 days; GSE990 myoblasts*:* G = 0-day, H = -2 days, I = -1 day; GSE3243 myotube: D = 4 days; and GSE3243 myoblast: K = -2 days; LLLT myoblast: E = LLL group; and myoblasts: J = control group. C) Principal Component Analysis (PCA) for clustering the global gene expression data from LLLT myoblasts with the transcriptomic data from the *in vitro* myogenesis study (myoblasts and myotubes) conducted by Tomczak et al. [22] (GSE990). CT: control group; LLL: Low-level Laser group; MB: myoblast; and MT: myotube

Discussion

Several studies have indicated that LLLT affects skeletal muscle cell proliferation and differentiation *in vivo* and *in vitro*. Although the therapeutic value of LLLT has become widely accepted, the global regulatory molecular mechanisms by which it exerts these effects on skeletal muscle cells remain largely unknown. In a comprehensive examination of global mRNA expression levels, we identified a large set of mRNAs that respond to changes following C2C12 myoblast LLLT and appear to play an important role in myoblasts proliferation and differentiation into myotubes. Furthermore, we demonstrated that the LLLT effects on C2C12 myoblast differentially regulate mRNAs that reveal a myotube-like transcriptional profile, generating further insights on the specific molecular changes underlying the effects of LLLT on skeletal muscle cells.

Initially, based on migration, proliferation, and cell viability parameters, we selected an appropriate time point, at 6 h post a single exposure of C2C12 cells to the laser radiation, to proceed to the transcriptomic analysis. These analyses showed that, after 6 h of LLLT, C2C12 myoblasts presented reduced migration and proliferation without affecting cell viability. These results are in accordance with a previous study performed in C2C12 cells, which also showed that laser treatment induced a decrease in the cell proliferation rate without affecting cell viability, while leading to the expression

of the early differentiation marker MyoD [10]. LLLT also has the potential to increase the survival of primary myogenic donor cells, promote their fusion with the host myofibers, and enhance their ability to recover [11]. Interestingly, LLLT in association with *Bothrops jararacussu* venom has been shown to promote C2C12 differentiation by up regulating myogenic factors [26].

On the other hand, Ben-Dov et al., [12] demonstrated that LLLT on primary rat satellite cell cultures induced cell cycle regulatory protein expression, increased satellite cell proliferation, and inhibited cell differentiation. LLLT also stimulated cell cycle entry and the accumulation of satellite cells around isolated single fibers [9]. Variable effects were achieved in a same study that used different LED light wavelengths, with blue (470 nm) or red (630 nm) LED light illumination decreasing or increasing C2C12 proliferation rates, respectively [8]. While there are no simple explanations to the apparent inconsistencies among these studies that have evaluated the effect of LLLT on proliferation and differentiation of skeletal muscle myogenic cells, it is clear that LLLT affect these processes and promotes or accelerates skeletal muscle regeneration [1–5].

To the best of our knowledge this is the first global transcriptome catalogue of skeletal muscle cells after LLLT. Our RNA-Seq analysis identified 514 DEG (p-value < 0.05 and fold change ≥ 1.2), of which 263 and 251 were up- or down-regulated, respectively. Importantly, the unsupervised hierarchical clustering analysis of the mRNAs expression data in C2C12 LLLT-treated myoblasts showed a biological replicate clustering and a segregation between CT and LLL groups. These data clearly indicate that the LLLT effects on myoblasts transcriptional regulation are not random, and that RNA-Seq is powerful tool to evaluated transcriptional changes promoted by LLLT in cultured cells.

Previously, Wu et al., [13] used a microarray analysis to identify transcriptome changes induced by LLLT in cultured mesenchymal stem cells, and identified 119 DEG (fold change ≥ 1.2). Zhang et al., [14] also used microarrays analysis to study the effect of LLLT on cultured human fibroblasts, and found 111 DEG by more than twofold. Noteworthy, the transcriptome changes between non-irradiated and irradiated in these previous studies show very few DEG in common. Our data from LLLT-treated myoblast had six DEG in common with one study [13], and three with the other [14]. Moreover, our RNA-Seq data identified a higher number of DEG when compared to these two previous microarray studies. Accordingly, our functional analysis also presented a higher number of categories that includes cell cycle, cell migration, response to stress, muscle cell proliferation, ribosome biogenesis, anatomical structure, DNA metabolic process, cell death, and blood vessel development. The comparison of these functional categories in which the DEG are classified may help to identify shared core molecular mechanisms underlying the effects of LLLT in different cell types. However, we did not identify functional categories affected by LLLT that overlap with C2C12 myoblasts when compared with mesenchymal stem cells [13] and fibroblasts [14]. These disparities in the number of the DEG and functional pathways among the studies may occur due to the different cells types or statistical cut-offs, or several laser-related factors such as wavelength of radiation, energy density, and time of irradiation.

To further validate our RNA-Seq results and better understand the effects of LLLT on myoblasts, we asked whether a sub-set of DEG in LLLT-myoblasts overlaps with Geo Expression Omnibus datasets (GEO990 [24] and GSE3243) experiments that evaluated transcriptome changes during *in vitro* myogenesis (myoblasts *vs* myotubes). Our LLLT-myoblasts data had 151 transcripts in common with one dataset (GEO990), 89 transcripts with the other (GSE3243), and 42 transcripts that overlap with both datasets. Although

included in different functional categories, these 42 transcripts are useful to indicate alterations triggered by LLLT in myoblast. It is interesting to note that *Hmga2* and *Ccnd1* were among these deregulated genes after LLLT; both were down-regulated and associated with ontology groups such as cellular response to irradiation, DNA damage checkpoint, regeneration, and cell morphogenesis involved in differentiation. Importantly, several studies have demonstrated a key role for Ccnd1 in promoting myoblast cell cycle withdrawal and terminal differentiation into myotubes [27–32]. Hmga2 has been also directly the regulation of connected to myoblast proliferation and differentiation; Hmga2, increases is coincident with satellite cell activation, and later its expression significantly declines correlating with fusion of myoblasts into myotubes [33]. Also in accordance with these literature data, our ontology analysis revealed that cell cycle pathway presented the higher enrichment (60%), and all the genes classified in this category were down-regulated. Together, these findings indicate that LLLT in C2C12 myoblast LLLT appear to play an important role in reducing myoblasts proliferation and inducing differentiation into myotubes.

Next, we performed a hierarchical cluster analysis with those 42 transcripts differentially expressed that overlap between GSE3243, GSE990 [24] and our data by using Euclidean distance similarity. Noteworthy, this clustering analysis confirmed that the LLLT-myoblasts have a transcriptional *myotube-like profile*, clustering away from the myoblast profile. Monici et al., 2013 [10] previously showed that laser treatment decreased cell proliferation associated with changes of cell morphology and cytoskeletal architecture leading to the formation of tube-like structures. These authors also evaluated the effect of LLLT on global protein expression in C2C12 myoblasts and identified 42 differently expressed proteins in LLLT-myoblasts. However, when we analyzed the DEG (GSE3243, GSE990[24], and our data) that overlap with the corresponding protein

products from Monici et al., 2013 [10], the proteomic data resulted in a lower number of overlapping to predict a transcriptional *myotube-like profile*. The intersection of all the four conditions tested also revealed that only the protein Proliferation-associated protein 2G4 (Pa2g4) that overlaps in all conditions. Pa2g4, also known as Ebp1, is expressed during myogenesis in satellite cells; however, its knockdown inhibits both proliferation and differentiation of C2C12 myoblasts and satellite cells, which also present a reduced capacity of myotube formation [34].

We also compared the differentially expressed genes in C2C12 myoblasts after LLLT with 154 Gene Sets derived from published in vitro muscle microarray studies available at Gene Expression Omnibus to confirm a global *myotube-like transcriptional profile* of the LLLT myoblasts. This analyses further demonstrated that all 514 DEG in myoblasts after LLLT highly overlaps with genes sets of differentiated myotubes from the study of Tomczak et al., [35], but surprisingly, also overlaps specifically with additional 22 gene sets from differentiated myotubes, and with one cardiotoxin injury model used to study muscle regeneration in mice [25].

Although our study design has proven useful, there were also limitations *in vivo* study that must be considered. Specifically, there is a diversity of studies that analyze the effects of LLLT on C2C12 myoblasts and other cell types. These studies apply several different laser-related parameters such as wavelength of radiation, energy density, and time of irradiation, making it difficult to select specific parameters to become the results comparable. Thus, further studies are needed to better establish how these laser-related parameters globally affect cellular and molecular mechanism in different cell types.

In summary, we demonstrate for the first time that LLLT regulates a set of mRNAs that control myoblasts proliferation and differentiation into myotubes. Importantly, this set of mRNAs revealed a myotube-like transcriptional profile in LLLT-myoblasts and

provide new insights to the understanding of the molecular mechanisms underlying the effects of LLLT on skeletal muscle cells.

Funding: This study was supported by grants from the São Paulo Research Foundation Brazil (FAPESP n° 2012/13961-6) and National Council for Scientific and Technological Development (CNPq n° 476399/2013-0).

Conflict of Interest: The authors declare that they have no conflict of interest.

Ethical approval: This article does not contain any studies with animals performed by any of the authors.

References

1. Vatansever F, Rodrigues NC, Assis LL, et al (2012) Low intensity laser therapy accelerates muscle regeneration in aged rats. Photonics Lasers Med 1:287–297 . doi: 10.1515/plm-2012-0035
2. Assis L, Moretti AIS, Abrahão TB, et al (2013) Low-level laser therapy (808 nm) contributes to muscle regeneration and prevents fibrosis in rat tibialis anterior muscle after cryolesion. Lasers Med Sci 28:947–955 . doi: 10.1007/s10103-012-1183-3
3. de Freitas CEA, Bertaglia RS, Vechetti Júnior IJ, et al (2015) High Final Energy of Low-Level Gallium Arsenide Laser Therapy Enhances Skeletal Muscle Recovery without a Positive Effect on Collagen Remodeling. Photochem Photobiol 91:n/a-n/a . doi: 10.1111/php.12446
4. Amaral AC, Parizotto NA, Salvini TF (2001) Dose-dependency of low-energy HeNe laser effect in regeneration of skeletal muscle in mice. Lasers Med Sci 16:44–51
5. Weiss N, Oron U (1992) Enhancement of muscle regeneration in the rat gastrocnemius muscle by low energy laser irradiation. Anat Embryol (Berl) 186:497–503
6. Buckingham M (2006) Myogenic progenitor cells and skeletal myogenesis in vertebrates. Curr Opin Genet Dev 16:525–32 . doi: 10.1016/j.gde.2006.08.008
7. Wang YX, Rudnicki MA (2011) Satellite cells, the engines of muscle repair. Nat Rev Mol Cell Biol 13:127–133 . doi: 10.1038/nrm3265
8. Teuschl A, Balmayor ER, Redl H, et al (2015) Phototherapy With LED Light Modulates Healing Processes in an In Vitro Scratch-Wound Model Using 3 Different Cell Types. Dermatologic Surg 41:261–268 . doi: 10.1097/DSS.0000000000000266
9. Shefer G, Partridge TA, Heslop L, et al (2002) Low-energy laser irradiation promotes the survival and cell cycle entry of skeletal muscle satellite cells. J Cell Sci 115:1461–9
10. Monici M, Cialdai F, Ranaldi F, et al (2013) Effect of IR laser on myoblasts: a proteomic study. Mol Biosyst 9:1147–61 . doi: 10.1039/c2mb25398d
11. Shefer G, Ben-Dov N, Halevy O, Oron U (2008) Primary myogenic cells see the light: improved survival of transplanted myogenic cells following low energy laser irradiation. Lasers Surg Med 40:38–45 . doi: 10.1002/lsm.20588
12. Ben-Dov N, Shefer G, Irinitchev A, et al (1999) Low-energy laser irradiation affects satellite cell proliferation and differentiation in vitro. Biochim Biophys Acta - Mol Cell Res 1448:372–380 . doi: 10.1016/S0167-4889(98)00147-5
13. Wu Y, Wang J, Gong D, et al (2012) Effects of low-level laser irradiation on mesenchymal stem cell proliferation: a microarray analysis. Lasers Med Sci 27:509–519 . doi: 10.1007/s10103-011-0995-x
14. Zhang Y, Song S, Fong C-C, et al (2003) cDNA microarray analysis of gene expression profiles in human fibroblast cells irradiated with red light. J Invest Dermatol 120:849–857 . doi: 10.1046/j.1523-1747.2003.12133.x
15. Trapnell C, Roberts A, Goff L, et al (2012) Differential gene and transcript expression analysis of RNA-seq experiments with TopHat and Cufflinks. Nat Protoc 7:562–78 . doi: 10.1038/nprot.2012.016
16. Shannon P, Markiel A, Ozier O, et al (2003) Cytoscape: a software environment for integrated models of biomolecular interaction networks. Genome Res 13:2498–504 . doi: 10.1101/gr.1239303

17. Bindea G, Mlecnik B, Hackl H, et al (2009) ClueGO: a Cytoscape plug-in to decipher functionally grouped gene ontology and pathway annotation networks. Bioinformatics 25:1091–3 . doi: 10.1093/bioinformatics/btp101
18. Aranda B, Blankenburg H, Kerrien S, et al (2011) PSICQUIC and PSISCORE: accessing and scoring molecular interactions. Nat Methods 8:528–9 . doi: 10.1038/nmeth.1637
19. Bindea G, Galon J, Mlecnik B (2013) CluePedia Cytoscape plugin: pathway insights using integrated experimental and in silico data. Bioinformatics 29:661–663 . doi: 10.1093/bioinformatics/btt019
20. Chen EY, Tan CM, Kou Y, et al (2013) Enrichr: interactive and collaborative HTML5 gene list enrichment analysis tool. BMC Bioinformatics 14:128 . doi: 10.1186/1471-2105-14-128
21. Kuleshov M V, Jones MR, Rouillard AD, et al (2016) Enrichr: a comprehensive gene set enrichment analysis web server 2016 update. Nucleic Acids Res 44:W90-7 . doi: 10.1093/nar/gkw377
22. Barrett T, Wilhite SE, Ledoux P, et al (2013) NCBI GEO: archive for functional genomics data sets--update. Nucleic Acids Res 41:D991-5 . doi: 10.1093/nar/gks1193
23. Edgar R, Domrachev M, Lash AE (2002) Gene Expression Omnibus: NCBI gene expression and hybridization array data repository. Nucleic Acids Res 30:207–10
24. Tomczak KK, Marinescu VD, Ramoni MF, et al (2003) Expression profiling and identification of novel genes involved in myogenic differentiation. FASEB J 17: . doi: 10.1096/fj.03-0568fje
25. Yan Z, Choi S, Liu X, et al (2003) Highly coordinated gene regulation in mouse skeletal muscle regeneration. J Biol Chem 278:8826–36 . doi: 10.1074/jbc.M209879200
26. Silva LMG, Da Silva CAA, Da Silva A, et al (2016) Photobiomodulation protects and promotes differentiation of C2C12 myoblast cells exposed to Snake venom. PLoS One 11:1–16 . doi: 10.1371/journal.pone.0152890
27. Albini S, Coutinho Toto P, Dall'Agnese A, et al (2015) Brahma is required for cell cycle arrest and late muscle gene expression during skeletal myogenesis. EMBO Rep 16:1037–50 . doi: 10.15252/embr.201540159
28. Guttridge DC, Albanese C, Reuther JY, et al (1999) NF-kappaB controls cell growth and differentiation through transcriptional regulation of cyclin D1. Mol Cell Biol 19:5785–99
29. Panda AC, Abdelmohsen K, Martindale JL, et al (2016) Novel RNA-binding activity of MYF5 enhances *Ccnd1/Cyclin D1* mRNA translation during myogenesis. Nucleic Acids Res gkw023 . doi: 10.1093/nar/gkw023
30. Skapek SX, Rhee J, Spicer DB, Lassar AB (1995) Inhibition of myogenic differentiation in proliferating myoblasts by cyclin D1-dependent kinase. Science 267:1022–4
31. Skapek SX, Rhee J, Kim PS, et al (1996) Cyclin-mediated inhibition of muscle gene expression via a mechanism that is independent of pRB hyperphosphorylation. Mol Cell Biol 16:7043–53
32. Zhang JM, Zhao X, Wei Q, Paterson BM (1999) Direct inhibition of G(1) cdk kinase activity by MyoD promotes myoblast cell cycle withdrawal and terminal differentiation. EMBO J 18:6983–93 . doi: 10.1093/emboj/18.24.6983
33. Li Z, Gilbert JA, Zhang Y, et al (2012) An HMGA2-IGF2BP2 Axis Regulates Myoblast Proliferation and Myogenesis. Dev Cell 23:1176–1188 . doi: 10.1016/j.devcel.2012.10.019

34. Figeac N, Serralbo O, Marcelle C, Zammit PS (2014) ErbB3 binding protein-1 (Ebp1) controls proliferation and myogenic differentiation of muscle stem cells. Dev Biol 386:135–151 . doi: 10.1016/j.ydbio.2013.11.017
35. Tomczak KK, Marinescu VD, Ramoni MF, et al (2004) Expression profiling and identification of novel genes involved in myogenic differentiation. Faseb J 18:403–405 . doi: 10.1096/fj.03-0568fje\r03-0568fje [pii]

ANEXO I

Table Supplementary 1 *Genes differentially expressed after low-level laser irradiation.*

Symbol	Description	ID	fold change	p value
Serpinb2	serine (or cysteine) peptidase inhibitor, clade B, member 2 [Source:MGI Symbol;Acc:MGI:97609]	ENSMUSG00000062345	-3.999398954	0.025955846
Gjb3	gap junction protein, beta 3 [Source:MGI Symbol;Acc:MGI:95721]	ENSMUSG00000042367	-3.433498299	0.000582023
Lce1g	late cornified envelope 1G [Source:MGI Symbol;Acc:MGI:1913445]	ENSMUSG00000027919	-2.985445223	0.002520492
Prl2c2	prolactin family 2, subfamily c, member 2 [Source:MGI Symbol;Acc:MGI:97618]	ENSMUSG00000079092	-2.467975714	0.000102734
Lrp2	low density lipoprotein receptor-related protein 2 [Source:MGI Symbol;Acc:MGI:95794]	ENSMUSG00000027070	-2.173024881	0.013088201
Ctgf	connective tissue growth factor [Source:MGI Symbol;Acc:MGI:95537]	ENSMUSG00000019997	-2.131538871	9.70E-08
Ngf	nerve growth factor [Source:MGI Symbol;Acc:MGI:97321]	ENSMUSG00000027859	-2.01613754	4.15E-05
Shank2	SH3/ankyrin domain gene 2 [Source:MGI Symbol;Acc:MGI:2671987]	ENSMUSG00000037541	-1.878258899	0.048516462
Hmga1	high mobility group AT-hook 1 [Source:MGI Symbol;Acc:MGI:96160]	ENSMUSG00000046711	-1.728715071	9.70E-08
Etv4	ets variant 4 [Source:MGI Symbol;Acc:MGI:99423]	ENSMUSG00000017724	-1.720927905	0.000668155
Siglecg	sialic acid binding Ig-like lectin G [Source:MGI Symbol;Acc:MGI:2443630]	ENSMUSG00000030468	-1.712048284	0.043672378
Hmga1-rs1	high mobility group AT-hook I, related sequence 1 [Source:MGI Symbol;Acc:MGI:96161]	ENSMUSG00000078249	-1.701951271	5.45E-10
Pparg	peroxisome proliferator activated receptor gamma [Source:MGI Symbol;Acc:MGI:97747]	ENSMUSG00000000440	-1.701209887	0.013478123
Tagln	transgelin [Source:MGI Symbol;Acc:MGI:106012]	ENSMUSG00000032085	-1.686138608	0.014709073
Ccnd1	cyclin D1 [Source:MGI Symbol;Acc:MGI:88313]	ENSMUSG00000070348	-1.685829908	7.36E-09
Tigit	T cell immunoreceptor with Ig and ITIM domains [Source:MGI Symbol;Acc:MGI:3642260]	ENSMUSG00000071552	-1.641660077	0.019177473
Hmga2	high mobility group AT-hook 2 [Source:MGI Symbol;Acc:MGI:101761]	ENSMUSG00000056758	-1.637526088	0.000184456
Gm7008	predicted gene 7008 [Source:MGI Symbol;Acc:MGI:3647211]	ENSMUSG00000035983	-1.626702086	0.001610793
Fosl1	fos-like antigen 1 [Source:MGI Symbol;Acc:MGI:107179]	ENSMUSG00000024912	-1.626375009	0.000373325
Chek1	checkpoint kinase 1 [Source:MGI Symbol;Acc:MGI:1202065]	ENSMUSG00000032113	-1.620200607	5.95E-05
Hbegf	heparin-binding EGF-like growth factor [Source:MGI Symbol;Acc:MGI:96070]	ENSMUSG00000024486	-1.617112886	0.049908928
Lrr1	leucine rich repeat protein 1 [Source:MGI Symbol;Acc:MGI:1916956]	ENSMUSG00000034883	-1.614364715	0.011401951
Ptgs2	prostaglandin-endoperoxide synthase 2 [Source:MGI Symbol;Acc:MGI:97798]	ENSMUSG00000032487	-1.58632756	0.002301965
Cbln1	cerebellin 1 precursor protein [Source:MGI Symbol;Acc:MGI:88281]	ENSMUSG00000031654	-1.581993289	0.001192388
Nhp2	NHP2 ribonucleoprotein [Source:MGI Symbol;Acc:MGI:1098547]	ENSMUSG00000001056	-1.577578709	0.000373325

Dlk2	delta-like 2 homolog (Drosophila) [Source:MGI Symbol;Acc:MGI:2146838]	ENSMUSG00000047428	-1.575630778	0.011268901
Taf4b	TATA-box binding protein associated factor 4b [Source:MGI Symbol;Acc:MGI:2152345]	ENSMUSG00000054321	-1.570235328	0.026512322
Timm8a1	translocase of inner mitochondrial membrane 8A1 [Source:MGI Symbol;Acc:MGI:1353433]	ENSMUSG00000048007	-1.560031151	0.021994405
Dnaaf2	dynein, axonemal assembly factor 2 [Source:MGI Symbol;Acc:MGI:1923566]	ENSMUSG00000020973	-1.556508357	0.028087699
Nptx1	neuronal pentraxin 1 [Source:MGI Symbol;Acc:MGI:107811]	ENSMUSG00000025582	-1.552314713	0.009377647
Kcnf1	potassium voltage-gated channel, subfamily F, member 1 [Source:MGI Symbol;Acc:MGI:2687399]	ENSMUSG00000051726	-1.532330665	0.012900431
Id1	inhibitor of DNA binding 1 [Source:MGI Symbol;Acc:MGI:96396]	ENSMUSG00000042745	-1.528796209	0.03375774
Ada	adenosine deaminase [Source:MGI Symbol;Acc:MGI:87916]	ENSMUSG00000017697	-1.525101346	0.037304681
Nop58	NOP58 ribonucleoprotein [Source:MGI Symbol;Acc:MGI:1933184]	ENSMUSG00000026020	-1.523077305	0.045651778
Dusp9	dual specificity phosphatase 9 [Source:MGI Symbol;Acc:MGI:2387107]	ENSMUSG00000031383	-1.517030267	0.018218872
Hells	helicase, lymphoid specific [Source:MGI Symbol;Acc:MGI:106209]	ENSMUSG00000025001	-1.516137452	0.012069084
Orc1	origin recognition complex, subunit 1 [Source:MGI Symbol;Acc:MGI:1328337]	ENSMUSG00000028587	-1.513930629	0.00296797
Dnph1	2'-deoxynucleoside 5'-phosphate N-hydrolase 1 [Source:MGI Symbol;Acc:MGI:3039376]	ENSMUSG00000040658	-1.505397629	0.014660876
Nup43	nucleoporin 43 [Source:MGI Symbol;Acc:MGI:1917162]	ENSMUSG00000040034	-1.498274282	0.005774114
Dph2	DPH2 homolog [Source:MGI Symbol;Acc:MGI:1914978]	ENSMUSG00000028540	-1.496171315	0.002301965
Nop56	NOP56 ribonucleoprotein [Source:MGI Symbol;Acc:MGI:1914384]	ENSMUSG00000027405	-1.495263688	4.82E-06
Gpatch4	G patch domain containing 4 [Source:MGI Symbol;Acc:MGI:1913864]	ENSMUSG00000028069	-1.495263004	0.000469333
Odc1	ornithine decarboxylase, structural 1 [Source:MGI Symbol;Acc:MGI:97402]	ENSMUSG00000011179	-1.492550749	0.001740595
Siah1b	seven in absentia 1B [Source:MGI Symbol;Acc:MGI:108063]	ENSMUSG00000040749	-1.489944949	0.006053516
Grwd1	glutamate-rich WD repeat containing 1 [Source:MGI Symbol;Acc:MGI:2141989]	ENSMUSG00000053801	-1.489643166	0.0003707
Tnfrsf12a	tumor necrosis factor receptor superfamily, member 12a [Source:MGI Symbol;Acc:MGI:1351484]	ENSMUSG00000023905	-1.482490429	0.021185738
Dkc1	dyskeratosis congenita 1, dyskerin [Source:MGI Symbol;Acc:MGI:1861727]	ENSMUSG00000031403	-1.482270223	0.020871414
Mybl2	myeloblastosis oncogene-like 2 [Source:MGI Symbol;Acc:MGI:101785]	ENSMUSG00000017861	-1.481944173	0.037710659
Chac1	ChaC, cation transport regulator 1 [Source:MGI Symbol;Acc:MGI:1916315]	ENSMUSG00000027313	-1.481828449	0.006419991
Hat1	histone aminotransferase 1 [Source:MGI Symbol;Acc:MGI:96013]	ENSMUSG00000027018	-1.480814415	0.000140019
Ccne2	cyclin E2 [Source:MGI Symbol;Acc:MGI:1329034]	ENSMUSG00000028212	-1.472808791	0.04659026
Ifrd1	interferon-related developmental regulator 1 [Source:MGI Symbol;Acc:MGI:1316717]	ENSMUSG00000001627	-1.471007832	0.016447423
Exosc8	exosome component 8 [Source:MGI Symbol;Acc:MGI:1916889]	ENSMUSG00000027752	-1.465885966	0.000271108
Chaf1b	chromatin assembly factor 1, subunit B (p60) [Source:MGI Symbol;Acc:MGI:1314881]	ENSMUSG00000022945	-1.463536977	0.000280963

Cst6	cystatin E/M [Source:MGI Symbol;Acc:MGI:1920970]	ENSMUSG00000024846	-1.459410818	0.031310718
Itgb7	integrin beta 7 [Source:MGI Symbol;Acc:MGI:96616]	ENSMUSG00000001281	-1.458730092	0.045412436
Slc19a1	solute carrier family 19 (folate transporter), member 1 [Source:MGI Symbol;Acc:MGI:103182]	ENSMUSG00000001436	-1.454755426	0.003555438
Samd11	sterile alpha motif domain containing 11 [Source:MGI Symbol;Acc:MGI:2446220]	ENSMUSG00000096351	-1.453157542	0.014908693
Wdr43	WD repeat domain 43 [Source:MGI Symbol;Acc:MGI:1919765]	ENSMUSG00000041057	-1.45079399	9.42E-05
Tfrc	transferrin receptor [Source:MGI Symbol;Acc:MGI:98822]	ENSMUSG00000022797	-1.446149263	0.028335471
Mcm10	minichromosome maintenance 10 replication initiation factor [Source:MGI Symbol;Acc:MGI:1917274]	ENSMUSG00000026669	-1.441496936	0.000778955
Lin54	lin-54 homolog (C. elegans) [Source:MGI Symbol;Acc:MGI:2140902]	ENSMUSG00000035310	-1.438182366	0.000902594
Dut	deoxyuridine triphosphatase [Source:MGI Symbol;Acc:MGI:1346051]	ENSMUSG00000027203	-1.437050468	0.024365941
Ccne1	cyclin E1 [Source:MGI Symbol;Acc:MGI:88316]	ENSMUSG00000002068	-1.434297676	0.018207607
Psph	phosphoserine phosphatase [Source:MGI Symbol;Acc:MGI:97788]	ENSMUSG00000029446	-1.433604657	0.001223852
Dis3	DIS3 homolog, exosome endoribonuclease and 3'-5' exoribonuclease [Source:MGI Symbol;Acc:MGI:1919912]	ENSMUSG00000033166	-1.430353962	0.000241973
Nop16	NOP16 nucleolar protein [Source:MGI Symbol;Acc:MGI:107862]	ENSMUSG00000025869	-1.428264533	0.001966742
Exosc1	exosome component 1 [Source:MGI Symbol;Acc:MGI:1913833]	ENSMUSG00000034321	-1.428047541	0.01971285
Enoph1	enolase-phosphatase 1 [Source:MGI Symbol;Acc:MGI:1915120]	ENSMUSG00000029326	-1.427224528	0.004190238
Recql4	RecQ protein-like 4 [Source:MGI Symbol;Acc:MGI:1931028]	ENSMUSG00000033762	-1.424414367	0.011243001
Dusp4	dual specificity phosphatase 4 [Source:MGI Symbol;Acc:MGI:2442191]	ENSMUSG00000031530	-1.42244133	0.002436045
Gemin6	gem (nuclear organelle) associated protein 6 [Source:MGI Symbol;Acc:MGI:1914492]	ENSMUSG00000055760	-1.421310221	0.024188138
Timeless	timeless circadian clock 1 [Source:MGI Symbol;Acc:MGI:1321393]	ENSMUSG00000039994	-1.413695834	0.002117843
Dimt1	DIM1 dimethyladenosine transferase 1-like (S. cerevisiae) [Source:MGI Symbol;Acc:MGI:1913504]	ENSMUSG00000021692	-1.413274625	0.028164931
Depdc7	DEP domain containing 7 [Source:MGI Symbol;Acc:MGI:2139258]	ENSMUSG00000027173	-1.412372658	0.033888309
Zmynd19	zinc finger, MYND domain containing 19 [Source:MGI Symbol;Acc:MGI:1914437]	ENSMUSG00000026974	-1.411384643	0.002997779
Phlda1	pleckstrin homology like domain, family A, member 1 [Source:MGI Symbol;Acc:MGI:1096880]	ENSMUSG00000020205	-1.411202468	0.006081444
Mthfd2	methylenetetrahydrofolate dehydrogenase (NAD+ dependent), methenyltetrahydrofolate cyclohydrolase [Source:MGI Symbol;Acc:MGI:1338850]	ENSMUSG00000005667	-1.410002998	0.029326612
Sema7a	sema domain, immunoglobulin domain (Ig), and GPI membrane anchor, (semaphorin) 7A [Source:MGI Symbol;Acc:MGI:1306826]	ENSMUSG00000038264	-1.40597123	0.019841311
Anxa3	annexin A3 [Source:MGI Symbol;Acc:MGI:1201378]	ENSMUSG00000029484	-1.404842386	0.041716576
Cdca7	cell division cycle associated 7 [Source:MGI Symbol;Acc:MGI:1914203]	ENSMUSG00000055612	-1.403134018	0.004880262

Gfer	growth factor, erv1 (S. cerevisiae)-like (augmenter of liver regeneration) [Source:MGI Symbol;Acc:MGI:107757]	ENSMUSG00000040888	-1.402402189	0.011243001
Twist2	twist basic helix-loop-helix transcription factor 2 [Source:MGI Symbol;Acc:MGI:104685]	ENSMUSG00000007805	-1.400511577	0.012646712
Sco2	SCO2 cytochrome c oxidase assembly protein [Source:MGI Symbol;Acc:MGI:3818630]	ENSMUSG00000091780	-1.399984311	0.043375173
Slc19a2	solute carrier family 19 (thiamine transporter), member 2 [Source:MGI Symbol;Acc:MGI:1928761]	ENSMUSG00000040918	-1.398488432	0.014709073
Cdt1	chromatin licensing and DNA replication factor 1 [Source:MGI Symbol;Acc:MGI:1914427]	ENSMUSG00000006585	-1.398094113	0.012069084
Rrp12	ribosomal RNA processing 12 homolog (S. cerevisiae) [Source:MGI Symbol;Acc:MGI:2147437]	ENSMUSG00000035049	-1.398065652	0.013842203
Mcm5	minichromosome maintenance complex component 5 [Source:MGI Symbol;Acc:MGI:103197]	ENSMUSG00000005410	-1.39655933	0.000280963
Ddx20	DEAD (Asp-Glu-Ala-Asp) box polypeptide 20 [Source:MGI Symbol;Acc:MGI:1858415]	ENSMUSG00000027905	-1.39652885	0.00546389
Trmt61a	tRNA methyltransferase 61A [Source:MGI Symbol;Acc:MGI:2443487]	ENSMUSG00000060950	-1.396196307	0.03580291
Cdc6	cell division cycle 6 [Source:MGI Symbol;Acc:MGI:1345150]	ENSMUSG00000017499	-1.391974715	0.006448572
Sephs2	selenophosphate synthetase 2 [Source:MGI Symbol;Acc:MGI:108388]	ENSMUSG00000049091	-1.39128338	0.013842203
Phgdh	3-phosphoglycerate dehydrogenase [Source:MGI Symbol;Acc:MGI:1355330]	ENSMUSG00000053398	-1.388493257	0.000280963
Arhgap22	Rho GTPase activating protein 22 [Source:MGI Symbol;Acc:MGI:2443418]	ENSMUSG00000063506	-1.387192495	0.000984343
Polr3g	polymerase (RNA) III (DNA directed) polypeptide G [Source:MGI Symbol;Acc:MGI:1914736]	ENSMUSG00000035834	-1.386196468	0.018218872
Dna2	DNA replication helicase/nuclease 2 [Source:MGI Symbol;Acc:MGI:2443732]	ENSMUSG00000036875	-1.386175408	0.020597543
Wdhd1	WD repeat and HMG-box DNA binding protein 1 [Source:MGI Symbol;Acc:MGI:2443514]	ENSMUSG00000037572	-1.385282825	0.002751174
Ncl	nucleolin [Source:MGI Symbol;Acc:MGI:97286]	ENSMUSG00000026234	-1.383652152	0.000241828
Srm	spermidine synthase [Source:MGI Symbol;Acc:MGI:102690]	ENSMUSG00000006442	-1.383199094	0.017185809
Chaf1a	chromatin assembly factor 1, subunit A (p150) [Source:MGI Symbol;Acc:MGI:1351331]	ENSMUSG00000002835	-1.380729014	0.000984343
Ska1	spindle and kinetochore associated complex subunit 1 [Source:MGI Symbol;Acc:MGI:1913718]	ENSMUSG00000036223	-1.380528068	0.015336476
Oraov1	oral cancer overexpressed 1 [Source:MGI Symbol;Acc:MGI:1919534]	ENSMUSG00000031072	-1.380262917	0.002997779
Nop2	NOP2 nucleolar protein [Source:MGI Symbol;Acc:MGI:107891]	ENSMUSG00000038279	-1.378196051	0.000902594
Ankrd1	ankyrin repeat domain 1 (cardiac muscle) [Source:MGI Symbol;Acc:MGI:1097717]	ENSMUSG00000024803	-1.376906041	0.001740595
Tipin	timeless interacting protein [Source:MGI Symbol;Acc:MGI:1921571]	ENSMUSG00000032397	-1.37657622	0.023163003
Setdb2	SET domain, bifurcated 2 [Source:MGI Symbol;Acc:MGI:2685139]	ENSMUSG00000071350	-1.376301497	0.048882303
Dctd	dCMP deaminase [Source:MGI Symbol;Acc:MGI:2444529]	ENSMUSG00000031562	-1.375784418	0.017097898
Itga6	integrin alpha 6 [Source:MGI Symbol;Acc:MGI:96605]	ENSMUSG00000027111	-1.375339181	0.008730364
Pole2	polymerase (DNA directed), epsilon 2 (p59 subunit) [Source:MGI Symbol;Acc:MGI:1197514]	ENSMUSG00000020974	-1.375238436	0.020597543
Tm4sf1	transmembrane 4 superfamily member 1 [Source:MGI Symbol;Acc:MGI:104678]	ENSMUSG00000027800	-1.374985069	0.045412436

Spdl1	spindle apparatus coiled-coil protein 1 [Source:MGI Symbol;Acc:MGI:1917635]	ENSMUSG00000069910	-1.373352511	0.022457628
Mcm3	minichromosome maintenance complex component 3 [Source:MGI Symbol;Acc:MGI:101845]	ENSMUSG00000041859	-1.372421431	0.000836895
Ppat	phosphoribosyl pyrophosphate amidotransferase [Source:MGI Symbol;Acc:MGI:2387203]	ENSMUSG00000029246	-1.371799933	0.033875221
Rrs1	ribosome biogenesis regulator 1 [Source:MGI Symbol;Acc:MGI:1929721]	ENSMUSG00000061024	-1.370966871	0.003818197
Fbxo5	F-box protein 5 [Source:MGI Symbol;Acc:MGI:1914391]	ENSMUSG00000019773	-1.370640366	0.006081444
Exo1	exonuclease 1 [Source:MGI Symbol;Acc:MGI:1349427]	ENSMUSG00000039748	-1.36871922	0.017332496
Nip7	NIP7, nucleolar pre-rRNA processing protein [Source:MGI Symbol;Acc:MGI:1913414]	ENSMUSG00000031917	-1.367172807	0.031672799
Nolc1	nucleolar and coiled-body phosphoprotein 1 [Source:MGI Symbol;Acc:MGI:1918019]	ENSMUSG00000015176	-1.367111058	0.001136736
Mcm4	minichromosome maintenance complex component 4 [Source:MGI Symbol;Acc:MGI:103199]	ENSMUSG00000022673	-1.367003817	0.000984343
Cdk1	cyclin-dependent kinase 1 [Source:MGI Symbol;Acc:MGI:88351]	ENSMUSG00000019942	-1.364770943	0.017332496
Ppan	peter pan homolog (Drosophila) [Source:MGI Symbol;Acc:MGI:2178445]	ENSMUSG00000004100	-1.363982975	0.007142522
Eif1ad	eukaryotic translation initiation factor 1A domain containing [Source:MGI Symbol;Acc:MGI:1917110]	ENSMUSG00000024841	-1.363472669	0.004094227
Mis18a	MIS18 kinetochore protein A [Source:MGI Symbol;Acc:MGI:1913828]	ENSMUSG00000022978	-1.36220571	0.039920152
Tk1	thymidine kinase 1 [Source:MGI Symbol;Acc:MGI:98763]	ENSMUSG00000025574	-1.361162884	0.001379194
Usp1	ubiquitin specific peptidase 1 [Source:MGI Symbol;Acc:MGI:2385198]	ENSMUSG00000028560	-1.360580496	0.003928587
Dbr1	debranching RNA lariats 1 [Source:MGI Symbol;Acc:MGI:1931520]	ENSMUSG00000032469	-1.359573218	0.0229276
Rps12-ps3	ribosomal protein S12, pseudogene 3 [Source:MGI Symbol;Acc:MGI:3704503]	ENSMUSG00000067038	-1.35952484	0.031222221
Tomt	transmembrane O-methyltransferase [Source:MGI Symbol;Acc:MGI:3769724]	ENSMUSG00000078630	-1.359348873	0.028627191
Fabp5	fatty acid binding protein 5, epidermal [Source:MGI Symbol;Acc:MGI:101790]	ENSMUSG00000027533	-1.3589403	0.004213014
Pa2g4	proliferation-associated 2G4 [Source:MGI Symbol;Acc:MGI:894684]	ENSMUSG00000025364	-1.357883953	0.000984343
Ak2	adenylate kinase 2 [Source:MGI Symbol;Acc:MGI:87978]	ENSMUSG00000028792	-1.357214133	0.003188695
Serpine1	serine (or cysteine) peptidase inhibitor, clade E, member 1 [Source:MGI Symbol;Acc:MGI:97608]	ENSMUSG00000037411	-1.356604818	0.002751174
Tsr1	TSR1 20S rRNA accumulation [Source:MGI Symbol;Acc:MGI:2144566]	ENSMUSG00000038335	-1.355350333	0.011355465
Ddx21	DEAD (Asp-Glu-Ala-Asp) box polypeptide 21 [Source:MGI Symbol;Acc:MGI:1860494]	ENSMUSG00000020075	-1.354281992	0.00109709
Ppih	peptidyl prolyl isomerase H [Source:MGI Symbol;Acc:MGI:106499]	ENSMUSG00000060288	-1.354025768	0.037710659
Pcna	proliferating cell nuclear antigen [Source:MGI Symbol;Acc:MGI:97503]	ENSMUSG00000027342	-1.35334772	0.004266124
Rcc1	regulator of chromosome condensation 1 [Source:MGI Symbol;Acc:MGI:1913989]	ENSMUSG00000028896	-1.352220089	0.006448572
Nek2	NIMA (never in mitosis gene a)-related expressed kinase 2 [Source:MGI Symbol;Acc:MGI:109359]	ENSMUSG00000026622	-1.350952172	0.004480671
Shmt2	serine hydroxymethyltransferase 2 (mitochondrial) [Source:MGI Symbol;Acc:MGI:1277989]	ENSMUSG00000025403	-1.34916689	0.00170814

Pik3cb	phosphatidylinositol 3-kinase, catalytic, beta polypeptide [Source:MGI Symbol;Acc:MGI:1922019]	ENSMUSG00000032462	-1.346164626	0.028683731
Wdr12	WD repeat domain 12 [Source:MGI Symbol;Acc:MGI:1927241]	ENSMUSG00000026019	-1.344977854	0.036804389
Nme1	NME/NM23 nucleoside diphosphate kinase 1 [Source:MGI Symbol;Acc:MGI:97355]	ENSMUSG00000037601	-1.344741493	0.045869631
Atp1b1	ATPase, Na+/K+ transporting, beta 1 polypeptide [Source:MGI Symbol;Acc:MGI:88108]	ENSMUSG00000026576	-1.342848188	0.012555649
Ccnb1	cyclin B1 [Source:MGI Symbol;Acc:MGI:88302]	ENSMUSG00000041431	-1.341173828	0.042949194
Ebna1bp2	EBNA1 binding protein 2 [Source:MGI Symbol;Acc:MGI:1916322]	ENSMUSG00000028729	-1.340619017	0.004480671
Qtrtd1	queuine tRNA-ribosyltransferase domain containing 1 [Source:MGI Symbol;Acc:MGI:1922194]	ENSMUSG00000022704	-1.340283705	0.0392801
Cirh1a	cirrhosis, autosomal recessive 1A (human) [Source:MGI Symbol;Acc:MGI:1096573]	ENSMUSG00000041438	-1.340228027	0.011355465
Gnl3	guanine nucleotide binding protein-like 3 (nucleolar) [Source:MGI Symbol;Acc:MGI:1353651]	ENSMUSG00000042354	-1.340203987	0.003207878
Prkg2	protein kinase, cGMP-dependent, type II [Source:MGI Symbol;Acc:MGI:108173]	ENSMUSG00000029334	-1.340103046	0.049261057
Ifrd2	interferon-related developmental regulator 2 [Source:MGI Symbol;Acc:MGI:1316708]	ENSMUSG00000010048	-1.339442149	0.021777147
Fxyd5	FXYD domain-containing ion transport regulator 5 [Source:MGI Symbol;Acc:MGI:1201785]	ENSMUSG00000009687	-1.338203737	0.013478123
Dck	deoxycytidine kinase [Source:MGI Symbol;Acc:MGI:102726]	ENSMUSG00000029366	-1.337675601	0.020446334
Ftsj3	FtsJ RNA methyltransferase homolog 3 (E. coli) [Source:MGI Symbol;Acc:MGI:1860295]	ENSMUSG00000020706	-1.336791776	0.003034541
Rad51ap1	RAD51 associated protein 1 [Source:MGI Symbol;Acc:MGI:1098224]	ENSMUSG00000030346	-1.336669184	0.049908928
Nasp	nuclear autoantigenic sperm protein (histone-binding) [Source:MGI Symbol;Acc:MGI:1355328]	ENSMUSG00000028693	-1.335282807	0.020597543
Dnajc9	DnaJ heat shock protein family (Hsp40) member C9 [Source:MGI Symbol;Acc:MGI:1915326]	ENSMUSG00000021811	-1.334379681	0.012069084
Asns	asparagine synthetase [Source:MGI Symbol;Acc:MGI:1350929]	ENSMUSG00000029752	-1.334265307	0.003702191
Umps	uridine monophosphate synthetase [Source:MGI Symbol;Acc:MGI:1298388]	ENSMUSG00000022814	-1.333037669	0.006906207
Atad5	ATPase family, AAA domain containing 5 [Source:MGI Symbol;Acc:MGI:2442925]	ENSMUSG00000017550	-1.331150502	0.021688656
Mtbp	Mdm2, transformed 3T3 cell double minute p53 binding protein [Source:MGI Symbol;Acc:MGI:2146005]	ENSMUSG00000022369	-1.331099144	0.012040486
Rad51	RAD51 recombinase [Source:MGI Symbol;Acc:MGI:97890]	ENSMUSG00000027323	-1.330242283	0.046178499
Aen	apoptosis enhancing nuclease [Source:MGI Symbol;Acc:MGI:1915298]	ENSMUSG00000030609	-1.329931148	0.010162844
Hspd1	heat shock protein 1 (chaperonin) [Source:MGI Symbol;Acc:MGI:96242]	ENSMUSG00000025980	-1.329345128	0.002201623
Ppa1	pyrophosphatase (inorganic) 1 [Source:MGI Symbol;Acc:MGI:97831]	ENSMUSG00000020089	-1.32790544	0.041226127
Eif5a	eukaryotic translation initiation factor 5A [Source:MGI Symbol;Acc:MGI:106248]	ENSMUSG00000078812	-1.326653358	0.017625834
Stil	Scl/Tal1 interrupting locus [Source:MGI Symbol;Acc:MGI:107477]	ENSMUSG00000028718	-1.326596612	0.022635088
Psat1	phosphoserine aminotransferase 1 [Source:MGI Symbol;Acc:MGI:2183441]	ENSMUSG00000024640	-1.323287513	0.005859364
Clspn	claspin [Source:MGI Symbol;Acc:MGI:2445153]	ENSMUSG00000042489	-1.323103473	0.009308656

Hmgb3	high mobility group box 3 [Source:MGI Symbol;Acc:MGI:1098219]	ENSMUSG00000015217	-1.319912763	0.016415614
Nup35	nucleoporin 35 [Source:MGI Symbol;Acc:MGI:1916732]	ENSMUSG00000026999	-1.3197382	0.034544604
Mcm2	minichromosome maintenance complex component 2 [Source:MGI Symbol;Acc:MGI:105380]	ENSMUSG00000002870	-1.318872319	0.004824129
Plk4	polo-like kinase 4 [Source:MGI Symbol;Acc:MGI:101783]	ENSMUSG00000025758	-1.317679013	0.00976649
Trip13	thyroid hormone receptor interactor 13 [Source:MGI Symbol;Acc:MGI:1916966]	ENSMUSG00000021569	-1.317642125	0.033083165
Dtl	denticleless E3 ubiquitin protein ligase [Source:MGI Symbol;Acc:MGI:1924093]	ENSMUSG00000037474	-1.317236154	0.023142218
Uhrf1	ubiquitin-like, containing PHD and RING finger domains, 1 [Source:MGI Symbol;Acc:MGI:1338889]	ENSMUSG00000001228	-1.314468001	0.004774209
Gm4737	predicted gene 4737 [Source:MGI Symbol;Acc:MGI:3643647]	ENSMUSG00000048087	-1.313819412	0.007282766
Ska3	spindle and kinetochore associated complex subunit 3 [Source:MGI Symbol;Acc:MGI:3041235]	ENSMUSG00000021965	-1.313195072	0.030288946
Ahcy	S-adenosylhomocysteine hydrolase [Source:MGI Symbol;Acc:MGI:87968]	ENSMUSG00000027597	-1.311868654	0.006053516
Ddah1	dimethylarginine dimethylaminohydrolase 1 [Source:MGI Symbol;Acc:MGI:1916469]	ENSMUSG00000028194	-1.310659932	0.031222221
Ncapg2	non-SMC condensin II complex, subunit G2 [Source:MGI Symbol;Acc:MGI:1923294]	ENSMUSG00000042029	-1.310364391	0.007865448
Smc2	structural maintenance of chromosomes 2 [Source:MGI Symbol;Acc:MGI:106067]	ENSMUSG00000028312	-1.31035061	0.031534732
Cdca7l	cell division cycle associated 7 like [Source:MGI Symbol;Acc:MGI:2384982]	ENSMUSG00000021175	-1.308581475	0.047054679
Nup85	nucleoporin 85 [Source:MGI Symbol;Acc:MGI:3046173]	ENSMUSG00000020739	-1.306648957	0.010025076
Ctps	cytidine 5'-triphosphate synthase [Source:MGI Symbol;Acc:MGI:1858304]	ENSMUSG00000028633	-1.306196014	0.011948334
Trmt6	tRNA methyltransferase 6 [Source:MGI Symbol;Acc:MGI:1914176]	ENSMUSG00000037376	-1.30546259	0.041129586
Tuba1b	tubulin, alpha 1B [Source:MGI Symbol;Acc:MGI:107804]	ENSMUSG00000023004	-1.304766996	0.004434301
Rad18	RAD18 E3 ubiquitin protein ligase [Source:MGI Symbol;Acc:MGI:1890476]	ENSMUSG00000030254	-1.303784397	0.03580291
Mcm6	minichromosome maintenance complex component 6 [Source:MGI Symbol;Acc:MGI:1298227]	ENSMUSG00000026355	-1.303748493	0.006414645
Snrpa1	small nuclear ribonucleoprotein polypeptide A' [Source:MGI Symbol;Acc:MGI:1916231]	ENSMUSG00000030512	-1.302699357	0.022647951
Prim1	DNA primase, p49 subunit [Source:MGI Symbol;Acc:MGI:97757]	ENSMUSG00000025395	-1.302451222	0.029361627
Alyref	Aly/REF export factor [Source:MGI Symbol;Acc:MGI:1341044]	ENSMUSG00000025134	-1.300115074	0.012040486
Taf1d	TATA-box binding protein associated factor, RNA polymerase I, D [Source:MGI Symbol;Acc:MGI:1922566]	ENSMUSG00000031939	-1.299484787	0.046448327
Nepro	nucleolus and neural progenitor protein [Source:MGI Symbol;Acc:MGI:2384836]	ENSMUSG00000036208	-1.299081987	0.04659026
Bcat1	branched chain aminotransferase 1, cytosolic [Source:MGI Symbol;Acc:MGI:104861]	ENSMUSG00000030268	-1.298037149	0.013211921
Cep57	centrosomal protein 57 [Source:MGI Symbol;Acc:MGI:1915551]	ENSMUSG00000031922	-1.29768963	0.035478032
Brca2	breast cancer 2, early onset [Source:MGI Symbol;Acc:MGI:109337]	ENSMUSG00000041147	-1.297674104	0.029361627
C330027C09Rik	RIKEN cDNA C330027C09 gene [Source:MGI Symbol;Acc:MGI:2146335]	ENSMUSG00000033031	-1.296908787	0.014455648

Id2	inhibitor of DNA binding 2 [Source:MGI Symbol;Acc:MGI:96397]	ENSMUSG00000020644	-1.295889174	0.031222221
Mak16	MAK16 homolog [Source:MGI Symbol;Acc:MGI:1915170]	ENSMUSG00000031578	-1.295350374	0.045651778
Hn1l	hematological and neurological expressed 1-like [Source:MGI Symbol;Acc:MGI:1196260]	ENSMUSG00000024165	-1.29306466	0.037304681
Alcam	activated leukocyte cell adhesion molecule [Source:MGI Symbol;Acc:MGI:1313266]	ENSMUSG00000022636	-1.29268419	0.035478032
Tomm5	translocase of outer mitochondrial membrane 5 homolog (yeast) [Source:MGI Symbol;Acc:MGI:1915762]	ENSMUSG00000078713	-1.291757917	0.044318489
Nup160	nucleoporin 160 [Source:MGI Symbol;Acc:MGI:1926227]	ENSMUSG00000051329	-1.290148409	0.021854725
Brix1	BRX1, biogenesis of ribosomes [Source:MGI Symbol;Acc:MGI:1915082]	ENSMUSG00000022247	-1.288525721	0.023409657
Snrpg	small nuclear ribonucleoprotein polypeptide G [Source:MGI Symbol;Acc:MGI:1915261]	ENSMUSG00000057278	-1.288431449	0.038451936
Lrp8	low density lipoprotein receptor-related protein 8, apolipoprotein e receptor [Source:MGI Symbol;Acc:MGI:1340044]	ENSMUSG00000028613	-1.288199346	0.017358299
Ube2c	ubiquitin-conjugating enzyme E2C [Source:MGI Symbol;Acc:MGI:1915862]	ENSMUSG00000001403	-1.286735542	0.01971285
Cenpi	centromere protein I [Source:MGI Symbol;Acc:MGI:2147897]	ENSMUSG00000031262	-1.286169627	0.037860174
Noc2l	NOC2 like nucleolar associated transcriptional repressor [Source:MGI Symbol;Acc:MGI:1931051]	ENSMUSG00000095567	-1.286148296	0.01971285
Naa25	N(alpha)-acetyltransferase 25, NatB auxiliary subunit [Source:MGI Symbol;Acc:MGI:2442563]	ENSMUSG00000042719	-1.284524873	0.019245715
Asf1b	anti-silencing function 1B histone chaperone [Source:MGI Symbol;Acc:MGI:1914179]	ENSMUSG00000005470	-1.284215533	0.013409351
Topbp1	topoisomerase (DNA) II binding protein 1 [Source:MGI Symbol;Acc:MGI:1920018]	ENSMUSG00000032555	-1.284058845	0.01617591
Gclc	glutamate-cysteine ligase, catalytic subunit [Source:MGI Symbol;Acc:MGI:104990]	ENSMUSG00000032350	-1.283875013	0.0229276
Gmps	guanine monophosphate synthetase [Source:MGI Symbol;Acc:MGI:2448526]	ENSMUSG00000027823	-1.283403776	0.018893234
Nsun2	NOL1/NOP2/Sun domain family member 2 [Source:MGI Symbol;Acc:MGI:107252]	ENSMUSG00000021595	-1.282912458	0.021777147
Brca1	breast cancer 1, early onset [Source:MGI Symbol;Acc:MGI:104537]	ENSMUSG00000017146	-1.281818068	0.033875221
Tubb4b	tubulin, beta 4B class IVB [Source:MGI Symbol;Acc:MGI:1915472]	ENSMUSG00000036752	-1.28092566	0.012693559
Mcm7	minichromosome maintenance complex component 7 [Source:MGI Symbol;Acc:MGI:1298398]	ENSMUSG00000029730	-1.280456706	0.01530219
Atad2	ATPase family, AAA domain containing 2 [Source:MGI Symbol;Acc:MGI:1917722]	ENSMUSG00000022360	-1.280097546	0.014709073
Ddx39	DEAD (Asp-Glu-Ala-Asp) box polypeptide 39 [Source:MGI Symbol;Acc:MGI:1915528]	ENSMUSG00000005481	-1.279452964	0.012631549
Mthfd1	methylenetetrahydrofolate dehydrogenase (NADP+ dependent), methenyltetrahydrofolate cyclohydrolase, formyltetrahydrofolate synthase [Source:MGI Symbol;Acc:MGI:1342005]	ENSMUSG00000021048	-1.278930204	0.021994405
Tcf19	transcription factor 19 [Source:MGI Symbol;Acc:MGI:103180]	ENSMUSG00000050410	-1.278284713	0.049908928
Gm10184	predicted pseudogene 10184 [Source:MGI Symbol;Acc:MGI:3704480]	ENSMUSG00000066878	-1.278266335	0.031534732
Fen1	flap structure specific endonuclease 1 [Source:MGI Symbol;Acc:MGI:102779]	ENSMUSG00000024742	-1.277812388	0.02932201
Ndc1	NDC1 transmembrane nucleoporin [Source:MGI Symbol;Acc:MGI:1920037]	ENSMUSG00000028614	-1.27725352	0.033875221

Gart	phosphoribosylglycinamide formyltransferase [Source:MGI Symbol;Acc:MGI:95654]	ENSMUSG00000022962	-1.274951684	0.028627191
Set	SET nuclear oncogene [Source:MGI Symbol;Acc:MGI:1860267]	ENSMUSG00000054766	-1.274555598	0.01530219
Pola1	polymerase (DNA directed), alpha 1 [Source:MGI Symbol;Acc:MGI:99660]	ENSMUSG00000006678	-1.274426547	0.033875221
Kif23	kinesin family member 23 [Source:MGI Symbol;Acc:MGI:1919069]	ENSMUSG00000032254	-1.274321928	0.023235285
Gclm	glutamate-cysteine ligase, modifier subunit [Source:MGI Symbol;Acc:MGI:104995]	ENSMUSG00000028124	-1.273747171	0.028112058
Skp2	S-phase kinase-associated protein 2 (p45) [Source:MGI Symbol;Acc:MGI:1351663]	ENSMUSG00000054115	-1.267738701	0.049908928
Mybbp1a	MYB binding protein (P160) 1a [Source:MGI Symbol;Acc:MGI:106181]	ENSMUSG00000040463	-1.266832636	0.018650284
Rif1	replication timing regulatory factor 1 [Source:MGI Symbol;Acc:MGI:1098622]	ENSMUSG00000036202	-1.266378058	0.042825447
Uck2	uridine-cytidine kinase 2 [Source:MGI Symbol;Acc:MGI:1931744]	ENSMUSG00000026558	-1.266333853	0.04265287
Rrm2	ribonucleotide reductase M2 [Source:MGI Symbol;Acc:MGI:98181]	ENSMUSG00000020649	-1.263050096	0.019841311
Fkbp4	FK506 binding protein 4 [Source:MGI Symbol;Acc:MGI:95543]	ENSMUSG00000030357	-1.26007739	0.024188138
Ddx18	DEAD (Asp-Glu-Ala-Asp) box polypeptide 18 [Source:MGI Symbol;Acc:MGI:1914192]	ENSMUSG00000001674	-1.256782001	0.049908928
Ckap2l	cytoskeleton associated protein 2-like [Source:MGI Symbol;Acc:MGI:1917716]	ENSMUSG00000048327	-1.253428495	0.04659026
Fbl	fibrillarin [Source:MGI Symbol;Acc:MGI:95486]	ENSMUSG00000046865	-1.253355183	0.045195528
Strap	serine/threonine kinase receptor associated protein [Source:MGI Symbol;Acc:MGI:1329037]	ENSMUSG00000030224	-1.251838032	0.035487966
Tacc3	transforming, acidic coiled-coil containing protein 3 [Source:MGI Symbol;Acc:MGI:1341163]	ENSMUSG00000037313	-1.251223446	0.04246107
Cyr61	cysteine rich protein 61 [Source:MGI Symbol;Acc:MGI:88613]	ENSMUSG00000028195	-1.25048435	0.033491177
Tfdp1	transcription factor Dp 1 [Source:MGI Symbol;Acc:MGI:101934]	ENSMUSG00000038482	-1.249411691	0.038291576
Nudc	nudC nuclear distribution protein [Source:MGI Symbol;Acc:MGI:106014]	ENSMUSG00000028851	-1.24921154	0.041716576
Rpa1	replication protein A1 [Source:MGI Symbol;Acc:MGI:1915525]	ENSMUSG00000000751	-1.246930142	0.037860174
Atic	5-aminoimidazole-4-carboxamide ribonucleotide formyltransferase/IMP cyclohydrolase [Source:MGI Symbol;Acc:MGI:1351352]	ENSMUSG00000026192	-1.246034716	0.040792682
Ect2	ect2 oncogene [Source:MGI Symbol;Acc:MGI:95281]	ENSMUSG00000027699	-1.24521703	0.048597581
Anln	anillin, actin binding protein [Source:MGI Symbol;Acc:MGI:1920174]	ENSMUSG00000036777	-1.244051358	0.036882929
Kif20a	kinesin family member 20A [Source:MGI Symbol;Acc:MGI:1201682]	ENSMUSG00000003779	-1.238385895	0.049261057
Atf4	activating transcription factor 4 [Source:MGI Symbol;Acc:MGI:88096]	ENSMUSG00000042406	-1.234770951	0.049908928
Tuba1c	tubulin, alpha 1C [Source:MGI Symbol;Acc:MGI:1095409]	ENSMUSG00000043091	-1.231181062	0.048535878
Sfxn3	sideroflexin 3 [Source:MGI Symbol;Acc:MGI:2137679]	ENSMUSG00000025212	1.245632761	0.048753594
Sparc	secreted acidic cysteine rich glycoprotein [Source:MGI Symbol;Acc:MGI:98373]	ENSMUSG00000018593	1.249692144	0.027493156
Kremen1	kringle containing transmembrane protein 1 [Source:MGI Symbol;Acc:MGI:1933988]	ENSMUSG00000020393	1.253684541	0.031534732

Igfbp2	insulin-like growth factor binding protein 2 [Source:MGI Symbol;Acc:MGI:96437]	ENSMUSG00000039323	1.25434281	0.031534732
Scd1	stearoyl-Coenzyme A desaturase 1 [Source:MGI Symbol;Acc:MGI:98239]	ENSMUSG00000037071	1.25622666	0.036021954
Bace1	beta-site APP cleaving enzyme 1 [Source:MGI Symbol;Acc:MGI:1346542]	ENSMUSG00000032086	1.256732985	0.037860174
Sdc2	syndecan 2 [Source:MGI Symbol;Acc:MGI:1349165]	ENSMUSG00000022261	1.261398962	0.021120456
Xdh	xanthine dehydrogenase [Source:MGI Symbol;Acc:MGI:98973]	ENSMUSG00000024066	1.261734692	0.038648635
Srpx2	sushi-repeat-containing protein, X-linked 2 [Source:MGI Symbol;Acc:MGI:1916042]	ENSMUSG00000031253	1.267954696	0.024188138
Thra	thyroid hormone receptor alpha [Source:MGI Symbol;Acc:MGI:98742]	ENSMUSG00000058756	1.2699653	0.048753594
Fhod3	formin homology 2 domain containing 3 [Source:MGI Symbol;Acc:MGI:1925847]	ENSMUSG00000034295	1.273974625	0.049908928
Rin2	Ras and Rab interactor 2 [Source:MGI Symbol;Acc:MGI:1921280]	ENSMUSG00000001768	1.273978402	0.03249814
Gulp1	GULP, engulfment adaptor PTB domain containing 1 [Source:MGI Symbol;Acc:MGI:1920407]	ENSMUSG00000056870	1.274292061	0.048853104
Acadm	acyl-Coenzyme A dehydrogenase, medium chain [Source:MGI Symbol;Acc:MGI:87867]	ENSMUSG00000062908	1.274624083	0.018934624
Fam234a	family with sequence similarity 234, member A [Source:MGI Symbol;Acc:MGI:2146854]	ENSMUSG00000024187	1.274667495	0.029835927
Flot1	flotillin 1 [Source:MGI Symbol;Acc:MGI:1100500]	ENSMUSG00000059714	1.275014739	0.031556676
Arsa	arylsulfatase A [Source:MGI Symbol;Acc:MGI:88077]	ENSMUSG00000022620	1.275201861	0.049908928
Fam102b	family with sequence similarity 102, member B [Source:MGI Symbol;Acc:MGI:3036259]	ENSMUSG00000040339	1.27524407	0.019896473
Utp14b	UTP14B small subunit processome component [Source:MGI Symbol;Acc:MGI:2445092]	ENSMUSG00000079470	1.275964258	0.049908928
Tapbp	TAP binding protein [Source:MGI Symbol;Acc:MGI:1201689]	ENSMUSG00000024308	1.277697389	0.019245715
Prrx1	paired related homeobox 1 [Source:MGI Symbol;Acc:MGI:97712]	ENSMUSG00000026586	1.279382856	0.012278563
C1qtnf3	C1q and tumor necrosis factor related protein 3 [Source:MGI Symbol;Acc:MGI:1932136]	ENSMUSG00000058914	1.279401349	0.023409657
Pcmtd2	protein-L-isoaspartate (D-aspartate) O-methyltransferase domain containing 2 [Source:MGI Symbol;Acc:MGI:1923927]	ENSMUSG00000027589	1.280306992	0.041716576
Birc2	baculoviral IAP repeat-containing 2 [Source:MGI Symbol;Acc:MGI:1197009]	ENSMUSG00000057367	1.281708596	0.035586884
Pik3r3	phosphatidylinositol 3 kinase, regulatory subunit, polypeptide 3 (p55) [Source:MGI Symbol;Acc:MGI:109277]	ENSMUSG00000028698	1.283168139	0.024677863
Pcnx	pecanex homolog (Drosophila) [Source:MGI Symbol;Acc:MGI:1891924]	ENSMUSG00000021140	1.284503198	0.019177473
Tcf4-018	transcription factor 4 [Source:MGI Symbol;Acc:MGI:98506]	ENSMUSG00000053477	1.284744499	0.014097135
Os9	amplified in osteosarcoma [Source:MGI Symbol;Acc:MGI:1924301]	ENSMUSG00000040462	1.285013528	0.020311919
Pik3r1	phosphatidylinositol 3-kinase, regulatory subunit, polypeptide 1 (p85 alpha) [Source:MGI Symbol;Acc:MGI:97583]	ENSMUSG00000041417	1.286868263	0.012275597
Dnal1	dynein, axonemal, light chain 1 [Source:MGI Symbol;Acc:MGI:1921462]	ENSMUSG00000042523	1.288381703	0.049908928
Matn2	matrilin 2 [Source:MGI Symbol;Acc:MGI:109613]	ENSMUSG00000022324	1.288872023	0.01530219

Lpin3	lipin 3 [Source:MGI Symbol;Acc:MGI:1891342]	ENSMUSG00000027412	1.28934558	0.044280512
Slc1a3	solute carrier family 1 (glial high affinity glutamate transporter), member 3 [Source:MGI Symbol;Acc:MGI:99917]	ENSMUSG00000005360	1.290453724	0.021777147
Lifr-203	leukemia inhibitory factor receptor [Source:MGI Symbol;Acc:MGI:96788]	ENSMUSG00000054263	1.29222933	0.037710659
Arhgef19	Rho guanine nucleotide exchange factor (GEF) 19 [Source:MGI Symbol;Acc:MGI:1925912]	ENSMUSG00000028919	1.293516282	0.019177473
Smad3	SMAD family member 3 [Source:MGI Symbol;Acc:MGI:1201674]	ENSMUSG00000032402	1.294761417	0.01971285
Ube2h	ubiquitin-conjugating enzyme E2H [Source:MGI Symbol;Acc:MGI:104632]	ENSMUSG00000039159	1.294762729	0.013842203
Mvp	major vault protein [Source:MGI Symbol;Acc:MGI:1925638]	ENSMUSG00000030681	1.295721063	0.013063538
Creld1	cysteine-rich with EGF-like domains 1 [Source:MGI Symbol;Acc:MGI:2152539]	ENSMUSG00000030284	1.296904669	0.042825447
Stat3	signal transducer and activator of transcription 3 [Source:MGI Symbol;Acc:MGI:103038]	ENSMUSG00000004040	1.296974826	0.009882913
Ptgfrn	prostaglandin F2 receptor negative regulator [Source:MGI Symbol;Acc:MGI:1277114]	ENSMUSG00000027864	1.298126736	0.006704121
Tgfbr2	transforming growth factor, beta receptor II [Source:MGI Symbol;Acc:MGI:98729]	ENSMUSG00000032440	1.299158756	0.006081444
Cp	ceruloplasmin [Source:MGI Symbol;Acc:MGI:88476]	ENSMUSG00000003617	1.299845093	0.011313788
Map1lc3a	microtubule-associated protein 1 light chain 3 alpha [Source:MGI Symbol;Acc:MGI:1915661]	ENSMUSG00000027602	1.300082493	0.044280512
Ppp1r14c	protein phosphatase 1, regulatory (inhibitor) subunit 14c [Source:MGI Symbol;Acc:MGI:1923392]	ENSMUSG00000040653	1.300629302	0.031534732
Olfml3	olfactomedin-like 3 [Source:MGI Symbol;Acc:MGI:1914877]	ENSMUSG00000027848	1.301095912	0.010381478
Mapre3	microtubule-associated protein, RP/EB family, member 3 [Source:MGI Symbol;Acc:MGI:2140967]	ENSMUSG00000029166	1.301150888	0.031534732
Pdcd4	programmed cell death 4 [Source:MGI Symbol;Acc:MGI:107490]	ENSMUSG00000024975	1.30249424	0.045412436
Rsrp1	arginine/serine rich protein 1 [Source:MGI Symbol;Acc:MGI:106498]	ENSMUSG00000037266	1.303650669	0.006906207
Nkd2	naked cuticle 2 homolog (Drosophila) [Source:MGI Symbol;Acc:MGI:1919543]	ENSMUSG00000021567	1.304552703	0.021777147
Capn6	calpain 6 [Source:MGI Symbol;Acc:MGI:1100850]	ENSMUSG00000067276	1.305035295	0.009630423
Mfsd12	major facilitator superfamily domain containing 12 [Source:MGI Symbol;Acc:MGI:3604804]	ENSMUSG00000034854	1.30719715	0.046777684
Lama4	laminin, alpha 4 [Source:MGI Symbol;Acc:MGI:109321]	ENSMUSG00000019846	1.308111083	0.034005422
Porcn	porcupine homolog (Drosophila) [Source:MGI Symbol;Acc:MGI:1890212]	ENSMUSG00000031169	1.310922244	0.034712785
Cxcr4	chemokine (C-X-C motif) receptor 4 [Source:MGI Symbol;Acc:MGI:109563]	ENSMUSG00000045382	1.312952799	0.012275597
Pcdh7	protocadherin 7 [Source:MGI Symbol;Acc:MGI:1860487]	ENSMUSG00000029108	1.314476161	0.024368735
P2rx4	purinergic receptor P2X, ligand-gated ion channel 4 [Source:MGI Symbol;Acc:MGI:1338859]	ENSMUSG00000029470	1.314559033	0.008861455
Filip1l	filamin A interacting protein 1-like [Source:MGI Symbol;Acc:MGI:1925999]	ENSMUSG00000043336	1.315636593	0.005717644
C1ra	complement component 1, r subcomponent A [Source:MGI Symbol;Acc:MGI:1355313]	ENSMUSG00000055172	1.317026873	0.012900431
Lmcd1	LIM and cysteine-rich domains 1 [Source:MGI Symbol;Acc:MGI:1353635]	ENSMUSG00000057604	1.317859882	0.049261057

Slc16a3	solute carrier family 16 (monocarboxylic acid transporters), member 3 [Source:MGI Symbol;Acc:MGI:1933438]	ENSMUSG00000025161	1.31838135	0.014812871
Klc4	kinesin light chain 4 [Source:MGI Symbol;Acc:MGI:1922014]	ENSMUSG00000003546	1.319076434	0.044280512
Slit2	slit homolog 2 (Drosophila) [Source:MGI Symbol;Acc:MGI:1315205]	ENSMUSG00000031558	1.319449331	0.012238248
Ccng2	cyclin G2 [Source:MGI Symbol;Acc:MGI:1095734]	ENSMUSG00000029385	1.319728613	0.011355465
Naglu	alpha-N-acetylglucosaminidase (Sanfilippo disease IIIB) [Source:MGI Symbol;Acc:MGI:1351641]	ENSMUSG00000001751	1.321172915	0.028164931
Ezh1	enhancer of zeste 1 polycomb repressive complex 2 subunit [Source:MGI Symbol;Acc:MGI:1097695]	ENSMUSG00000006920	1.323128977	0.012069084
Gas1	growth arrest specific 1 [Source:MGI Symbol;Acc:MGI:95655]	ENSMUSG00000052957	1.324012042	0.002274993
Ghr	growth hormone receptor [Source:MGI Symbol;Acc:MGI:95708]	ENSMUSG00000055737	1.32426376	0.007619161
Mtus1	mitochondrial tumor suppressor 1 [Source:MGI Symbol;Acc:MGI:2142572]	ENSMUSG00000045636	1.32660216	0.011355465
Dtna	dystrobrevin alpha [Source:MGI Symbol;Acc:MGI:106039]	ENSMUSG00000024302	1.327557427	0.016672611
Chrna1	cholinergic receptor, nicotinic, alpha polypeptide 1 (muscle) [Source:MGI Symbol;Acc:MGI:87885]	ENSMUSG00000027107	1.327861691	0.002394027
Clip3	CAP-GLY domain containing linker protein 3 [Source:MGI Symbol;Acc:MGI:1923936]	ENSMUSG00000013921	1.328148069	0.02230728
Dopey2	dopey family member 2 [Source:MGI Symbol;Acc:MGI:1917278]	ENSMUSG00000022946	1.329797725	0.02048745
Lgals3bp	lectin, galactoside-binding, soluble, 3 binding protein [Source:MGI Symbol;Acc:MGI:99554]	ENSMUSG00000033880	1.330562804	0.046057413
Olfml2b	olfactomedin-like 2B [Source:MGI Symbol;Acc:MGI:2443310]	ENSMUSG00000038463	1.330642877	0.047849193
Cd82	CD82 antigen [Source:MGI Symbol;Acc:MGI:104651]	ENSMUSG00000027215	1.332433065	0.002520492
Ets2	E26 avian leukemia oncogene 2, 3' domain [Source:MGI Symbol;Acc:MGI:95456]	ENSMUSG00000022895	1.332806503	0.04659026
Plpp3	phospholipid phosphatase 3 [Source:MGI Symbol;Acc:MGI:1915166]	ENSMUSG00000028517	1.334197617	0.013221608
Fbxo32	F-box protein 32 [Source:MGI Symbol;Acc:MGI:1914981]	ENSMUSG00000022358	1.334376202	0.01971285
Acsl3	acyl-CoA synthetase long-chain family member 3 [Source:MGI Symbol;Acc:MGI:1921455]	ENSMUSG00000032883	1.335671809	0.001740595
Stat5a	signal transducer and activator of transcription 5A [Source:MGI Symbol;Acc:MGI:103036]	ENSMUSG00000004043	1.336440009	0.03825052
Pbxip1	pre B cell leukemia transcription factor interacting protein 1 [Source:MGI Symbol;Acc:MGI:2441670]	ENSMUSG00000042613	1.33699108	0.028799309
Kbtbd11	kelch repeat and BTB (POZ) domain containing 11 [Source:MGI Symbol;Acc:MGI:1922151]	ENSMUSG00000055675	1.338783709	0.012278563
Tmem123	transmembrane protein 123 [Source:MGI Symbol;Acc:MGI:1919179]	ENSMUSG00000050912	1.338982182	0.001223852
Pld3	phospholipase D family, member 3 [Source:MGI Symbol;Acc:MGI:1333782]	ENSMUSG00000003363	1.342991674	0.003565618
Ccdc8	coiled-coil domain containing 8 [Source:MGI Symbol;Acc:MGI:3612184]	ENSMUSG00000041117	1.344420623	0.02853252
Klhl24	kelch-like 24 [Source:MGI Symbol;Acc:MGI:1923035]	ENSMUSG00000062901	1.344750294	0.003034541
BC034090	cDNA sequence BC034090 [Source:MGI Symbol;Acc:MGI:2672904]	ENSMUSG00000033722	1.348449322	0.042464287
Ralgds	ral guanine nucleotide dissociation stimulator [Source:MGI Symbol;Acc:MGI:107485]	ENSMUSG00000026821	1.348858818	0.010121449

Abcd1	ATP-binding cassette, sub-family D (ALD), member 1 [Source:MGI Symbol;Acc:MGI:1349215]	ENSMUSG00000031378	1.349416724	0.016644256
Uckl1	uridine-cytidine kinase 1-like 1 [Source:MGI Symbol;Acc:MGI:1915806]	ENSMUSG00000089917	1.354881331	0.030006497
Mxra8	matrix-remodelling associated 8 [Source:MGI Symbol;Acc:MGI:1922011]	ENSMUSG00000029070	1.355312157	0.006081444
Gm2a	GM2 ganglioside activator protein [Source:MGI Symbol;Acc:MGI:95762]	ENSMUSG00000000594	1.355344733	0.012069084
Ccdc80	coiled-coil domain containing 80 [Source:MGI Symbol;Acc:MGI:1915146]	ENSMUSG00000022665	1.355752128	0.001109029
Pdgfrl	platelet-derived growth factor receptor-like [Source:MGI Symbol;Acc:MGI:1916047]	ENSMUSG00000031595	1.357062335	0.008724909
Pcx	pyruvate carboxylase [Source:MGI Symbol;Acc:MGI:97520]	ENSMUSG00000024892	1.35743111	0.004774209
C1rl	complement component 1, r subcomponent-like [Source:MGI Symbol;Acc:MGI:2660692]	ENSMUSG00000038527	1.358489539	0.025955846
Dtx3l	deltex 3-like, E3 ubiquitin ligase [Source:MGI Symbol;Acc:MGI:2656973]	ENSMUSG00000049502	1.358830295	0.049908928
Fosl2	fos-like antigen 2 [Source:MGI Symbol;Acc:MGI:102858]	ENSMUSG00000029135	1.361419529	0.019245715
Mmp14	matrix metallopeptidase 14 (membrane-inserted) [Source:MGI Symbol;Acc:MGI:101900]	ENSMUSG00000000957	1.363102355	0.040904066
Lmf1	lipase maturation factor 1 [Source:MGI Symbol;Acc:MGI:1923733]	ENSMUSG00000002279	1.363372679	0.038943902
Ttyh3	tweety family member 3 [Source:MGI Symbol;Acc:MGI:1925589]	ENSMUSG00000036565	1.363387415	0.042949194
Tmem140	transmembrane protein 140 [Source:MGI Symbol;Acc:MGI:1915737]	ENSMUSG00000057137	1.364730518	0.009377647
Fam53b	family with sequence similarity 53, member B [Source:MGI Symbol;Acc:MGI:1925188]	ENSMUSG00000030956	1.36663627	0.018661713
Creb3l2	cAMP responsive element binding protein 3-like 2 [Source:MGI Symbol;Acc:MGI:2442695]	ENSMUSG00000038648	1.367061489	0.031222221
Thsd7a	thrombospondin, type I, domain containing 7A [Source:MGI Symbol;Acc:MGI:2685683]	ENSMUSG00000032625	1.367084412	0.01590799
Zfp36l1	zinc finger protein 36, C3H type-like 1 [Source:MGI Symbol;Acc:MGI:107946]	ENSMUSG00000021127	1.372195964	0.039714464
Ypel3	yippee-like 3 (Drosophila) [Source:MGI Symbol;Acc:MGI:1913340]	ENSMUSG00000042675	1.37466696	0.027651431
Svil	supervillin [Source:MGI Symbol;Acc:MGI:2147319]	ENSMUSG00000024236	1.374810335	0.039714464
Sepp1	selenoprotein P, plasma, 1 [Source:MGI Symbol;Acc:MGI:894288]	ENSMUSG00000064373	1.37698271	0.017649779
Plat	plasminogen activator, tissue [Source:MGI Symbol;Acc:MGI:97610]	ENSMUSG00000031538	1.377058008	0.003902526
Abtb1	ankyrin repeat and BTB (POZ) domain containing 1 [Source:MGI Symbol;Acc:MGI:1933148]	ENSMUSG00000030083	1.378213154	0.043327195
Narf	nuclear prelamin A recognition factor [Source:MGI Symbol;Acc:MGI:1914858]	ENSMUSG00000000056	1.378553295	0.002536224
Fam214b	family with sequence similarity 214, member B [Source:MGI Symbol;Acc:MGI:2441854]	ENSMUSG00000036002	1.384844297	0.022647951
Sulf2	sulfatase 2 [Source:MGI Symbol;Acc:MGI:1919293]	ENSMUSG00000006800	1.384967129	0.001134395
Fzd1	frizzled class receptor 1 [Source:MGI Symbol;Acc:MGI:1196625]	ENSMUSG00000044674	1.385246653	0.001693481
Dusp27	dual specificity phosphatase 27 (putative) [Source:MGI Symbol;Acc:MGI:2685055]	ENSMUSG00000026564	1.385428678	0.011788007
Antxr1	anthrax toxin receptor 1 [Source:MGI Symbol;Acc:MGI:1916788]	ENSMUSG00000033420	1.386187764	0.000984343

Ucp2	uncoupling protein 2 (mitochondrial, proton carrier) [Source:MGI Symbol;Acc:MGI:109354]	ENSMUSG00000033685	1.387022386	0.010162844
Mrgprf	MAS-related GPR, member F [Source:MGI Symbol;Acc:MGI:2384823]	ENSMUSG00000031070	1.388747773	0.004915017
Plekhg4	pleckstrin homology domain containing, family G (with RhoGef domain) member 4 [Source:MGI Symbol;Acc:MGI:2142544]	ENSMUSG00000014782	1.388936293	0.042825447
Ogn	osteoglycin [Source:MGI Symbol;Acc:MGI:109278]	ENSMUSG00000021390	1.390417311	0.031727329
Bcas3	breast carcinoma amplified sequence 3 [Source:MGI Symbol;Acc:MGI:2385848]	ENSMUSG00000059439	1.390556447	0.024365941
Sema3d	sema domain, immunoglobulin domain (Ig), short basic domain, secreted, (semaphorin) 3D [Source:MGI Symbol;Acc:MGI:1860118]	ENSMUSG00000040254	1.392101216	0.00170814
Gadd45a	growth arrest and DNA-damage-inducible 45 alpha [Source:MGI Symbol;Acc:MGI:107799]	ENSMUSG00000036390	1.393515512	0.001905899
Sh3d19	SH3 domain protein D19 [Source:MGI Symbol;Acc:MGI:1350923]	ENSMUSG00000028082	1.393664251	0.002520492
Tgfb3	transforming growth factor, beta 3 [Source:MGI Symbol;Acc:MGI:98727]	ENSMUSG00000021253	1.39670446	0.005859364
Irgq	immunity-related GTPase family, Q [Source:MGI Symbol;Acc:MGI:2667176]	ENSMUSG00000041037	1.398030009	0.008209336
Mmp19	matrix metallopeptidase 19 [Source:MGI Symbol;Acc:MGI:1927899]	ENSMUSG00000025355	1.400429914	0.006063904
Rbms3	RNA binding motif, single stranded interacting protein [Source:MGI Symbol;Acc:MGI:2444477]	ENSMUSG00000039607	1.40128896	0.017649779
Pi15	peptidase inhibitor 15 [Source:MGI Symbol;Acc:MGI:1934659]	ENSMUSG00000067780	1.401379245	0.000918143
Mmp2	matrix metallopeptidase 2 [Source:MGI Symbol;Acc:MGI:97009]	ENSMUSG00000031740	1.403043674	0.000902594
C1qtnf6	C1q and tumor necrosis factor related protein 6 [Source:MGI Symbol;Acc:MGI:1919959]	ENSMUSG00000022440	1.404466801	0.007312526
Ticam1	toll-like receptor adaptor molecule 1 [Source:MGI Symbol;Acc:MGI:2147032]	ENSMUSG00000047123	1.405167599	0.006053516
Cfh	complement component factor h [Source:MGI Symbol;Acc:MGI:88385]	ENSMUSG00000026365	1.407333606	0.017358299
Tap2	transporter 2, ATP-binding cassette, sub-family B (MDR/TAP) [Source:MGI Symbol;Acc:MGI:98484]	ENSMUSG00000024339	1.40785906	0.012275597
Unc5c	unc-5 netrin receptor C [Source:MGI Symbol;Acc:MGI:1095412]	ENSMUSG00000059921	1.409018207	0.002929157
Ficd	FIC domain containing [Source:MGI Symbol;Acc:MGI:1098550]	ENSMUSG00000053334	1.409068431	0.028087699
Ptgis	prostaglandin I2 (prostacyclin) synthase [Source:MGI Symbol;Acc:MGI:1097156]	ENSMUSG00000017969	1.410203111	0.003555438
Vldlr	very low density lipoprotein receptor [Source:MGI Symbol;Acc:MGI:98935]	ENSMUSG00000024924	1.414394581	0.020871414
Mxd4	Max dimerization protein 4 [Source:MGI Symbol;Acc:MGI:104991]	ENSMUSG00000037235	1.415168137	0.000184456
Cbr2	carbonyl reductase 2 [Source:MGI Symbol;Acc:MGI:107200]	ENSMUSG00000025150	1.41647738	0.000874401
Col3a1	collagen, type III, alpha 1 [Source:MGI Symbol;Acc:MGI:88453]	ENSMUSG00000026043	1.42015321	0.04265287
Kcnj2	potassium inwardly-rectifying channel, subfamily J, member 2 [Source:MGI Symbol;Acc:MGI:104744]	ENSMUSG00000041695	1.421889222	8.92E-05
Trp53inp2	transformation related protein 53 inducible nuclear protein 2 [Source:MGI Symbol;Acc:MGI:1915978]	ENSMUSG00000038375	1.422578681	0.000262485

Thbs2	thrombospondin 2 [Source:MGI Symbol;Acc:MGI:98738]	ENSMUSG00000023885	1.423354016	0.003034541
Wisp2	WNT1 inducible signaling pathway protein 2 [Source:MGI Symbol;Acc:MGI:1328326]	ENSMUSG00000027656	1.424690919	0.01741594
C1s1	complement component 1, s subcomponent 1 [Source:MGI Symbol;Acc:MGI:1355312]	ENSMUSG00000038521	1.425881221	0.004785485
Prickle1	prickle planar cell polarity protein 1 [Source:MGI Symbol;Acc:MGI:1916034]	ENSMUSG00000036158	1.426039436	0.04659026
Axin2	axin 2 [Source:MGI Symbol;Acc:MGI:1270862]	ENSMUSG00000000142	1.430801448	0.00546389
Sulf1	sulfatase 1 [Source:MGI Symbol;Acc:MGI:2138563]	ENSMUSG00000016918	1.43256503	0.000902594
Cdhr1	cadherin-related family member 1 [Source:MGI Symbol;Acc:MGI:2157782]	ENSMUSG00000021803	1.433926856	0.041716576
Bcl2l11	BCL2-like 11 (apoptosis facilitator) [Source:MGI Symbol;Acc:MGI:1197519]	ENSMUSG00000027381	1.434559378	0.02498071
Nsg1	neuron specific gene family member 1 [Source:MGI Symbol;Acc:MGI:109149]	ENSMUSG00000029126	1.437262269	4.15E-05
Slc7a2	solute carrier family 7 (cationic amino acid transporter, y+ system), member 2 [Source:MGI Symbol;Acc:MGI:99828]	ENSMUSG00000031596	1.439714378	0.003103043
Afap1l2	actin filament associated protein 1-like 2 [Source:MGI Symbol;Acc:MGI:2147658]	ENSMUSG00000025083	1.444907186	0.013885936
Adamts4	a disintegrin-like and metallopeptidase (reprolysin type) with thrombospondin type 1 motif, 4 [Source:MGI Symbol;Acc:MGI:1339949]	ENSMUSG00000006403	1.448785782	0.008087445
Hoxc6	homeobox C6 [Source:MGI Symbol;Acc:MGI:96197]	ENSMUSG00000001661	1.452873668	0.026263324
Lrrc17	leucine rich repeat containing 17 [Source:MGI Symbol;Acc:MGI:1921761]	ENSMUSG00000039883	1.454845533	6.02E-05
Ephb6	Eph receptor B6 [Source:MGI Symbol;Acc:MGI:1096338]	ENSMUSG00000029869	1.455393547	0.003034541
Dtx4	deltex 4, E3 ubiquitin ligase [Source:MGI Symbol;Acc:MGI:2672905]	ENSMUSG00000039982	1.457010823	0.000187439
Macrod1	MACRO domain containing 1 [Source:MGI Symbol;Acc:MGI:2147583]	ENSMUSG00000036278	1.45819272	0.043295022
Inhbb	inhibin beta-B [Source:MGI Symbol;Acc:MGI:96571]	ENSMUSG00000037035	1.45917153	0.011765321
Casp12	caspase 12 [Source:MGI Symbol;Acc:MGI:1312922]	ENSMUSG00000025887	1.459772032	0.000477638
Ogdhl	oxoglutarate dehydrogenase-like [Source:MGI Symbol;Acc:MGI:3616088]	ENSMUSG00000021913	1.463811517	0.047890332
Kdm7a	lysine (K)-specific demethylase 7A [Source:MGI Symbol;Acc:MGI:2443388]	ENSMUSG00000042599	1.464637325	0.000984343
Txnip	thioredoxin interacting protein [Source:MGI Symbol;Acc:MGI:1889549]	ENSMUSG00000038393	1.46474697	0.000421946
AI464131	expressed sequence AI464131 [Source:MGI Symbol;Acc:MGI:2140300]	ENSMUSG00000046312	1.465419466	0.001143032
Calcoco1	calcium binding and coiled coil domain 1 [Source:MGI Symbol;Acc:MGI:1914738]	ENSMUSG00000023055	1.468858449	0.011355465
Whrn	whirlin [Source:MGI Symbol;Acc:MGI:2682003]	ENSMUSG00000039137	1.470336707	0.046448327
Pdgfra	platelet derived growth factor receptor, alpha polypeptide [Source:MGI Symbol;Acc:MGI:97530]	ENSMUSG00000029231	1.472131483	0.001429892
Col6a2	collagen, type VI, alpha 2 [Source:MGI Symbol;Acc:MGI:88460]	ENSMUSG00000020241	1.472480178	0.036856582
Hs3st1	heparan sulfate (glucosamine) 3-O-sulfotransferase 1 [Source:MGI Symbol;Acc:MGI:1201606]	ENSMUSG00000051022	1.472761857	0.000167229

A4galt	alpha 1,4-galactosyltransferase [Source:MGI Symbol;Acc:MGI:3512453]	ENSMUSG00000047878	1.475219825	0.000116336
Coro2b	coronin, actin binding protein, 2B [Source:MGI Symbol;Acc:MGI:2444283]	ENSMUSG00000041729	1.478329002	0.003034541
Cd200	CD200 antigen [Source:MGI Symbol;Acc:MGI:1196990]	ENSMUSG00000022661	1.479552233	0.041330937
Hsd3b7	hydroxy-delta-5-steroid dehydrogenase, 3 beta- and steroid delta-isomerase 7 [Source:MGI Symbol;Acc:MGI:2141879]	ENSMUSG00000042289	1.480296916	0.000594708
Islr	immunoglobulin superfamily containing leucine-rich repeat [Source:MGI Symbol;Acc:MGI:1349645]	ENSMUSG00000037206	1.482660926	1.03E-05
Fam46a	family with sequence similarity 46, member A [Source:MGI Symbol;Acc:MGI:2670964]	ENSMUSG00000032265	1.484721296	0.015055278
Slc43a2	solute carrier family 43, member 2 [Source:MGI Symbol;Acc:MGI:2442746]	ENSMUSG00000038178	1.494204605	0.002579876
Emilin1	elastin microfibril interfacer 1 [Source:MGI Symbol;Acc:MGI:1926189]	ENSMUSG00000029163	1.494698401	0.002520492
Dio2	deiodinase, iodothyronine, type II [Source:MGI Symbol;Acc:MGI:1338833]	ENSMUSG00000007682	1.494779904	0.00022752
Alox5ap	arachidonate 5-lipoxygenase activating protein [Source:MGI Symbol;Acc:MGI:107505]	ENSMUSG00000060063	1.495118524	0.007619161
Rac3	RAS-related C3 botulinum substrate 3 [Source:MGI Symbol;Acc:MGI:2180784]	ENSMUSG00000018012	1.498116197	0.042290597
Prelp	proline arginine-rich end leucine-rich repeat [Source:MGI Symbol;Acc:MGI:2151110]	ENSMUSG00000041577	1.500111956	0.038451936
Pnrc1	proline-rich nuclear receptor coactivator 1 [Source:MGI Symbol;Acc:MGI:1917838]	ENSMUSG00000040128	1.500184229	0.000243602
Fcgrt	Fc receptor, IgG, alpha chain transporter [Source:MGI Symbol;Acc:MGI:103017]	ENSMUSG00000003420	1.500933667	4.15E-05
Rassf2	Ras association (RalGDS/AF-6) domain family member 2 [Source:MGI Symbol;Acc:MGI:2442060]	ENSMUSG00000027339	1.502629926	0.000384691
Angpt4	angiopoietin 4 [Source:MGI Symbol;Acc:MGI:1336887]	ENSMUSG00000027460	1.509910104	0.001478659
Ophn1	oligophrenin 1 [Source:MGI Symbol;Acc:MGI:2151070]	ENSMUSG00000031214	1.513475339	0.002389393
Sema6c	sema domain, transmembrane domain (TM), and cytoplasmic domain, (semaphorin) 6C [Source:MGI Symbol;Acc:MGI:1338032]	ENSMUSG00000038777	1.515506807	0.031624186
Zim1	zinc finger, imprinted 1 [Source:MGI Symbol;Acc:MGI:1341879]	ENSMUSG00000002266	1.521400389	0.009961883
Col6a1	collagen, type VI, alpha 1 [Source:MGI Symbol;Acc:MGI:88459]	ENSMUSG00000001119	1.526986007	0.008826785
Fmo1	flavin containing monooxygenase 1 [Source:MGI Symbol;Acc:MGI:1310002]	ENSMUSG00000040181	1.528265944	0.000415164
Nfatc4	nuclear factor of activated T cells, cytoplasmic, calcineurin dependent 4 [Source:MGI Symbol;Acc:MGI:1920431]	ENSMUSG00000023411	1.53324678	0.028087699
Daam2	dishevelled associated activator of morphogenesis 2 [Source:MGI Symbol;Acc:MGI:1923691]	ENSMUSG00000040260	1.534495188	0.034756348
Gm5662	predicted gene 5662 [Source:MGI Symbol;Acc:MGI:3648257]	ENSMUSG00000079029	1.538616457	0.047965926
Lix1	limb and CNS expressed 1 [Source:MGI Symbol;Acc:MGI:1913893]	ENSMUSG00000047786	1.543658814	0.008766801
Fgfr4	fibroblast growth factor receptor 4 [Source:MGI Symbol;Acc:MGI:95525]	ENSMUSG00000005320	1.553691663	0.032664303
Sema6a	sema domain, transmembrane domain (TM), and cytoplasmic domain, (semaphorin) 6A [Source:MGI Symbol;Acc:MGI:1203727]	ENSMUSG00000019647	1.559804685	0.019841311

Kdm5b	lysine (K)-specific demethylase 5B [Source:MGI Symbol;Acc:MGI:1922855]	ENSMUSG00000042207	1.561087005	0.042825447
Mmp28	matrix metallopeptidase 28 (epilysin) [Source:MGI Symbol;Acc:MGI:2153062]	ENSMUSG00000020682	1.561331311	0.001178146
Ugt1a6a	UDP glucuronosyltransferase 1 family, polypeptide A6A [Source:MGI Symbol;Acc:MGI:2137698]	ENSMUSG00000054545	1.561806264	0.004480671
Car3	carbonic anhydrase 3 [Source:MGI Symbol;Acc:MGI:88270]	ENSMUSG00000027559	1.578791226	0.002012428
Gm12258	predicted gene 12258 [Source:MGI Symbol;Acc:MGI:3651534]	ENSMUSG00000072915	1.581995196	0.028335471
Fbxl13	F-box and leucine-rich repeat protein 13 [Source:MGI Symbol;Acc:MGI:2443416]	ENSMUSG00000048520	1.587323322	0.003103043
Pcdhb20	protocadherin beta 20 [Source:MGI Symbol;Acc:MGI:2136758]	ENSMUSG00000046191	1.587666882	0.007142522
Car2	carbonic anhydrase 2 [Source:MGI Symbol;Acc:MGI:88269]	ENSMUSG00000027562	1.587714395	0.001223852
Spon2	spondin 2, extracellular matrix protein [Source:MGI Symbol;Acc:MGI:1923724]	ENSMUSG00000037379	1.588956989	6.00E-06
Gm8113	predicted gene 8113 [Source:MGI Symbol;Acc:MGI:3648791]	ENSMUSG00000089901	1.592214833	0.000218027
Ssc5d	scavenger receptor cysteine rich family, 5 domains [Source:MGI Symbol;Acc:MGI:3606211]	ENSMUSG00000035279	1.593609617	0.042825447
Pdlim3	PDZ and LIM domain 3 [Source:MGI Symbol;Acc:MGI:1859274]	ENSMUSG00000031636	1.594200302	0.002192009
Frmpd1	FERM and PDZ domain containing 1 [Source:MGI Symbol;Acc:MGI:2446274]	ENSMUSG00000035615	1.594244911	0.006448572
Aldh3b1	aldehyde dehydrogenase 3 family, member B1 [Source:MGI Symbol;Acc:MGI:1914939]	ENSMUSG00000024885	1.597916999	0.001421423
Sfrp2	secreted frizzled-related protein 2 [Source:MGI Symbol;Acc:MGI:108078]	ENSMUSG00000027996	1.60073797	0.002394027
Pnmal2	PNMA-like 2 [Source:MGI Symbol;Acc:MGI:3645856]	ENSMUSG00000070802	1.60455815	0.009417407
Ryr3	ryanodine receptor 3 [Source:MGI Symbol;Acc:MGI:99684]	ENSMUSG00000057378	1.609336155	0.036882929
Pik3ip1	phosphoinositide-3-kinase interacting protein 1 [Source:MGI Symbol;Acc:MGI:1917016]	ENSMUSG00000034614	1.61338316	5.21E-06
Lzts1	leucine zipper, putative tumor suppressor 1 [Source:MGI Symbol;Acc:MGI:2684762]	ENSMUSG00000036306	1.628255171	0.016720641
Igfbp5	insulin-like growth factor binding protein 5 [Source:MGI Symbol;Acc:MGI:96440]	ENSMUSG00000026185	1.638850986	0.002520492
Tbc1d16	TBC1 domain family, member 16 [Source:MGI Symbol;Acc:MGI:2652878]	ENSMUSG00000039976	1.641147314	9.42E-05
Sobp	sine oculis-binding protein homolog (Drosophila) [Source:MGI Symbol;Acc:MGI:1924427]	ENSMUSG00000038248	1.641568139	0.000743314
Tcp11l2	t-complex 11 (mouse) like 2 [Source:MGI Symbol;Acc:MGI:2444679]	ENSMUSG00000020034	1.667083561	0.000421946
Ch25h	cholesterol 25-hydroxylase [Source:MGI Symbol;Acc:MGI:1333869]	ENSMUSG00000050370	1.673810191	0.003063044
Vsir	V-set immunoregulatory receptor [Source:MGI Symbol;Acc:MGI:1921298]	ENSMUSG00000020101	1.683522665	1.36E-05
P2rx6	purinergic receptor P2X, ligand-gated ion channel, 6 [Source:MGI Symbol;Acc:MGI:1337113]	ENSMUSG00000022758	1.683869597	0.000241973
Kank1	KN motif and ankyrin repeat domains 1 [Source:MGI Symbol;Acc:MGI:2147707]	ENSMUSG00000032702	1.688161345	0.003218377
Chrng	cholinergic receptor, nicotinic, gamma polypeptide [Source:MGI Symbol;Acc:MGI:87895]	ENSMUSG00000026253	1.689423538	0.002301965
Fads6	fatty acid desaturase domain family, member 6 [Source:MGI Symbol;Acc:MGI:3039592]	ENSMUSG00000044788	1.697952193	0.001144895

Fndc1	fibronectin type III domain containing 1 [Source:MGI Symbol;Acc:MGI:1915905]	ENSMUSG00000071984	1.714938415	0.031534732
Csf2rb2	colony stimulating factor 2 receptor, beta 2, low-affinity (granulocyte-macrophage) [Source:MGI Symbol;Acc:MGI:1339760]	ENSMUSG00000071714	1.726029426	0.004124492
Nrep	neuronal regeneration related protein [Source:MGI Symbol;Acc:MGI:99444]	ENSMUSG00000042834	1.726196715	1.49E-06
Cmbl	carboxymethylenebutenolidase-like (Pseudomonas) [Source:MGI Symbol;Acc:MGI:1916824]	ENSMUSG00000022235	1.734912337	0.046185124
Etl4	enhancer trap locus 4 [Source:MGI Symbol;Acc:MGI:95454]	ENSMUSG00000036617	1.744398398	0.036441045
Htra3	HtrA serine peptidase 3 [Source:MGI Symbol;Acc:MGI:1925808]	ENSMUSG00000029096	1.749655479	0.044280512
Enpp2	ectonucleotide pyrophosphatase/phosphodiesterase 2 [Source:MGI Symbol;Acc:MGI:1321390]	ENSMUSG00000022425	1.750912805	0.004266124
C1qtnf1	C1q and tumor necrosis factor related protein 1 [Source:MGI Symbol;Acc:MGI:1919254]	ENSMUSG00000017446	1.764319874	5.45E-10
Gm8300	predicted gene 8300 [Source:MGI Symbol;Acc:MGI:3643794]	ENSMUSG00000079034	1.764522771	0.031222221
Aldh1l1	aldehyde dehydrogenase 1 family, member L1 [Source:MGI Symbol;Acc:MGI:1340024]	ENSMUSG00000030088	1.791705027	0.00976649
Lrrn1	leucine rich repeat protein 1, neuronal [Source:MGI Symbol;Acc:MGI:106038]	ENSMUSG00000034648	1.79434983	0.010861458
Il13ra2	interleukin 13 receptor, alpha 2 [Source:MGI Symbol;Acc:MGI:1277954]	ENSMUSG00000031289	1.817825956	0.002520492
Gpr153	G protein-coupled receptor 153 [Source:MGI Symbol;Acc:MGI:1916157]	ENSMUSG00000042804	1.83913058	0.000292763
Csf2rb	colony stimulating factor 2 receptor, beta, low-affinity (granulocyte-macrophage) [Source:MGI Symbol;Acc:MGI:1339759]	ENSMUSG00000071713	1.855188285	5.86E-07
Maf	avian musculoaponeurotic fibrosarcoma oncogene homolog [Source:MGI Symbol;Acc:MGI:96909]	ENSMUSG00000055435	1.899229279	9.74E-09
Bmf	BCL2 modifying factor [Source:MGI Symbol;Acc:MGI:2176433]	ENSMUSG00000040093	1.960300303	0.000184456
Slc6a2	solute carrier family 6 (neurotransmitter transporter, noradrenalin), member 2 [Source:MGI Symbol;Acc:MGI:1270850]	ENSMUSG00000055368	1.961926471	0.005884226
Gm11007	predicted gene 11007 [Source:MGI Symbol;Acc:MGI:3779223]	ENSMUSG00000094475	1.97423218	0.031726069
Plxdc1	plexin domain containing 1 [Source:MGI Symbol;Acc:MGI:1919574]	ENSMUSG00000017417	2.006381745	0.028764789
Gdpd2	glycerophosphodiester phosphodiesterase domain containing 2 [Source:MGI Symbol;Acc:MGI:1918834]	ENSMUSG00000019359	2.038358931	0.020516157
Parp14	poly (ADP-ribose) polymerase family, member 14 [Source:MGI Symbol;Acc:MGI:1919489]	ENSMUSG00000034422	2.058918209	0.005990343
Tgm2	transglutaminase 2, C polypeptide [Source:MGI Symbol;Acc:MGI:98731]	ENSMUSG00000037820	2.095412967	1.12E-07
Slc2a13	solute carrier family 2 (facilitated glucose transporter), member 13 [Source:MGI Symbol;Acc:MGI:2146030]	ENSMUSG00000036298	2.098957471	0.000128746
Olfml2a	olfactomedin-like 2A [Source:MGI Symbol;Acc:MGI:2444741]	ENSMUSG00000046618	2.215388226	0.022516668
Robo2	roundabout guidance receptor 2 [Source:MGI Symbol;Acc:MGI:1890110]	ENSMUSG00000052516	2.248610704	0.017358299
Srgap1	SLIT-ROBO Rho GTPase activating protein 1 [Source:MGI Symbol;Acc:MGI:2152936]	ENSMUSG00000020121	2.302216214	0.03825052

B3galt1	UDP-Gal:betaGlcNAc beta 1,3-galactosyltransferase, polypeptide 1 [Source:MGI Symbol;Acc:MGI:1349403]	ENSMUSG00000034780	2.375218519	0.017649779
Adamts16	a disintegrin-like and metallopeptidase (reprolysin type) with thrombospondin type 1 motif, 16 [Source:MGI Symbol;Acc:MGI:2429637]	ENSMUSG00000049538	2.553641602	0.000215353
Ifit3	interferon-induced protein with tetratricopeptide repeats 3 [Source:MGI Symbol;Acc:MGI:1101055]	ENSMUSG00000074896	2.558035634	0.032523003
Kcnj16	potassium inwardly-rectifying channel, subfamily J, member 16 [Source:MGI Symbol;Acc:MGI:1314842]	ENSMUSG00000051497	2.568062903	0.00109709
Xpnpep2	X-prolyl aminopeptidase (aminopeptidase P) 2, membrane-bound [Source:MGI Symbol;Acc:MGI:2180001]	ENSMUSG00000037005	2.79820134	0.023017937
Hfe	hemochromatosis [Source:MGI Symbol;Acc:MGI:109191]	ENSMUSG00000006611	3.162128799	0.034712785
Dhx58	DEXH (Asp-Glu-X-His) box polypeptide 58 [Source:MGI Symbol;Acc:MGI:1931560]	ENSMUSG00000017830	4.194419265	0.001122482
Faim2	Fas apoptotic inhibitory molecule 2 [Source:MGI Symbol;Acc:MGI:1919643]	ENSMUSG00000023011	6.17885431	0.027387161

ANEXO II

Table S2 *Enrichment analysis of differentially expressed genes in C2C12 myoblasts after LLLT*

GOID	GOTerm	p value	% Associated Genes	Nr. Genes	Associated Genes Found
GO:0010634	positive regulation of epithelial cell migration	350.0E-15	10.68	11.00	[Angpt4, Anxa3, Bcas3, Enpp2, Hbegf, Plpp3, Prl2c2, Ptgs2, Sparc, Srpx2, Tgfbr2]
GO:0045765	regulation of angiogenesis	350.0E-15	8.49	18.00	[Angpt4, Anxa3, Brca1, Ddah1, Enpp2, Id1, Prl2c2, Ptgis, Ptgs2, Serpine1, Sfrp2, Sparc, Srpx2, Sulf1, Tcf4, Tgfbr2, Thbs2, Tnfrsf12a]
GO:0006268	DNA unwinding involved in DNA replication	32.0E-18	62.50	5.00	[Mcm2, Mcm4, Mcm6, Mcm7, Rad51]
GO:0006270	DNA replication initiation	32.0E-18	50.00	12.00	[Ccne1, Ccne2, Cdc6, Cdt1, Mcm10, Mcm2, Mcm3, Mcm4, Mcm5, Mcm6, Mcm7, Pola1]
GO:0006261	DNA-dependent DNA replication	32.0E-18	19.61	20.00	[Brca2, Ccne1, Ccne2, Cdc6, Cdt1, Dna2, Fen1, Mcm10, Mcm2, Mcm3, Mcm4, Mcm5, Mcm6, Mcm7, Pcna, Pola1, Pole2, Prim1, Rad51, Tipin]
GO:0044774	mitotic DNA integrity checkpoint	990.0E-21	13.56	8.00	[Bcat1, Ccnd1, Cdk1, Clspn, Fbxo5, Hmga2, Oraov1, Tipin]
GO:0000077	DNA damage checkpoint	990.0E-21	10.48	11.00	[Bcat1, Brca1, Ccnd1, Cdk1, Chek1, Clspn, Dtl, Fbxo5, Hmga2, Oraov1, Tipin]
GO:0032392	DNA geometric change	8.8E-6	19.23	10.00	[Dna2, Hmgb3, Mcm2, Mcm3, Mcm4, Mcm5, Mcm6, Mcm7, Rad51, Recql4]
GO:0006335	DNA replication-dependent nucleosome assembly	8.8E-6	41.67	5.00	[Asf1b, Chaf1a, Chaf1b, Hat1, Nasp]
GO:0010942	positive regulation of cell death	71.0E-9	6.19	36.00	[Ankrd1, Atf4, Axin2, Bcl2l11, Bmf, Clip3, Ctgf, Cyr61, Ddx20, Ect2, Eif5a, Fndc1, Fosl1, Gadd45a, Hmga2, Hspd1, Inhbb, Itga6, Mybbp1a, Nfatc4, Pdcd4, Phlda1, Pparg, Ptgis, Ptgs2, Rassf2, Sfrp2, Slit2, Smad3, Tgfb3, Tgm2, Tnfrsf12a, Txnip, Ucp2, Unc5c, Xdh]
GO:0031099	regeneration	930.0E-12	10.11	19.00	[Anxa3, Atic, Ccnb1, Ccnd1, Ccne1, Cdk1, Ezh1, Hfe, Ifrd1, Lifr, Matn2, Ncl, Nrep, Pparg, Ppat, Prrx1, Sulf2, Tgfbr2, Ucp2]
GO:0071478	cellular response to radiation	910.0E-15	9.63	13.00	[Bcat1, Chek1, Ect2, Gadd45a, Hmga2, Nfatc4, Noc2l, Pcna, Pik3r1, Ptgs2, Rad51, Rad51ap1, Sfrp2]
GO:0031570	DNA integrity checkpoint	910.0E-15	11.50	13.00	[Bcat1, Brca1, Ccnd1, Cdk1, Cdt1, Chek1, Clspn, Dna2, Dtl, Fbxo5, Hmga2, Oraov1, Tipin]
GO:0000076	DNA replication checkpoint	910.0E-15	38.46	5.00	[Cdt1, Clspn, Dna2, Oraov1, Tipin]
GO:0006282	regulation of DNA repair	910.0E-15	12.33	9.00	[Axin2, Brca1, Chek1, Hmga2, Pcna, Rad51, Rad51ap1, Rif1, Usp1]

GO:0009314	response to radiation	910.0E-15	6.19	27.00	[Aen, Asns, Bcat1, Brca1, Brca2, Ccnd1, Chek1, Col3a1, Dtl, Ect2, Gadd45a, Hmga2, Id2, Nfatc4, Noc2l, Pcna, Pik3r1, Pparg, Ptgs2, Rad18, Rad51, Rad51ap1, Sfrp2, Slc1a3, Tipin, Topbp1, Usp1]
GO:0009411	response to UV	910.0E-15	9.49	13.00	[Bcat1, Brca2, Ccnd1, Chek1, Dtl, Nfatc4, Noc2l, Pcna, Pik3r1, Ptgs2, Rad18, Tipin, Usp1]
GO:0033002	muscle cell proliferation	61.0E-6	8.50	13.00	[Ccnb1, Cdk1, Hbegf, Id2, Igfbp5, Orc1, Pparg, Ptgs2, Skp2, Stat3, Sulf1, Tgfbr2, Tk1]
GO:0000904	cell morphogenesis involved in differentiation	370.0E-9	5.10	39.00	[Alcam, Antxr1, Axin2, Cxcr4, Etv4, Fbxo5, Flot1, Gas1, Hmga2, Id1, Id2, Ifrd1, Itgb7, Kank1, Lrp8, Lrrn1, Lzts1, Matn2, Nfatc4, Ngf, Nptx1, Ogn, Prelp, Rac3, Robo2, Sdc2, Sema3d, Sema6a, Sema6c, Sema7a, Sfrp2, Slc1a3, Slit2, Smad3, Strap, Tgfb3, Tnfrsf12a, Unc5c, Vldlr]
GO:0001558	regulation of cell growth	370.0E-9	6.32	23.00	[Csf2rb, Ctgf, Cyr61, Dnph1, Gas1, Hbegf, Htra3, Ifrd1, Igfbp2, Igfbp5, Mmp14, Ngf, Ppan, Pparg, Sema3d, Sema6a, Sema6c, Sema7a, Sfrp2, Slit2, Smad3, Tnfrsf12a, Wisp2]
GO:0051271	negative regulation of cellular component movement	350.0E-15	7.14	17.00	[Ada, Angpt4, Col3a1, Igfbp5, Kank1, Mmp28, Sema3d, Sema6a, Sema6c, Sema7a, Serpine1, Sfrp2, Slit2, Srgap1, Stat3, Strap, Sulf1]
GO:0040013	negative regulation of locomotion	44.0E-6	6.98	18.00	[Ada, Angpt4, Col3a1, Igfbp5, Kank1, Mmp28, Robo2, Sema3d, Sema6a, Sema6c, Sema7a, Serpine1, Sfrp2, Slit2, Srgap1, Stat3, Strap, Sulf1]
GO:0030334	regulation of cell migration	44.0E-6	5.57	37.00	[Ada, Angpt4, Anxa3, Bcas3, Col3a1, Cxcr4, Cyr61, Enpp2, Fbxo5, Hbegf, Igfbp5, Kank1, Lama4, Mmp14, Mmp28, Mtus1, Pdgfra, Pik3r1, Plpp3, Prl2c2, Ptgs2, Sema3d, Sema6a, Sema6c, Sema7a, Serpine1, Sfrp2, Slit2, Smad3, Sparc, Srgap1, Srpx2, Stat3, Strap, Sulf1, Tgfbr2, Unc5c]
GO:0010769	regulation of cell morphogenesis involved in differentiation	44.0E-6	6.74	23.00	[Axin2, Fbxo5, Id1, Ifrd1, Kank1, Lrp8, Lzts1, Nfatc4, Ngf, Ogn, Rac3, Robo2, Sdc2, Sema3d, Sema6a, Sema6c, Sema7a, Sfrp2, Slit2, Smad3, Strap, Tgfb3, Tnfrsf12a]
GO:0031668	cellular response to extracellular stimulus	1.1E-12	8.13	17.00	[Asns, Atf4, Ccne1, Fosl1, Fzd1, Hfe, Inhbb, Itga6, Map1lc3a, Mybbp1a, Ppan, Pparg, Sfrp2, Skp2, Tfrc, Ucp2, Vldlr]
GO:1903034	regulation of response to wounding	120.0E-9	6.05	24.00	[Ada, Alox5ap, Birc2, C1qtnf1, C1qtnf3, Casp12, Cfh, Fam46a, Hbegf, Hspd1, Kank1, Pdgfra, Plpp3, Pparg, Ptgis, Ptgs2, Sema7a, Serpine1, Slc7a2, Slit2, Smad3, Stat5a, Tgfbr2, Tnfrsf12a]
GO:0000154	rRNA modification	5.8E-6	30.00	6.00	[Dimt1, Dkc1, Ftsj3, Nhp2, Nop56, Nop58]